九州大学学術情報リポジトリ Kyushu University Institutional Repository

STRUCTURAL IN-PLANE BEHAVIOR OF MASONRY WALLS EXTERNALLY RETROFITTED WITH FIBER REINFORCED MATERIALS

ザマニ, アハリゴラムレザ

https://doi.org/10.15017/1398305

出版情報:九州大学, 2013, 博士(工学), 課程博士

バージョン:

権利関係:全文ファイル公表済

STRUCTURAL IN-PLANE BEHAVIOR OF MASONRY WALLS EXTERNALLY RETROFITTED WITH FIBER REINFORCED MATERIALS

By Gholamreza ZAMANI AHARI

A thesis submitted to the Graduate School of Human-Environment Studies, Department of Architecture, Kyushu University in partial fulfillment of the requirements for the degree of Doctor of Engineering

June 2013

ACKNOWLEDGEMENTS

I wish to express my special appreciation to my thesis supervisor, Professor Kentaro Yamaguchi for his great support, interest and encouragement during the experimental and analytical work of this thesis.

Special thanks are also due to Professor Akihiko Kawano, my thesis co-supervisor, for his invaluable help and comments during the research period. Also, sincere thanks to Professor Tatsuo Kanno, my thesis co-supervisor, for his great support and valuable advices.

I am also thankful to Professor Masakatsu Miyajima from Kanazawa University for his great support during this study.

Distinguished thanks to Dr. Tetsushi Kanda from Kajima Corporation for his precious information and comments. Acknowledgement is also toward Professor Jason Ingham from University of Auckland for useful papers and advices.

My sincere appreciation is extended to Mr. Hiroaki Kubotera from structural laboratory of Department of Architecture, Kyushu University for his valuable help during the experimental work of this research. I am also thankful to all master and undergraduate students of the Professor Yamaguchi's laboratory for their great help and friendly attitude. Further, sincere thanks to the staff of Kajima Corporation, Futase Yogyo Corporation and Fibex Co., Ltd. for their contribution to the experimental work of this study.

This study was not possible without Japanese government scholarship (Ministry of Education, Culture, Sports, Science and Technology (MEXT)) for international Ph.D program. Also, the experimental work of this thesis was supported by Grant-in-Aid for Scientific Research from MEXT. These supports are very gratefully acknowledged.

At last but not the least, I thank my family for everything they did, and are still doing for me.

Gholamreza ZAMANI AHARI

June 2013

TABLE OF CONTENTS

CHAPTER 1. INTRODUCTION	1
1.1 An Overview on Masonry Construction.	1
1.2 Masonry Types.	2
1.3 Seismic Performance of Unreinforced Masonry (URM)	2
1.4 Vulnerability Resources of URM Buildings	3
1.5 Research Objective.	4
1.6 Thesis Organization.	5
References	6
CHAPTER 2. STRUCTURAL BEHAVIOR OF UNREINFORCED MA	SONRY
WALLS	8
2.1 Mechanical Characteristics of URM Walls.	8
2.1.1 Uniaxial Compressive Strength	9
2.1.2 Shear Strength	16
2.1.3 Tensile Strength.	18
2.1.4 Masonry under Biaxial Stress State	21
2.2 Tension Softening.	22
2.3 Masonry under Cyclic Loading.	22
2.4 Failure Criterion of Unreinforced Masonry.	24
2.5 In-plane Behavior of URM Walls.	27
References	37
CHAPTER 3. SEISMIC RETROFITTING OF UNREINFORCED MAS	ONRY
WALLS	41
3.1 Retrofit Strategies of Masonry	41
3.2 Conventional Retrofit Techniques of URM	44
3.2.1 Surface Treatment.	44
3.2.2 Injection.	50

3.2.3 Confinement.	51
3.2.4 Center Core.	51
3.2.5 Base Isolation.	52
3.3 Retrofitting with Engineered Cementitious Composites	52
3.4 Effectiveness of the URM Retrofitting Methods	53
References	58
CHAPTER 4. MODELING OF MASONRY	62
4.1 Modeling Approaches for URM	63
4.1.1 Heterogeneous Modeling	64
4.1.2 Homogeneous Modeling	65
4.1.3 Homogenization Theory	66
4.2 Modeling Procedure in Simple Micro-Model Technique	68
4.2.1 Tangential Behavior	68
4.2.2 Normal Behavior	68
4.2.3 Cohesive Behavior	68
4.2.4 Damage Criterion.	69
4.3 Modeling of ECC and AFRP Retrofitted Masonry	69
4.3.1 ECC Retrofitting Model	70
4.3.2 AFRP Retrofitting Model	72
References	73
CHAPTER 5. EXPERIMENTAL PROGRAM	76
5.1 Objective and Scope of Experiments	76
5.2 ECC Retrofitting.	76
5.2.1 Outline of Experiment	76
5.2.2 Characterization of ECC.	77
5.2.3 Properties of Masonry Brick	82
5.2.4 Properties of Bed Joint Mortar	84
5.2.5 Masonry Test Specimens	86
5 2 6 Test Dragadura	90

5.2.7 Test Results and Discussion.	91
5.2.8 Conclusion Remarks for ECC Retrofitting.	100
5.3 AFRP Retrofitting.	101
5.3.1 Outline of Experiment.	101
5.3.2 Material and Specimen Specification.	101
5.3.3 Shear Stress and Strain in Diagonal Specimens.	106
5.3.4 Test Results and Discussion.	107
5.3.5 Comparison to Other Retrofitting Methods	112
5.3.6 Conclusion Remarks for AFRP Retrofitting.	113
References	114
CHAPTER 6. ANALYTICAL STUDY	116
6.1 Analysis Procedure.	116
6.2 Simple Shear Model for ECC Retrofitted Triplet Specimens	116
6.3 Numerical Micro-Model Analysis of ECC Retrofitted Triplet Specimens	120
6.3.1 Material Properties	120
6.3.2 Discretization of Model.	122
6.3.3 Characteristics of Interface.	122
6.3.4 Shear Load Resistance-Displacement Behavior	127
6.3.5 Results and Discussion.	127
6.4 Shear Strength Evaluation of AFRP Retrofitted Diagonal Specimens	129
6.5 Numerical Micro-Model Analysis of AFRP Retrofitted Diagonal Specimens	133
6.5.1 Material Properties.	134
6.5.2 Discretization of Model	135
6.5.3 Characteristics of Interface.	137
6.5.4 Load-Displacement Behavior	138
6.5.5 Results and Discussion.	138
References	141
CHAPTER 7. SUMMARY AND CONCLUSION	142
7.1 Summary	142

7.2 Findings and Conclusion.	144
7.3 Future Work	146

LIST OF FIGURES

Figure 1.1 Bam historical masonry castle before and after 2003 Bam earthquake (Iran))3
Figure 1.2 Typical failure mechanisms of URM structures.	4
Figure 2.1 States of stress in masonry under various loading conditions	9
Figure 2.2 Uniaxial compressive behavior of masonry under loading normal to the bed	
Joints	10
Figure 2.3 Typical stress-strain diagram of masonry for different types of brick	15
Figure 2.4 Common shear test methods of masonry	17
Figure 2.5 Failure of masonry under tensile stress.	18
Figure 2.6 Stress-strain diagram of masonry under tensile load parallel to bed joint morta	ar18
Figure 2.7 Test setup for tensile strength of masonry parallel to the bed joints	19
Figure 2.8 Biaxial stress envelopes for masonry in three orientation degrees	21
Figure 2.9 Typical tensile stress-strain models of materials.	23
Figure 2.10 Typical behavior of different type of materials under cyclic loading	23
Figure 2.11 Modes of failure of URM under biaxial loading	25
Figure 2.12 Typical failure surface of masonry	26
Figure 2.13 Simplified failure envelopes of URM.	26
Figure 2.14 In-plane failure patterns of URM wall.	28
Figure 2.15 In-plane failure modes of a laterally loaded URM wall	29
Figure 2.16 Horizontal force versus horizontal deformation in case of mortar failure	30
Figure 2.17 Horizontal force versus horizontal deformation in case of mortar-brick failure	re30
Figure 2.18 Local failure patterns of URM wall.	31
Figure 2.19 Local failure patterns URM wall with opening.	31
Figure 2.20 Generalized force-deformation relation for masonry elements	32
Figure 2.21 URM wall under horizontal lateral loading.	33
Figure 3.1 Seismic assessment of URM structures	43
Figure 3.2 Externally retrofitted wall in shotcrete method.	45
Figure 3.3 Steel wire mesh applied to the surface of URM wall	47

Figure 3.4 Vertical and diagonal steel bracing.	49
Figure 3.5 Grout injection.	50
Figure 3.6 Confinement of URM wall by tie column.	51
Figure 3.7 High deformability of ECC composite.	53
Figure 4.1 Modeling approaches for masonry	65
Figure 4.2 Typical linear traction-separation model	69
Figure 4.3 Perfect elasto-plastic tensile stress-strain relation of ECC	71
Figure 4.4 Elasto-plastic tensile stress-strain diagram for AFRP-resin	72
Figure 5.1 ECC mortar mixture.	79
Figure 5.2 Flow test on ECC mortar	79
Figure 5.3 Compressive test on ECC.	79
Figure 5.4 Compressive failure of ECC	79
Figure 5.5 Bending test on ECC.	79
Figure 5.6 Flexural failure of ECC.	79
Figure 5.7 Compressive stress-strain diagram of ECC mortar (28 days age)	80
Figure 5.8 Extreme fiber stress-strain diagram of ECC mortar (28 days age)	81
Figure 5.9 Compressive strength versus time diagram of ECC mortar	81
Figure 5.10 Masonry unit brick specimens.	82
Figure 5.11 Compressive stress-strain diagram of masonry unit brick (UBH series)	83
Figure 5.12 Compressive test on bed joint mortar.	84
Figure 5.13 Compressive stress-strain diagram of bed joint mortar	85
Figure 5.14 Extreme fiber stress-strain diagram of bed joint mortar	85
Figure 5.15 Masonry specimen forms.	86
Figure 5.16 Retrofitted masonry unit bricks.	87
Figure 5.17 Construction of UT specimens.	88
Figure 5.18 Construction of UP specimens.	88
Figure 5.19 Molding of RT specimens.	88
Figure 5.20 Molding of RP specimens.	88
Figure 5.21 Retrofitting of RT specimens	88

Figure 5.22 ECC retrofitted masonry specimens.	90
Figure 5.23 Failure mode of masonry unit bricks	91
Figure 5.24 Compressive strength of masonry unit bricks	92
Figure 5.25 Failure mode of masonry triplet specimens	92
Figure 5.26 Shear strain in masonry triplet specimens	93
Figure 5.27 Shear stress-strain diagram of masonry triplet specimens aged 378 days	94
Figure 5.28 Shear strength of masonry triplet specimens aged 42 days	95
Figure 5.29 Shear strength of masonry triplet specimens aged 378 days	95
Figure 5.30 Failure mode of masonry prism specimens	96
Figure 5.31 Compressive stress-strain diagram of masonry prism specimens aged 42 days	97
Figure 5.32 Compressive strength of masonry prism specimens aged 42 days	97
Figure 5.33 Compressive strength of masonry prism specimens aged 378 days	98
Figure 5.34 Maximum compressive load carried by masonry prism specimens	
aged 42 days	98
Figure 5.35 Maximum compressive load carried by masonry prism specimens	
aged 378 days	99
Figure 5.36 Configuration of prism test.	100
Figure 5.37 Configuration of diagonal compression test	102
Figure 5.38 Specimen types (AFRP Retrofitting)	103
Figure 5.39 Application of primer	104
Figure 5.40 Surface treatment using putty	104
Figure 5.41 Application of adhesive.	104
Figure 5.42 Removing air with roller	104
Figure 5.43 Coating with adhesive.	104
Figure 5.44 Wrapping confining bands	104
Figure 5.45 Application of AFRP band to URM wall	105
Figure 5.46 Shear strain in diagonal specimen	106
Figure 5.47 Failure mode of retrofitted specimens type A.	108
Figure 5.48 Failure mode of bare and retrofitted specimens type B	109

Figure 5.49 Shear stress-strain diagram of specimens type A.	110
Figure 5.50 Shear stress-strain diagram of specimens type B.	110
Figure 5.51 Shear strength of specimen series A.	111
Figure 5.52 Shear strength of specimen series B.	111
Figure 6.1 Crack propagation in ECC retrofitted triplet specimens	117
Figure 6.2 Shear force equilibrium in ECC retrofitted triplet specimens	117
Figure 6.3 Perfect elasto-plastic tensile stress-strain relation of ECC	121
Figure 6.4 Model of unreinforced triplet specimens	123
Figure 6.5 Model of retrofitted triplet specimens	123
Figure 6.6 Typical linear traction-separation model	125
Figure 6.7 Shear bond stress vs displacement for calibrated unreinforced model and	
experimental data	126
Figure 6.8 Shear load resistance vs deflection for specimens 10RT2 and 10RT3	128
Figure 6.9 Shear load resistance vs deflection for specimens 20RT1 and 20RT2	128
Figure 6.10 Elasto-plastic tensile stress-strain diagram for AFRP-resin	135
Figure 6.11 Model of unreinforced diagonal specimen	136
Figure 6.12 Model of AFRP retrofitted diagonal specimen	136
Figure 6.13 In-plane strain in the AFRP retrofitted specimen.	138
Figure 6.14 Vertical compressive load vs deflection for specimen type B21 and B22	139

LIST OF TABLES

Table 2.1 Failure types of URM wall in FEMA 356 and ASCE 41	35
Table 3.1 Advantages and disadvantages of URM retrofitting methods	54
Table 4.1 Required parameters for URM in simplified modeling technique	70
Table 4.2 Required parameters for ECC modeling.	71
Table 4.3 Required parameters for AFRP modeling.	72
Table 5.1 ECC mix proportion.	78
Table 5.2 Properties of PVA fiber	78
Table 5.3 ECC test sample properties	78
Table 5.4 Mechanical properties of ECC mortar.	80
Table 5.5 Properties of masonry unit brick series UBH and RBH	83
Table 5.6 Properties of masonry unit brick series UBB.	83
Table 5.7 Bed joint mortar test sample properties	84
Table 5.8 Mechanical properties of bed joint mortar	84
Table 5.9 Masonry specimen types (ECC retrofitting).	87
Table 5.10 Specimen specifications (AFRP Retrofitting)	102
Table 5.11 Aramid sheet specifications	103
Table 5.12 Aramid sheet material specifications	103
Table 5.13 Comparison of AFRP retrofitting to other methods	112
Table 6.1 Experimental and analytical shear strength of ECC retrofitted triplet specim	ens119
Table 6.2 Parameters of bilinear tensile constitute law for ECC model	121
Table 6.3 Stiffness coefficients of traction-separation for ECC retrofitted model	126
Table 6.4 Experimental and analytical shear load capacity and failure displacement	
of specimens 10RT3 and 20RT1	129
Table 6.5 Experimental and analytical shear resistance of AFRP retrofitted specimens	132
Table 6.6 Effective tensile strain of AFRP and efficiency ratio with and without	
confining bands	132
Table 6.7 Aramid sheet material specifications.	135

Table 6.8 Stiffness coefficients of traction-separation for AFRP retrofitted model.	138
Table 6.9 Experimental and analytical results for peak compressive load of	
specimens B21 and B22	140

NOTATION

	6-46
α	factor for uniaxial compressive strength of masonry prism (relation (2.1))
α	factor for a fixed-free cantilevered wall and for a fixed-fixed pier (relation (2.20))
γ	shear strain in masonry triplet
δ	vertical displacement at the point of failure in prism specimen (relation (2.1))
δ	relative displacement of the two adjacent brick in triplet specimen (relation (5.1))
δ	average vertical displacements in prism specimen (relation (5.4))
δ_{ecc}	displacement of ECC retrofit layer in triplet specimen
δ_{H}	relative deformation of diagonal specimen in horizontal direction
δ_{m}	displacement of masonry in triplet specimen
δ_{n}	normal separation in interface
δ_s,δ_t	tangential separation in interface
δ_{V}	relative deformation of diagonal specimen in vertical direction
3	normal strain in masonry prism specimen
ϵ_{frpe}	effective strain of FRP
$\epsilon_{\text{frp,ec}}$	effective strain for experimental data of AFRP retrofitting (with confining)
$\epsilon_{\text{frp,ew}}$	effective strain for analytical results of AFRP retrofitting (without confining)
$\epsilon_{\text{frp},u}$	ultimate failure tensile strain of FRP
$\epsilon_{tu,b}$	ultimate tensile strain of ECC obtained from bending test
ϵ_{u}	ultimate tensile strain of ECC in bilinear elasto-plastic model
ϵ_{u}	ultimate tensile strain of AFRP-resin in bilinear elasto-plastic model
ϵ_{y}	yield tensile strain of AFRP-resin in bilinear elasto-plastic model
θ	Inclination degree in diagonal masonry specimens
μ	friction coefficient of brick-mortar interface
ν_{b}	Poisson's ratio of brick
ν_{m}	Poisson's ratio of mortar
$ ho_{frp}$	FRP area fraction

compressive strength of unit brick σ_{cb}

mean compressive strength of brick $\sigma_{cb,m}$

compressive strength of mortar σ_{cm}

mean compressive strength of mortar $\sigma_{\text{cm},m}$

compressive strength of masonry wall σ_{cw} compressive loading perpendicular to bed joint mortar

τ shear stress in masonry

 σ_{n}

bond (initial) strength between brick and mortar τ_0

critical shear stress in brick-mortar interface just before sliding τ_{crit}

masonry sectional area subjected to shear Α

ECC sectional area subjected to shear loading A_{ecc}

net area of the mortared/grouted brick section A_n

 A_v effective shear area of masonry

В binder content in ECC

cement content in mortar c

d effective depth of specimen (relation (6.12))

d distance between the brick centers in triplet masonry (relation (5.1))

D depth of masonry specimens (Figure 5.15 and 5.38)

 $d_{\rm f}$ PVA fiber diameter of ECC

deformability of retrofitted masonry specimen D_{RM}

 D_{URM} deformability of URM specimen

 E_b modulus of elasticity of brick

cЕ elastic modulus of ECC obtained from compression test

PVA fiber elastic modulus $E_{\rm f}$

 $E_{\text{frp}} \\$ elastic modulus of FRP

 E_{m} Young's modulus of masonry (relations (2.7)-(2.11))

 E_{m} modulus of elasticity of mortar (relation (2.12))

 f_a lower bound axial compressive stress of masonry

 f_b compressive strength of brick f_{bt,fl} flexural tensile strength of brick

f_{cb} compressive strength of brick

f_{cm} compressive strength of mortar

f_{cw} compressive strength of masonry wall

f_m compressive strength of mortar

 f_{sh} shear strength of mortar

 f_{sh0} shear bond strength between brick and mortar

 f_{ta} normal bond strength between brick and bed joint mortar

f_{tb} tensile strength of ECC obtained from bending test

 $f_{th,b}$ tensile strength of brick in the direction of its height

 $f_{t,ma}$ tensile strength of masonry

f_{tu} ultimate tensile stress of ECC obtained from uniaxail tensile test

f_{tu,b} ultimate tensile stress of ECC obtained from bending test

 $f_{t,un}$ tensile strength of unit brick

 f_{vecc} characteristic shear strength of ECC

 $f_{vk} \qquad \quad \text{characteristic shear strength of } URM$

f'dt lower bound diagonal tensile strength of URM

 f'_m compressive strength of masonry

G_m shear modulus of masonry

H height of masonry specimen

h_b height of brick

 h_{eff} effective height of the wall (relation (2.20))

h_{eff} wall height to the point of lateral load (relations (2.17)-(2.18))

h_m height (thickness) of mortar

 h_{un} height of unit brick

h_w height of masonry wall

Ig moment of inertia of uncracked wall cross section

K factor for different compositions of brick and mortar

K_n normal stiffness of contact

K_{nn} normal cohesive stiffness of contact

K_{ss}, K_{tt} tangential stiffness of contact

L length of the wall (relation (2.20))

L distance between second and fourth bricks in prism specimen (relation (5.4))

 l_0 overlap length of bricks

L_f PVA fiber length of ECC

m ratio of elastic modulus of brick and mortar

N initial compressive load normal to brick-mortar interface

P compressive load

P_E expected axial compressive force in masonry

P_{max} maximum experimental compressive load of masonry specimens

t thickness of masonry specimen

r ratio of height of brick and mortar (relation (2.12))

r FRP efficiency factor (relation (6.12))

r_c efficiency factor for AFRP retrofitting with confining

r_w efficiency factor for AFRP retrofitting without confining

s sand content

t_{ecc} thickness of ECC layer

t_i thickness of bed joint mortar

t_n normal traction stress in contact

t_s,t_t tangential traction stress in contact

 t_n^0 maximum normal stress of contact

 t_s^0, t_t^0 maximum tangential stress of contact

V shear capacity of retrofitted masonry

V_{ana} predicted shear load resistance by analytical model

V_{bis} lateral load which results in sliding at bed joint

V_{ecc} provided shear load resistance by ECC retrofit layer

V_{exp} experimental shear load resistance of retrofitted masonry specimens

V_f PVA fiber volume fraction in ECC

V_{FRP} shear capacity of FRP retrofitting

V_m shear load resistance of unreinforced masonry

 $\begin{array}{ll} v_{\text{me}} & & \text{expected bed joint sliding shear strength} \\ V_{\text{RM}} & & \text{shear capacity of retrofitted masonry} \end{array}$

V_{URM} shear capacity of unreinforced masonry

W water content

W width of masonry specimen (Figure 5.15 and 5.38)

ABSTRACT

There is a high stock of existing buildings including historical and cultural monuments around world constructed with unreinforced masonry (URM). In recent earthquakes, it has been proved that many of URM structures such as ordinary houses, schools and so far, are highly vulnerable and as a result there is a serious need for proposing appropriate seismic retrofitting techniques for them.

Load bearing unreinforced masonry walls are one of the most vulnerable parts of the URM structures. Their inadequate in-plane and out-of-plane seismic responses are responsible for the partial damages and also total collapse of the unreinforced masonry buildings.

This thesis focuses on the in-plane retrofitting of the unreinforced masonry walls. Improvement of in-plane behavior of URM wall by means of suitable retrofitting methods was the main objective of this research work.

An extensive investigation was conducted on the existing URM retrofit strategies and techniques. As a result, it was revealed that the surface treatment is the most suitable method from both applicability and cost-performance viewpoints in the case that wall covering is acceptable due to the altering the architectural features. Among the materials which have been examined in the surface treatment category, ones with higher deformation and tensile capacity exhibit better in-plane retrofit performance in terms of the shear resistance and deformability.

Retrofitting of URM wall with engineered cementitious composite (ECC) as a relatively new composite material was investigated in this study. ECC is a cement-based composite material with a strain-hardening tensile behavior and an excellent capability to control the width of crack. Improvement in the in-plane characteristics of the URM wall was evaluated through a series of tests conducted on small-size specimens. Monotonic shear and compression tests have been conducted on the unreinforced and retrofitted specimens.

Significant enhancement in the shear strength and deformation capacity was observed applying this retrofit method.

Also aramid fiber reinforced polymer (AFRP) sheet with light weight and good workability was utilized as a retrofit solution for URM walls. In order to eliminate the premature debonding behavior of the AFRP sheet, confining bands were utilized in this study. Diagonal compression test was conducted on the unreinforced and AFRP retrofitted specimens and the performance of the retrofit method and confining bands were evaluated. Experimental results showed that the shear capacity and deformability of URM were improved considerably. Also the debonding behavior of AFRP sheet was successfully controlled by the confining band system.

In order to predict the in-plane behavior of the retrofitted URM with both of the above mentioned methods (ECC and AFRP), analytical study was performed. A simple shear model was introduced for the ECC retrofitted masonry and the obtained results were validated with experimental data. This model showed a good agreement with experimental results in case of thin layers of ECC overlay.

Efficient strain approach, which has been originally developed for design of the FRP retrofitted concrete elements, was adopted for AFRP-URM with confining bands. The contribution of the confining bands to the efficient design strain of AFRP sheet was evaluated and discussed. As a result, it was found out that the application of these bands to thinner AFRP sheet leads to a more efficiency.

Numerical analysis was conducted on the retrofitted masonry specimens. Simple micro-model strategy was adopted employing finite element method. An elasto-plastic tensile model was adopted for ECC. In case of AFRP retrofitting, a new approach was proposed as a bilinear tensile model for AFRP-resin assemblage. The results of both analytical models showed good agreement with experimental results in terms of the load resistance and deformability.

As the result of this research work, it was concluded that both ECC and AFRP (with confining band system) retrofitting can be considered as suitable methods for in-plane enhancement of URM walls. Moreover, the adopted and proposed analytical models can

simulate the elastic and post-cracking behaviors of the retrofitted masonry with a fine accuracy and consequently can be useful for retrofit design.

Chapter 1

INTRODUCTION

1.1 An Overview on Masonry Construction

Based on the historical explorations, bricks were first fired around 3500 BC in Mesopotamia, present Iraq ^[1]. Masonry has been known as one of the oldest construction types and there is a high stock of masonry buildings around world including historical monuments which have being used for thousands of years or even up to now. It is estimated that more than 70% of the worldwide building inventory is masonry type ^[2]. Availability of materials and workmanship, enough local knowledge of constitutes like brick, stone, timber and mortar have made the masonry construction an attractive choice for building owners. Masonry can be considered strong and durable for gravitational loads. However due to the inherent structural deficiencies and material weakness of masonry, it has been proved that they are extremely vulnerable during earthquake events which resulted in high number of casualties ^[3,4]. Therefore, this type of buildings should be considered for retrofitting and strengthening against earthquake-induced loads. From a performance-based design viewpoint, the minimum requirements for life safety of the users of these building must be fulfilled. The first step for the retrofitting of this type of structures is a deep understanding of their structural characteristics and vulnerabilities.

Despite of easy construction and popularity of masonry, its structural behavior is complex ^[5]. The analysis of masonry structures poses important challenges because of their geometrical complexity, variability of the properties of traditional materials, different building techniques, lack of appropriate design and evaluation codes and little knowledge on the existing damages from previous loading experiences which affect these types of structures throughout their lifetime. Masonry is an anisotropic, non-linear composite material which its mechanical characteristics depend highly on the properties of constitutes and loading direction ^[6].

1.2 Masonry Types

Plain, reinforced and confined masonry are the common types of masonry buildings around world. Plain masonry can be categorized to adobe masonry, stone masonry and unreinforced masonry (URM). Major differences between these three groups come from the brick and bed joint mortar types and their assemblage system. In adobe buildings, unburned bricks are laid using mud mortar. For stone masonry, middle size natural stones are laid instead of brick using either cement-based mortars or mud.

Unreinforced masonry structures are represented by burned bricks which are assembled with cementitious mortar. The type of roof system in URM buildings is different depending on the environmental situation and local available materials. Timber plain roof, wooden inclined roofs, are roofs and reinforced concrete slabs are common types of roof system in the URM structures.

1.3 Seismic Performance of Unreinforced Masonry (URM)

Collapse of URM structures in earthquakes caused a great loss of human and financial resources around world. Experiences from past earthquakes such as ones occurred in Pakistan (2009), China (2008) and Iran (2003) [7,8] have shown high seismic vulnerability of URM. As a tragic example, the worst death toll from an earthquake in the past century occurred in 1976 in China (T'ang Shan province) where it was estimated that 240,000 people lost their lives [9]. Common damage patterns of URM reported in the past earthquake events are as follows [10]:

- Collapse of chimneys and plaster cracks
- Shear cracks in the walls, mainly starting from corners of openings
- Partial or complete out-of-plane wall collapse due to lack of wall to wall and wall to roof anchorage. In extreme cases this is accompanied by partial or total collapse of floor and roof structures
- Total collapse of walls and entire building

Evidence from the recent earthquakes has confirmed that the overall performance of URM buildings is dependent on parameters such as the wall stability, type of roof system, quality of mortar and geometrical features.

Material non-linearity along with geometrical non-linear behavior caused by progressive cracking is known as an inherent characteristic of unreinforced masonry. The severity of damages in Arge-Bam historical masonry castle (Iran) before and after 2003 earthquake is shown in Figure 1.1.





Figure 1.1 Bam historical masonry castle before and after 2003 Bam earthquake (Iran) [12]

1.4 Vulnerability Resources of URM Buildings

Among the mentioned failure patterns, it has been proved that the failure of load bearing walls is mostly responsible for damages and collapse of URM structures [11]. Unreinforced load bearing masonry walls are the major load resisting system of URM structures and damages induced in these walls play the key role in the damage or total collapse of URM structures. The typical failure modes of URM walls are shown in Figure 1.2.

Two major failure modes of URM walls are in-plane and out-of-plane modes ^[14]. Considering the tridimensional nature of earthquake waves, actual failure mode of URM walls are a combination of these modes.

In order to understand the causes and progress mechanism of these failure modes, plenty of experimental and analytical efforts have been done by researchers around world.

In-plane damages of URM wall due to the inertia forces parallel to the wall plane proved to be an important reason for the shear strength degradation of URM structures ^[15]. Due to this fact, in-plan retrofitting of URM walls must be considered as an important part of a strengthening plan.

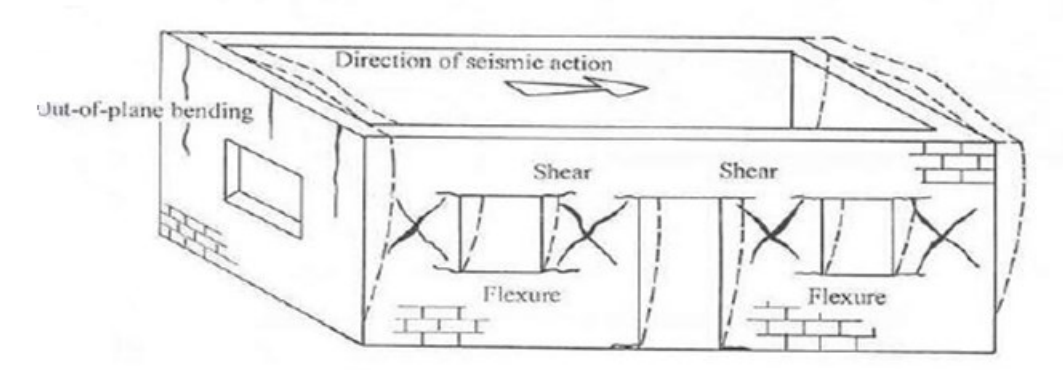


Figure 1.2 Typical failure mechanisms of URM structures [13]

1.5 Research Objective

As it was mentioned before, URM walls should be strengthened against earthquake loads. Among the failure modes of these walls, few research programs have been contributed to the in-plane behavior of the retrofitted masonry. Moreover, the majority of these research works have been concentrated on the effectiveness study of the retrofitting methods and the study about the mechanism of rehabilitation has been omitted in most of them.

In recent years, composite industry has opened new doors for retrofitting of URM introducing high performance composite materials such as fiber reinforced polymers (FRP) and engineered cementitious composites (ECC). These relatively new developed materials exhibit high strength, ductility and durability.

As an experimental and analytical study, this thesis aims towards study of the in-plane behavior of the URM wall retrofitted with ECC composites and aramid fiber reinforced polymers (AFRP). Developing appropriate analytical models for prediction of the structural response of retrofitted URM walls against in-plane loads was another goal of this study.

Application of ECC for retrofit purpose is in the efficiency study stage and very few information is available about the behavior of the ECC retrofitted masonry walls.

In case of AFRP and FRP retrofitting in general, there are few studies about the in-plane response of the retrofitted wall compare to the out-of-plane research works. Debonding is a characteristic behavior of FRP products which eliminates their retrofit efficiency. In this

research work, in order to avoid this undesirable effect, confining band system was applied. The performance of AFRP retrofitting using this system was evaluated and discussed.

1.6 Thesis Organization

This dissertation was organized in seven chapters based on the steps followed during the research period.

A general overview on masonry buildings, types of construction and its seismic response were introduced in Chapter 1.

Chapter 2 deals with the structural behavior of unreinforced masonry wall. In particular, in-plane mechanical characteristic and failure modes of URM walls were investigated based on previous experimental studies and earthquake experiences.

The retrofit policies and available conventional rehabilitation techniques for unreinforced masonry were introduced in Chapter 3. Based on the structural effectiveness and other remarkable parameters of these retrofitting techniques, performance of them was compared to each other and evaluated.

The modeling strategies of URM wall were discussed in Chapter 4. The numerical analysis conducted in the current study was based on the introduced strategies in this chapter.

The conducted experimental program and obtained results were explained in Chapter 5. These tests were carried out on the ECC and AFRP retrofitted masonry wall specimens. The performance of each method was evaluated and discussed.

Chapter 6 deals with analytical and numerical studies on the retrofitted masonry with ECC and AFRP. The results obtained from these analytical studies were validated by the corresponding experimental data.

The summary, major finding and conclusion remarks of this research were described in Chapter 7. Also, recommendations for future studies were mentioned.

References

- [1] D'Ayala, D. Unreinforced brick masonry construction. Major construction types, unreinforced masonry introduction, World Housing Encyclopedia.
- [2] Matthys, H., Noland, L. (1989). Proceedings of an international seminar on evaluation, strengthening and retrofitting masonry buildings, TMS, Colorado, USA.
- [3] Abrams, D.P. (2001). Performance-based engineering concepts for unreinforced masonry building structures, Progress in Structural Engineering and Materials. Vol. 3, issue 1, pp. 48-56.
- [4] Page, A.W. (1995). Unreinforced masonry structures- An Australian overview. Pacific conference on earthquake engineering, PCEE 95, Melbourne.
- [5] Lourenco, P.B., Milani, G., Tralli, A. and Zucchini, A. (2007). Analysis of masonry structures: review of and recent trends in homogenization techniques. Can. J. Civ. Eng. 34, pp.1443-1457.
- [6] Mosalam, K., Glascoe, L., Bernier, J. (2009). Mechanical properties of unreinforced brick masonry, Section1. Lawrence Livermore National Laboratory, report LLNL-TR-417646.
- [7] Mostafaei, H., Toshimi, K. (2004). Investigation and analysis of damage to buildings during the 2003 Bam earthquake. Bull, Earth, Res, Inst, Univ. Tokyo, Vol.79, pp. 107-132.
- [8] Shibaya, A., Ghayamghamian, M., Hisada, Y. (2004). Building damage and seismic intensity in Bam city from the 2003 Bam, Iran, earthquake. Bull, Earth, Res, Inst, Univ. Tokyo, Vol. 79, pp. 81-93.
- [9] Kusky, T.M. (2003). Geological hazards a sourcebook. ISBN: 1-57356-469-9.
- [10] Zamani Ahari, G., Yamaguchi, K. (2010). A Proposal of the most suitable retrofitting methods for URM Structures in Iran- An extensive review of recent techniques-. Journal of Habitat Engineering, Vol. 2, Number 2, pp.105-114.
- [11] Maffei, J., Bazzurro, P., Marrow, J., Goretti, A. (2006). Recent Italian Earthquakes: Examination of Structural Vulnerability, Damage, and Post-Earthquake Practices. Earthquake Engineering Research Institute, ISBN: 1-932884-12-2.

- [12] Manafpour, A. R. (2008). BAM EARTHQUAKE, IRAN: LESSONS ON THE SEISMIC BEHAVIOUR OF BUILDING STRUCTURES. The 14th World Conference on Earthquake Engineering, China.
- [13] Arya A.S. (2007). Seismic Assessment of Masonry Buildings. Earthquake Disaster Reduction Masonry Building Design and Construction, New Delhi, India.
- [14] ElGawady, M.A., Lestuzzi, P. and Badoux, M. (2006). Retrofitting of masonry walls using shotcrete. NZSEE conference, paper No. 45.
- [15] Calvi, G.M., Kingsley, G.R., Magenes, G. (1996). Testing of unreinforced masonry structures for seismic assessment. Earthquake Spectra, Vol.12, No.1, pp.145-162.

Chapter 2

STRUCTURAL BEHAVIOR OF UNREINFORCED MASONRY WALLS

3.1 Mechanical Characteristics of URM Walls

Masonry is a composite anisotropic material and its mechanical behavior is highly dependent on the properties of constitutes. As a simple description, masonry consists of bricks joined together by bed joint mortar. The bricks and mortar have their own specific properties that make a non-homogeneous assemblage when combined together in the URM wall construction.

The non-homogeneous behavior of URM is also a cause of its construction method in which each piece is joined to another and consequently there is no way to ensure that every brick is placed in exactly the same way as the rest of the bricks. Also, the brick and mortar have varying properties in the different parts of the structure. Moreover, cracking generated during the loading adds more complexity to the overall behavior of URM and known as the main reason for the non-linear behavior of the wall. The main behavioral characteristics of URM can be summarized as the following facts [1]:

- 1) Mechanical behavior is non-homogeneous.
- 2) URM does not show an isotropic behavior.
- 3) Tensile strength is very low and in most of the cases it is close to zero.
- 4) Compressive response is brittle type without any yield point.
- 5) Stress-strain relation is neither linear nor elastic.

This level of complication makes it as an essential to use some simplifying assumptions for analyzing and evaluation of URM structures and URM wall in particular. A popular assumption generally adopted is that masonry is isotropic and homogeneous. Moreover at small levels of stress, the behavior of URM can be assumed as linear-elastic.

In order to evaluate the performance of a URM wall and adopting an adequate retrofit strategy, the basic mechanical behavior of masonry should be properly understood. Principal mechanical characteristics of masonry – such as compressive, shear and tensile strength – and

also behavior of masonry under biaxial loading state are discussed in this chapter. Tension softening behavior of URM is described as the next part. Because of the reversal nature of seismic loads, cyclic response of URM is introduced as well. Failure criterion of URM under various loading regimes is discussed as the next. Then the in-plane behavior of URM wall is described.

The states of stress in masonry in general loading conditions are shown as a simple illustration in Figure 2.1 [1].

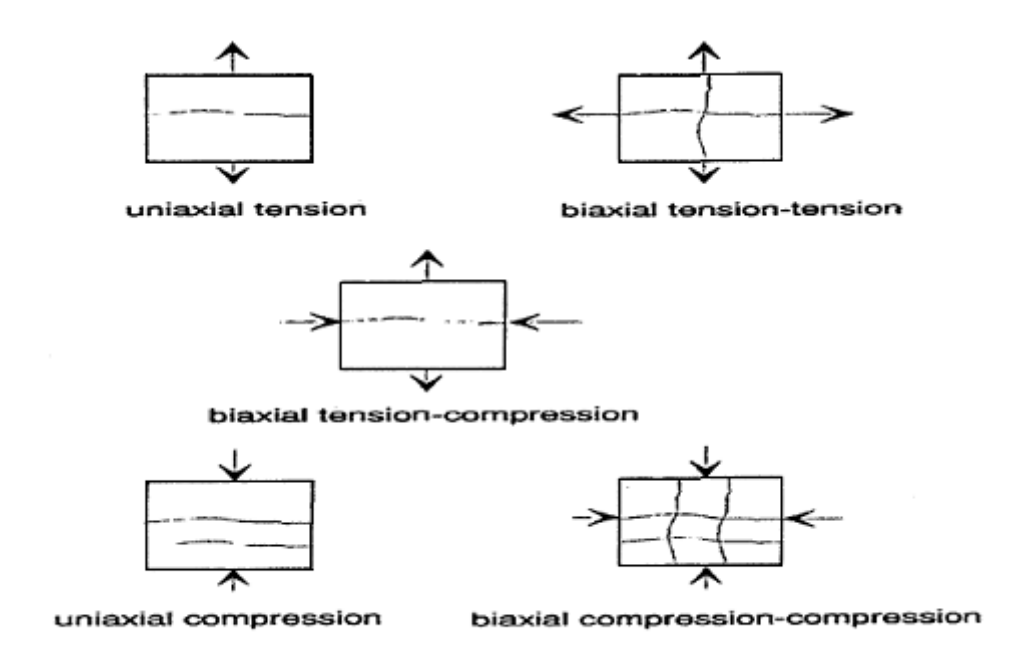


Figure 2.1 States of stress in masonry under various loading conditions [1]

3.1.1 Uniaxial Compressive Strength

The compressive strength of masonry in the direction normal to the bed joints is generally considered as the main design property of masonry. The common method for obtaining this property is uniaxial compression test on masonry prism specimens. The test configuration is shown in Figure 2.2(a) [2]. Although still there is not a common agreement on reliability of this method among researchers, it is the suggested method in several design codes [3].

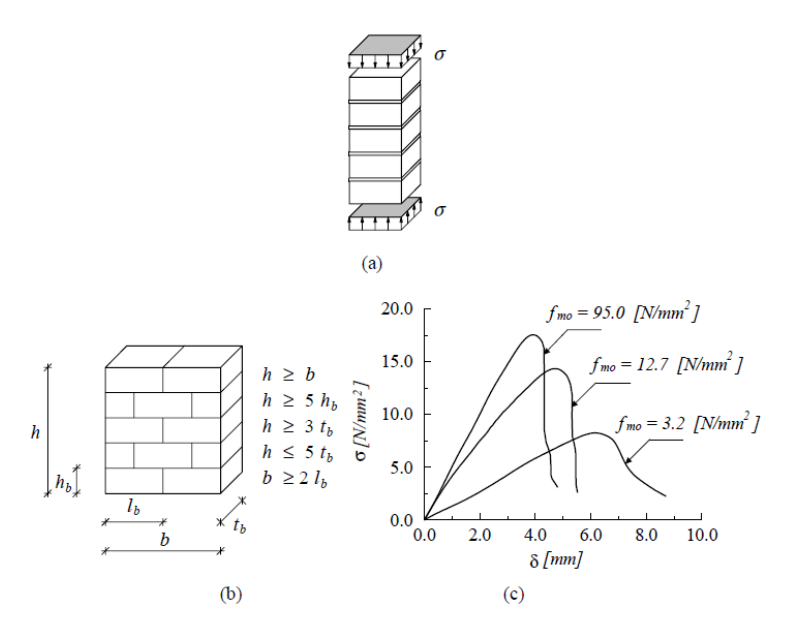


Figure 2.2 Uniaxial compressive behavior of masonry under loading normal to the bed joints [4]

- (a) Stacked bond prism (b) Schematic representation of RILEM test specimen
- (c) Experimental stress-displacement diagrams for prisms made of mortar with various compressive strength

Also as a common role it was accepted that the uniaxial compressive strength of masonry in the direction normal to the bed joints can be obtained from the RILEM test which is shown in Figure 2.2(b). Some stress-displacement diagrams for masonry prisms made by various mortars are shown in Figure 2.2 (c) [4].

The main trigger for failure of masonry prism in axial loading is the difference in elastic properties of the unit and mortar ^[5]. Two states of stress are generated in this loading type as triaxial compression in bed joint mortar and compression-biaxial tension in brick. As the process of the failure, two stages have been observed ^[3]:

- 1) Normal cracking of the brick in the direction of the specimen centerline
- 2) Widening of the cracks and splitting of the specimen

The maximum compressive strength of mortar is an important factor for the compressive strength of the whole specimen as it was shown for bricks with different compressive strength in Figure 2.2 (c).

As it was mentioned before, several parameters contribute to the compressive strength of brick masonry walls. Basically, the compressive strength of masonry is dependent on the mechanical properties of brick and mortar and their interaction which took place in their interface. Also considering the anisotropic behavior of masonry, the geometry feature such as the brick laying technique plays an important role. Therefore, a wide range of quantitative and qualitative factors contribute to the compressive behavior of the masonry wall.

Unlike the uniaxial compression test in the direction normal to bed joint mortar, the compressive behavior of masonry in the direction parallel to the bed joints still have not been studied properly. The ratio between the uniaxial compressive strength parallel and normal to the bed joints varies from 0.2 to 0.8 ^[6]. These ratios were obtained from tests on the masonry samples of solid and perforated clay units, calcium silicate units, lightweight concrete units and aerated concrete units.

In order to have a unified method to evaluate the compressive strength of masonry and using them in design process, some masonry codes introduced test methods which are mainly based on the specific specimen geometry and loading configuration. Also the acceptance criteria for existing masonry walls are based on these testing methods.

However, in the absence of such tests, some specific amounts for compressive strength of masonry were recommended by these codes as the minimum values that can be used as an initial design amounts.

As it was frequently reported in literature, there is two types of study on the determination of the compressive strength of masonry such as experimental (empirical) and analytical. Here, some of these models are described in brief as follows.

Empirical models have been obtained from different experimental research methods and composed of simple expressions, using two principal mechanical parameters of the masonry constitutes: the compressive strength of the mortar (f_m) and the one of the brick (f_b) .

The empirical models are simple to use and this fact has made them so popular and even they are indicated as design relations in various codes such as ENV 1996 ^[7], the ACI Standard 530 ^[8] and the British Standard BD 21 ^[9].

Some analytical models [10-14] have been proposed to determine the compressive strength of masonry structures. These models try to obtain the compressive strength of the brick and mortar combination from theoretical principles, starting from a series of mechanical hypotheses and applying equilibrium and compatibility equations. Although most of these models assume that the bond between bricks and mortar remains intact when either brick or mortar fails, it has been shown that this is not completely correct. The models are also highly complex, require a variety of parameters (geometry, brick and mortar compressive strengths, elasticity modulus and Poisson coefficient) and obtain expressions in which some of the factors are interrelated [15].

Compressive strength of URM is generally obtained from experiments on small-size prism specimens with height of at least 3 brick units. Specimens are tested under vertical increasing load in a uniform rate until the failure of the prism. Since the initial strains of prism specimens are not reliable, vertical displacements measured between two points of the prism in the height of the specimen were used to calculate the normal compressive strain.

Also in slender specimens, the effect of slenderness should be taken into account. In slender specimens, compressive strength obtained from test is generally lower than the actual value. So the amount obtained from test is increased by a factor. This factor is generally calculated with the following relation:

$$\alpha = \frac{t}{t - \delta} \tag{2.1}$$

where, t is the thickness of the specimen and δ is the value of displacement recorded by vertical displacement transducers at the point of the failure or maximum vertical load bearing capacity of the specimen. This factor is limited to 15%.

As an empirical relation, the compressive strength of a masonry prism can be calculated based on the compressive strength of brick (f_b) and mortar (f_m) which is recommended by ENV 1996 design code ^[7],

$$f_k = K f_b^{0.65} f_m^{0.25}$$
 (MPa)

The value of factor K for different compositions of brick and mortar varies between 0.4-0.6 and depends on the masonry group classification indicated in the code.

The compressive strength of masonry may vary from 5 MPa to 100 MPa and a minimum strength of 12.5 MPa is recommended by masonry design codes.

In standard ASTM C 67, a reduction factor is used for the calculation of compressive strength in masonry prisms with height-to-thickness ratios less than five. As the test observation, in low height prism specimens, failure started from a series of vertical tensile cracks and ultimate compressive load bearing capacity of the specimen achieved when the compressive stress in mortar exceed the allowable one ^[16].

D'Ayala [17] based on the compressive strength of brick and mortar, proposed the following relation for compressive strength of masonry,

$$\sigma_{cw} = 0.538\sigma_{cm} + 0.241\sigma_{cb} \tag{2.3}$$

in which, σ_{cw} , σ_{cm} and σ_{cb} are the compressive strength of masonry wall, mortar and unit brick, respectively.

Considering the height of brick and bed joint mortar, the above relation can be normalized and re-written as,

$$\frac{f_{cw}}{h_w} = 0.0216 \left[\frac{f_{cb}}{h_b} + \frac{f_{cm}}{h_m} \right] \tag{2.4}$$

where,

f_{cw} compressive strength of masonry wall

f_{cm} compressive strength of mortar

f_{cb} compressive strength of brick

h_w height of masonry wall

h_m height (thickness) of mortar

h_b height of brick

As another method, the following equation was introduced for calculation of the compressive strength of masonry [13],

$$\sigma_{cw} = \frac{f_{bt,fl}}{v_b + \frac{mv_m - v_b}{1 + mr}}$$
(2.5)

in which,

f_{bt,fl} flexural tensile strength of brick

v_b Poisson's ratio of brick

v_m Poisson's ratio of mortar

$$m = \frac{E_b}{E_m}$$

$$r = \frac{H_b}{H_m}$$

Also the following equation was proposed by Mehlmann [18] which uses the mean values of the compressive strength of brick and mortar,

$$\sigma_{cw} = 0.83 \sigma_{cb,m}^{0.66} \sigma_{cm,m}^{0.18} \tag{2.6}$$

where, $\sigma_{cb,m}$ and $\sigma_{cm,m}$ are the mean compressive strength of brick and mortar, respectively.

Powell and Hodgkinson [19] introduced typical stress-strain diagrams for different types of bricks as shown in Figure 2.3.

The modulus of elasticity (E_m) is always needed for evaluation and analysis of masonry structures. Currently the most common methods are based on the empirical relations.

In these methods the main attempt was on the determination of the modulus of elasticity based on empirical relations from the compressive strength of masonry. Some of them are introduced as follows [16]:

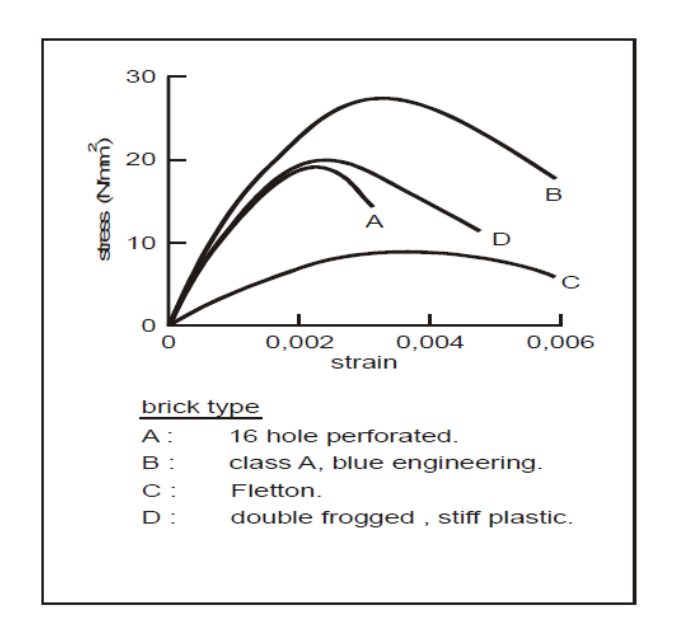


Figure 2.3 Typical stress-strain diagram of masonry for different types of brick [19]

$$E_m = 750 f'_m$$
 and 20.5 GPa as the maximum amount (MIA, 1998) (2.7)

$$E_m = 400 f_m' \sim 1000 f_m'$$
 (Sahlin, 1971) (2.8)

$$E_m = 2116\sqrt{f_m'}$$
 (Schubert, 1982) (2.9)

$$E_{m} = 1180 f_{m}^{\prime} = 0.83$$
 (Sinha and Pedreschi, 1983) (2.10)

$$E_m = 1000 f_m'$$
 (Bull, 2001) (2.11)

As an attempt to find a relationship between the Young's modulus of masonry and the ones for brick and mortar, the following relation was introduced by Binda [13],

$$E = E_b \frac{1+r}{r + \frac{E_b}{E_m}}$$
(2.12)

r ratio of the height of the brick and mortar

E_b, E_m the modulus of elasticity of brick and mortar

2.1.2 Shear Strength

Shear strength of URM is highly dependent on its failure mode and based on the experimental observations, two type of failure mode as shear failures could be happen as follows,

- Failure in brick-mortar interface or mortar in itself (sliding)
- Splitting failure

It must be mentioned that splitting failure may consist of direct or zigzag shaped sliding as well.

1) Sliding failure

There are different methods for determination of sliding shear strength of masonry. Two famous techniques which are widely used for this purpose are direct shear and triplet tests. The various methods in this regard are shown as schematic illustrations in Figure 2.4 [20].

In these methods the classic Coulomb equation is used as follows,

$$\tau = \tau_0 + \mu N \tag{2.13}$$

in which,

- τ shear strength of masonry
- τ_0 bond (initial) strength between brick and mortar
- μ friction coefficient of brick-mortar interface
- N initial normal compressive load

For different brick and mortar types, the value of μ varies between 0.3 and 1.04.

2) Splitting failure

As it was stated before, splitting failure mode of masonry is represented by progressive cracks passing the bed joints or bricks or both of them. In order to determine shear strength of the masonry in case of the occurrence of this failure mode, the most common test method is

diagonal compression (or tension in some documents) test which is recommended by some masonry design codes such as ASTM E519 as shown in Figure 2.4 (h).

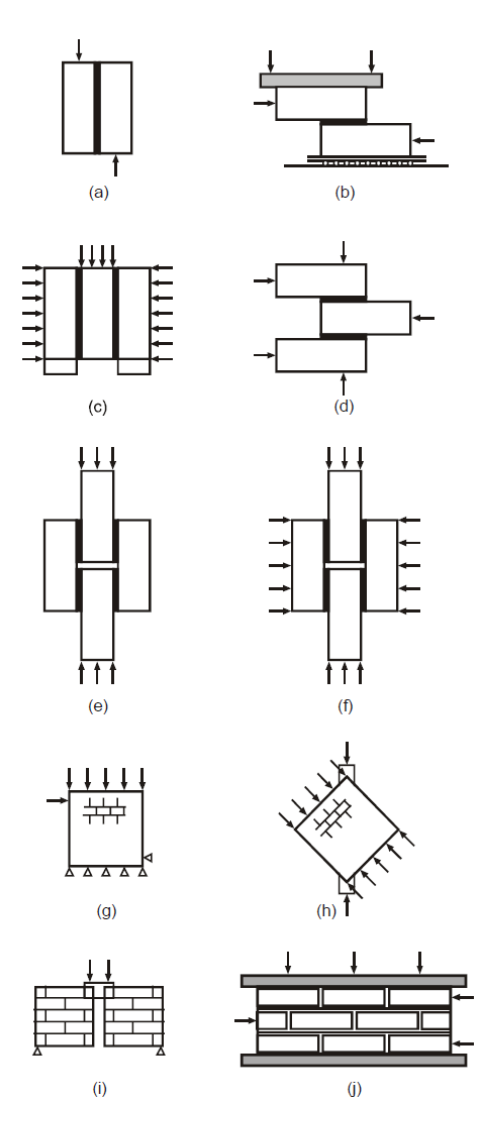


Figure 2.4 Common shear test methods of masonry [20]

Masonry specimens used for the ASTM test methods holds an aspect ratio equal to one. They were placed between two loading shoes in a diagonal way. Displacement meters such as LVDT transducers are utilized in horizontal and vertical directions to record the

displacements of the specimen in these two directions. According to Mohr circle, stress situation in this method leads to pure shear as a point. About the Poisson's ratio of masonry the common assumption is about 0.25 which leads to a shear modulus equal to 0.4E. This value for shear modulus is recommended by ENV code as well.

2.1.3 Tensile Strength

The tension strength of masonry compared to its compression strength is very small and even in some cases it is close to zero.

The failure pattern in tension depends on the direction of the loading whether is perpendicular or parallel to the direction of bed joint mortar as shown in Figure 2.5. The shear strength of brick and mortar and also the tensile strength of brick govern this type of failure [21].

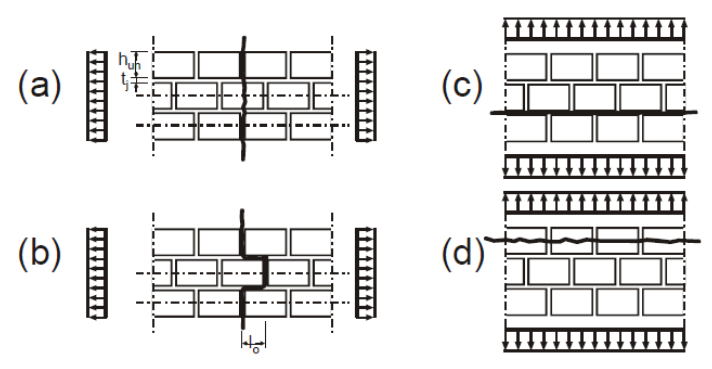


Figure 2.5 Failure of masonry under tensile stress [21]

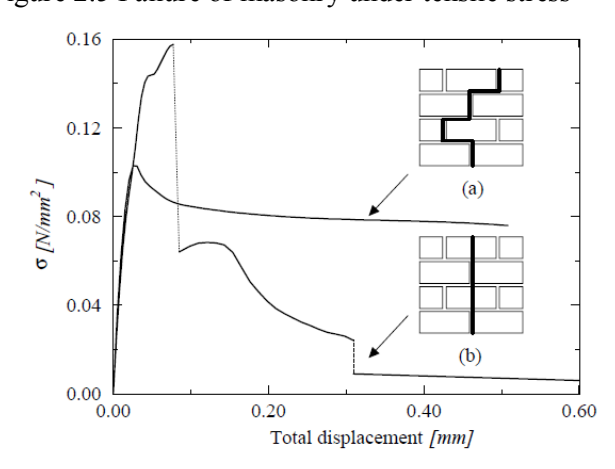


Figure 2.6 Stess-strain diagram of masonry under tensile load parallel to bed joint mortar [22]

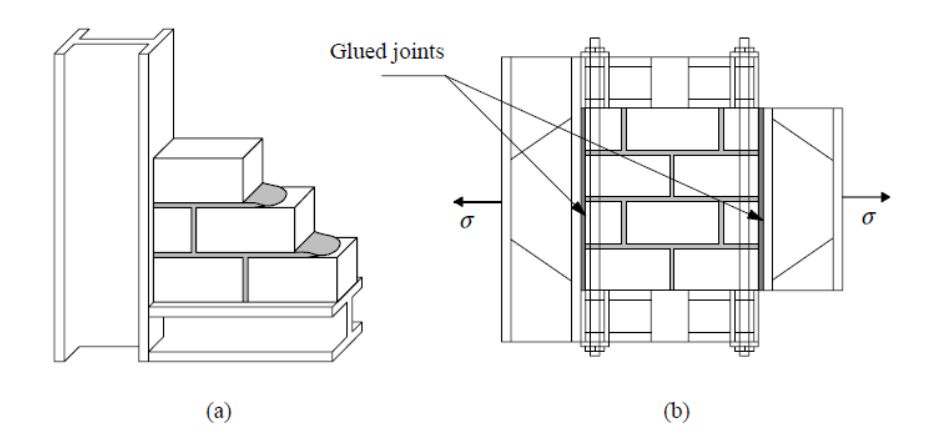


Figure 2.7 Test setup for tensile strength of masonry parallel to the bed joints ^[22], (a) construction of test specimen; (b) test specimen before 90° rotation and testing

The stress-strain relation diagram and the related test configuration are shown in Figures 2.6 and 2.7, respectively.

The tensile behavior of masonry in two direction, normal and parallel to bed joint mortar are discussed as follows,

a) Tension normal to the bed joint mortar direction

In this loading direction there are two possible failure modes, cracking in bed joint mortar or masonry unit bricks. Therefore, the strength values are the tensile strength of brick in the direction of its height or the normal bond strength between the unit and the bed joint mortar.

The masonry tension strength can be calculated as the minimum value obtained from the following relations [21]

$$f_{t,ma} = f_{th,b}$$

$$f_{t,ma} = f_{ta}$$
(2.14)

b) Tension parallel to the bed joint mortar direction

In this loading direction there are two possible failure modes, shear cracking in bed joint mortar or tensile cracking in masonry unit bricks as shown in Figure 2.5. Hence, shear bond

strength between brick and mortar or the tensile strength of the mortar and masonry unit brick in the direction of its length governs the failure pattern. The possible failure cases are discussed as follows.

a) Case 1: Tensile cracking in bed joint mortar and brick

This case happens when there is high unit/mortar shear strength and the masonry units are of poor quality and/or there is a high compressive strength normal to the bed joint.

The following relation can be used to calculate the tensile strength of the masonry in this case,

$$f_{t,ma} \cdot (h_{un} + t_{j}) = f_{t,un} \cdot h_{un} / 2$$

$$f_{t,ma} = 0.5 \cdot f_{t,un} \cdot \frac{1}{1 + t_{j/h_{un}}}$$
(2.15)

b) Case 2: Tensile and shear cracking in bed joint mortar

When there is a high unit tensile strength and the mortar tensile strength or shear bond strength between brick and mortar is small and/or the compressive strength normal to the bed joints is small, this mode of failure may happen. In this case the tensile strength of masonry can be calculated by the following relation,

$$f_{t,ma} \cdot (h_{un} + t_j) = f_{sh} \cdot l_0$$

$$f_{t,ma} = (f_{sh0} + \mu \cdot \sigma_n) \frac{l_0}{1 + t_j / h_{un}}$$
(2.16)

where,

f_{t,ma} tensile strength of brick in longitudinal direction

t_i height of the mortar

h_{un} height of brick

f_{sh0} bond strength between brick and mortar

l₀ overlap length

μ friction coefficient

σ_n compressive loading perpendicular to bed joint mortar

The shear bond strength between unit and bed mortar is generally ranging between 0.5 and $1.0 \text{ N}/\text{mm}^2$ [21].

2.1.4 Masonry under Biaxial Stress State

The behavior of masonry under biaxial states of stress cannot be completely obtained from the constitutive behavior under uniaxial loading conditions such as compressive, shear and tensile behaviors. Some research works have been conducted on the masonry under biaxial stress condition in order to catch a strength envelope [23,24]. However as it was reported, due to anisotropic characteristics of masonry, the biaxial behavior of masonry cannot be stated based on the principal stresses. The above mentioned envelope based on the principal stresses and rotation angle was proposed by Page [23,24] through a series of experiments conducted on the specimens constructed with half-scale brick.

Both the orientation of the principal stresses with regard to the material axes and the principal stress ratio considerably influence the failure mode and strength ^[25].

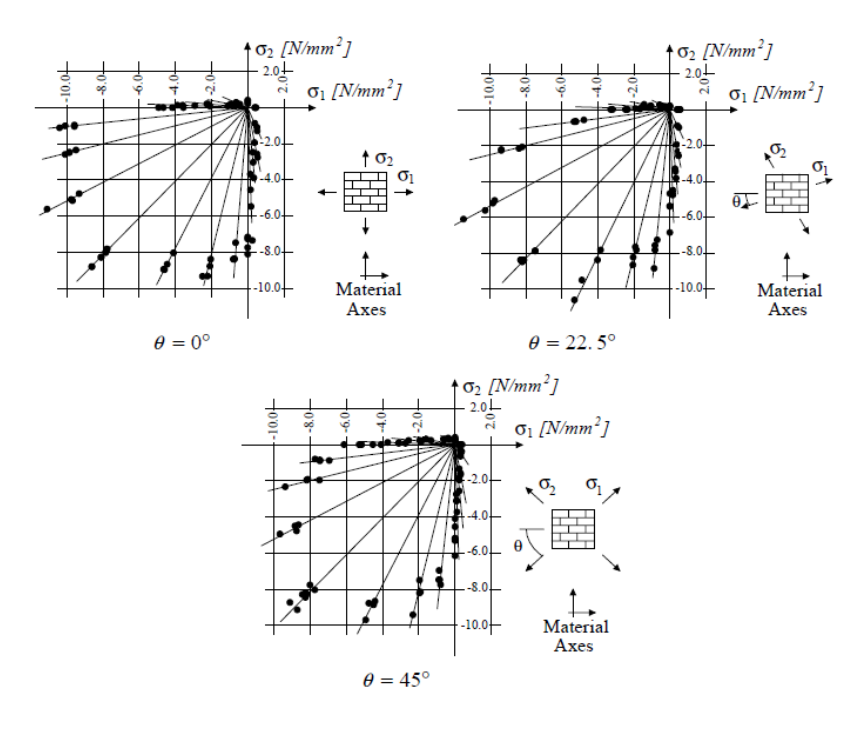


Figure 2.8 Biaxial stress envelopes for masonry in three orientation degrees [23,24]

However, it was stated that the validity of the envelopes shown in Figure 2.8 are limited for a certain type of masonry and specimen geometry. Therefore, different strength envelopes might be found for other type of brick and mortar or specimen shape.

Similar studies have been done on the hollow clay, calcium-silicate and concrete bricks in other research works [26,27,28].

3.2 Tension Softening

Softening is a gradual decrease of mechanical resistance under a continuous increase of deformation applied to a material or structure. This behavior plays a key role in quasi-brittle and brittle materials such as brick and mortar. Quasi-brittle materials fail due to a progressive internal cracking. The reason for this behavior can be explained by non-homogeneity of material, anisotropic behavior and material defects. There are two type of cracks may be generated in these materials as micro and macro cracks. Micro cracks may exist before any loading. Such cracks exist in mortar and brick because of shrinkage during the hardening and burning process, respectively. Micro cracks have insignificant effect on the mechanical behavior of the material until they start to grow and join together which lead to the generation of the macro cracks. Unlike micro cracks, macro cracking occurs generally after increasing the strain due to loading. Growth of macro cracks results in a decrease in material resistance and even after unloading this process is irreversible. This kind of behavior has been studied for three principal mechanical characteristics of brittle materials such as compressive, shear and tensile as reported in literature [29,30].

Some typical stress-strain models for the post-peak tensile behavior of materials are shown in Figure 2.9 [31]. Among them, models (c) and (d) can provide a reliable description for tension softening behavior of URM [2].

2.3 URM under Cyclic Loading

Because of the cyclic nature of the seismic loads, in order to grasp a complete structural model, behavior of URM under cyclic loading should be considered in the evaluation and retrofit process.

The typical material behaviors under cyclic loading are shown in Figure 2.10 [25]. There

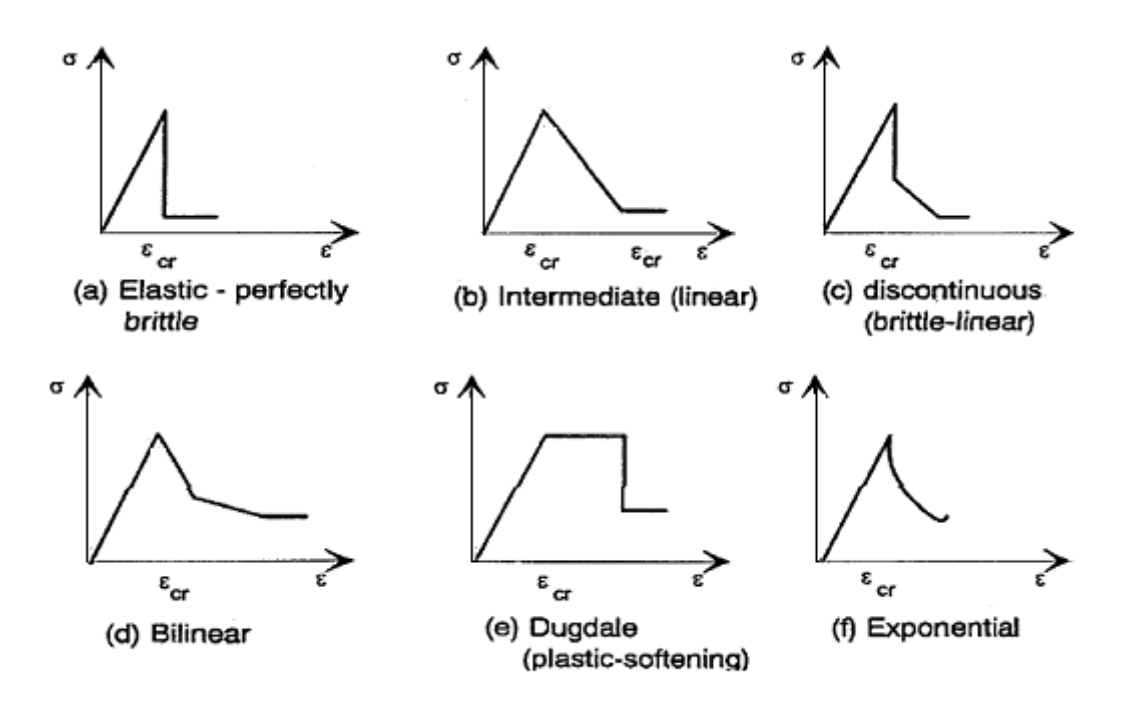


Figure 2.9 Typical tensile stress-strain models of materials [31]

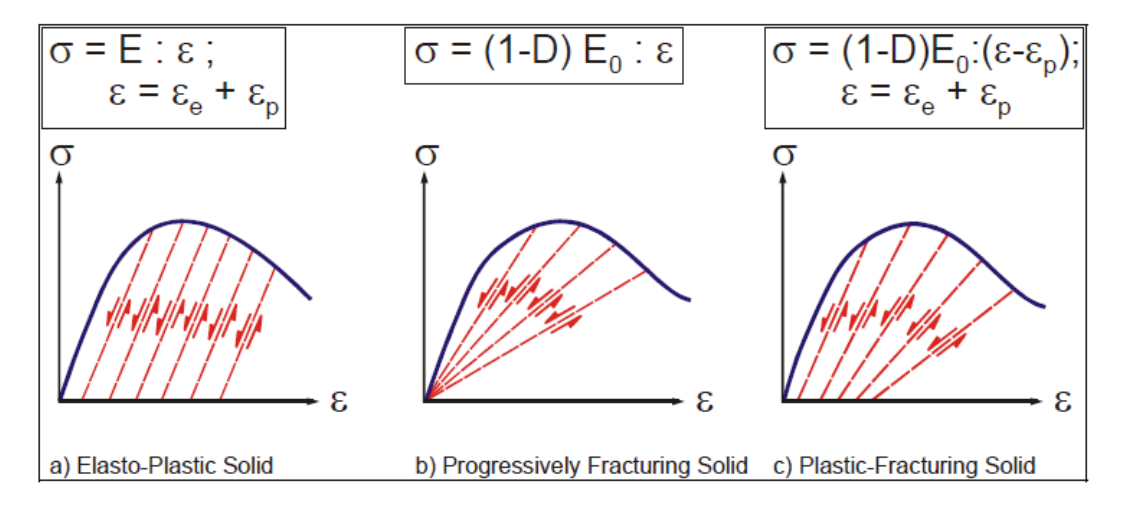


Figure 2.10 Typical behavior of different type of materials under cyclic loading [25]

are three types of behavior such as elasto-plastic, progressive fracture and plastic fracture.

a) Elasto-palstic

Elasto-plastic materials exhibit plastic strain during unloading and the straight unloadreload path lines are parallel to the initial tangent line of the material (shown in Figure 2.10(a)). It means that the plastic deformation does not change the stiffness. Also the plastic deformation is the main reason for non-linear behavior of the material. Theory of plasticity describes the behavior of materials of this type.

b) Progressively fracturing

The behavior of these materials is shown in Figure 2.10(b). During the unloading material returns to zero state of stress and no plastic deformation generate. However the stiffness of material degrades with increase in strain and this stiffness degradation is responsible for the non-linear behavior of material. The theory of continuum damage can explain the behavior of materials in this type.

c) Plastic fracturing

This behavior is shown in Figure 2.10(c) and it is a combination of the above mentioned two behaviors. This behavior can be studied by the damage theory combined with the plasticity theory.

URM exhibits a considerable stiffness degradation and also decrease in compressive strength (softening). In the other words, the progressively fracturing behavior can be a fine representative for URM structural behavior and damage mechanics can explain the behavior of URM and its failure mechanism.

As shown in Figure 2.10(b) and 2.10(c), the damage coefficient (D) acts as a multiplier to the tangential modulus of elasticity (E_0) in stress-strain relation.

2.4 Failure Criterion of Unreinforced Masonry

As it was stated before, masonry is a non-homogenous material and it is not possible to predict the failure of masonry just by its principal mechanical characteristics. In the other hand, in order to retrofit the URM, the failure criteria of it should be understood.

URM exhibits a directional behavior in which the bed joint mortar act as the weakest plane and under biaxial stress state, this fact should be taken into account.

Failure occurs in bed joint mortar, brick-mortar interface and bricks. In different loading conditions, various combinations of failure pattern may be took place.

The failure modes of URM (constructed with clay bricks) subjected to various in-plane loading conditions are shown in Figure 2.11. Different combinations of loading in some inclination degrees were applied to URM. The cracking pattern in case of uniaxial tensile, tension-compression and uniaxial compression loading cases for each loading direction has been investigated. In case of biaxial compression loading, failure took place as splitting in bricks at the middle of its thickness and in a direction normal to bed joints. However, still there is not enough knowledge about the failure pattern under tension-tension biaxial combination.

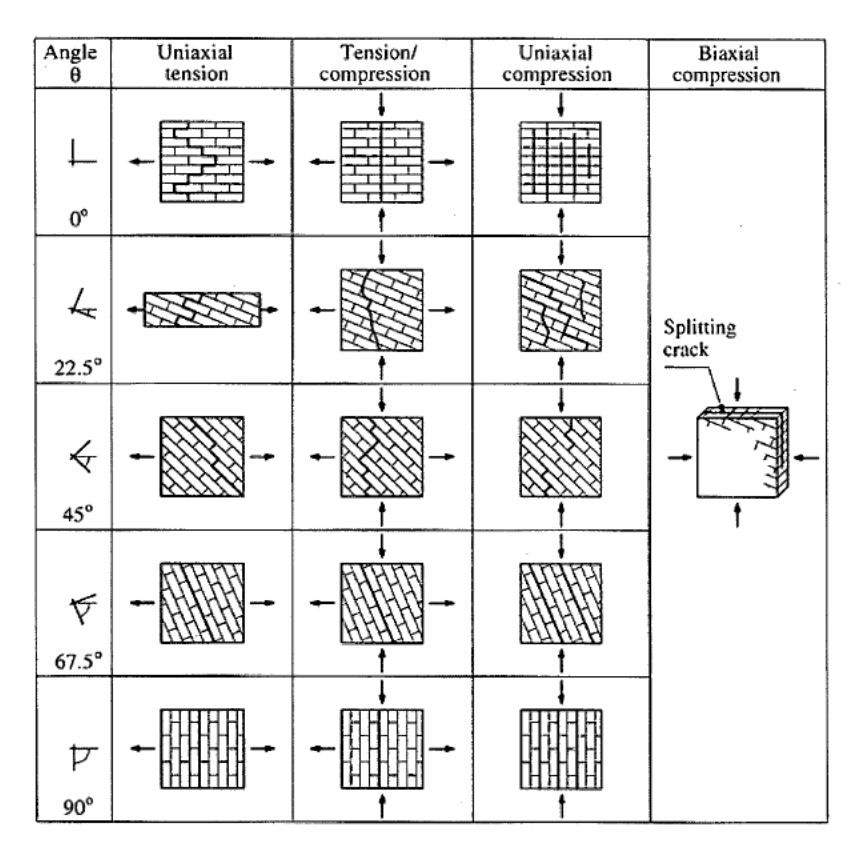


Figure 2.11 Modes of failure of URM under biaxial loading [32]

Generation of friction between brick and mortar in case of biaxial compression loading leads to a high compressive strength.

The typical biaxial failure surface of URM is shown in Figure 2.12. As it can be seen from the failure surface, two failure regimes exist as crushing and tensile. In case of crushing, Von Mises criterion was used to describe this condition.

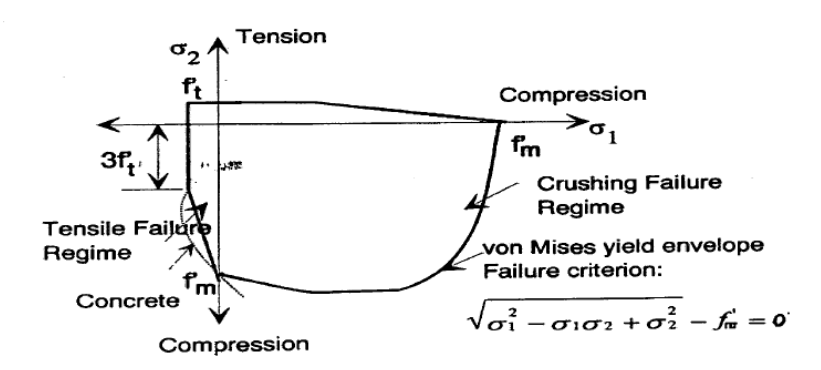


Figure 2.12 Typical failure surface of masonry [2]

However, it should be mentioned that the effect of bed joint mortar was not considered in this failure surface, so the reliability of it is questionable. In the other words, in-plane failure of URM cannot be described in terms of principal stresses only [2].

Zhuge [33], proposed a simple failure envelope for URM based on the biaxial and Coulomb shear failure models.

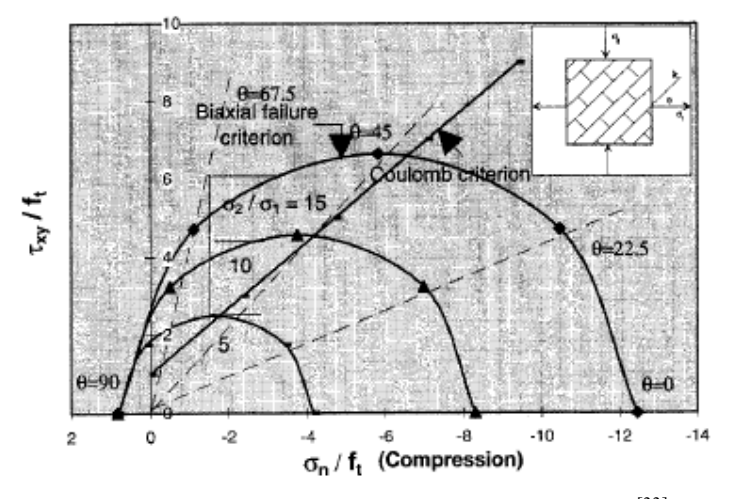


Figure 2.13 Simplified failure envelopes of URM [33]

The ubiquitous joint model combined with biaxial and Coulomb shear failure was presented in the model. The ubiquitous joint model is an anisotropic plasticity model which assumes a series of weak planes embedded in a Mohr-Coulomb solid. The model was first developed by Zienkiewicz and Pande for analyzing rock material with multiple planes of weakness. In this model, failure may occur either in the solid or along the slip (weak) plane, or both, depending on the material properties of the solid and weak plane, the stress state, and the angle of the weak planes [33].

As it can be seen from Figure 2.13, the model was proposed for three ratios of principal stresses (5,10 and 15) and four orientation degrees. Also a straight line representing the Coulomb failure criteria is included in the envelope.

As it was seen during the tests conducted by Page [34], in low ratios of the principal stresses and orientation degree between 45 and 90, shear failure is governing.

2.5 In-plane Behavior of URM Walls

As it was discussed in the first chapter the in-plane behavior of the masonry wall plays a key role in the seismic behavior of the URM structure during earthquakes. So the mechanism of this behavior and affecting parameters should be understood. As it was reported in several research works, the in-plane behavior of URM wall depends on numerous parameters such as the applied load combination, wall geometry and properties of the constituent materials and also the nature of loading (monotonic or cyclic) [33].

Regions with high possibility of failure occurrence are shown in Figure 2.14 [35]. However in case of low compressive pre-loading, URM wall tend to rock and in this case the whole rotate on the edge of the wall.

As it was indicated in research reports and also some masonry design codes, there are two major failure modes under in-plane loading as,

- 1) Shear failure
- 2) Flexural failure

In case of shear failure, two failure patterns may occur:

a) Shear sliding

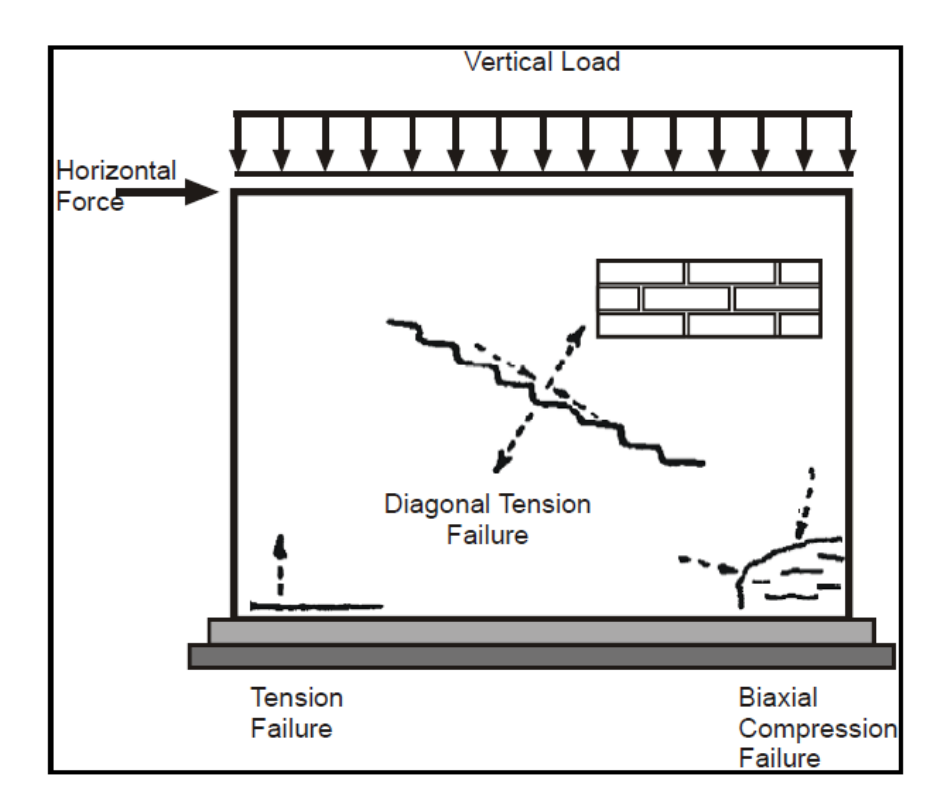


Figure 2.14 In-plane failure patterns of URM wall [35]

b) Diagonal shear

As the flexural failure, there are three possible failure patterns:

- c) Rocking
- d) Toe crushing
- e) Flexural cracking at the heel

The above mentioned failure modes and patterns of URM under in-plane loading are shown in Figure $2.15\,^{[36]}$.

The mechanism of these failure modes and the process of their progression are discussed in this part. The objective of study on the failure modes is to evaluate the behavior of masonry wall during the failure and prioritizing of them in order to adopt an adequate retrofit strategy.

When the aspect ratio of URM wall (ratio of wall's height to length) is small (short wall),

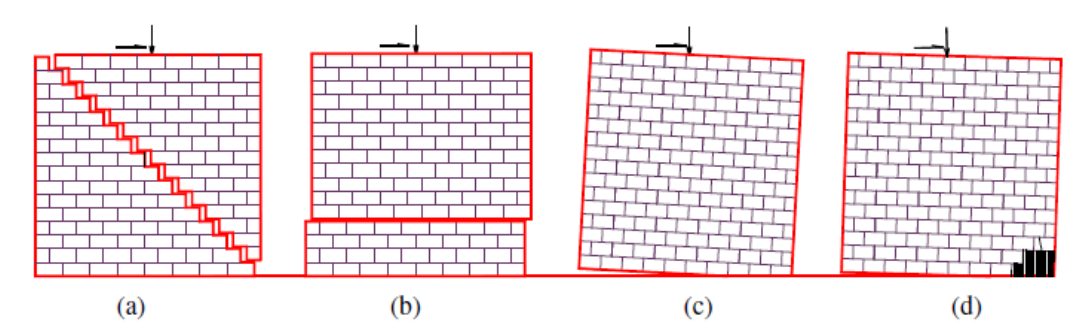


Figure 2.15 In-plane failure modes of a laterally loaded URM wall ^[36]: a) shear failure, b) sliding failure, c) rocking failure, and d) toe crushing

shear failure occurs which is a brittle type failure. Also in case of low vertical pressure and low strength mortar, cracks form in the head and bed joints and may lead to rocking or stepwise cracking. In case of rocking failure, when the compressive stresses in toe part of the wall exceed the allowable one, toe crushing occurs.

In case of cyclic loading, failure mode of URM wall is mainly dependent on the amount of the vertical load and tensile strength of bricks.

As cyclic response under low vertical loads, the wall shows large deformations with constant strength as shown in Figure 2.16 [37]. The opening of the cracks generally occur in bed joint mortars after several runs of cyclic loading and compressive crushing in wall corners lead to the wall failure. This type of failure can dissipate relatively high energy and can be considered as a ductile failure.

However in case of high vertical load and bricks with small tensile strength, the cracks are formed in both of the joint mortar and bricks. The failure of wall occurs suddenly with high stiffness degrading which dissipate small amount of energy as shown in Figure 2.17 [37]. This type of failure is brittle.

Failure states in different parts of a URM wall is summarized in Figure 2.18 ^[25]. As it can be seen from this figure, in center part of the wall, mixed regime of failures may happen which depends on the amount of vertical load and aspect ratio of the wall.

In case of wall with opening, these failure states are shown in Figure 2.19 [25].

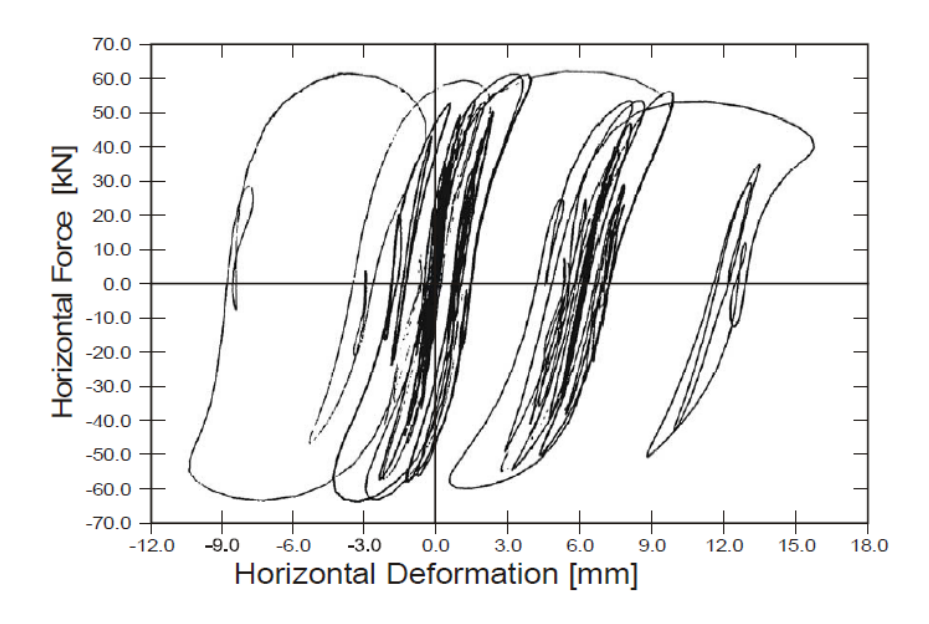


Figure 2.16 Horizontal force versus horizontal deformation in case of mortar failure [37]

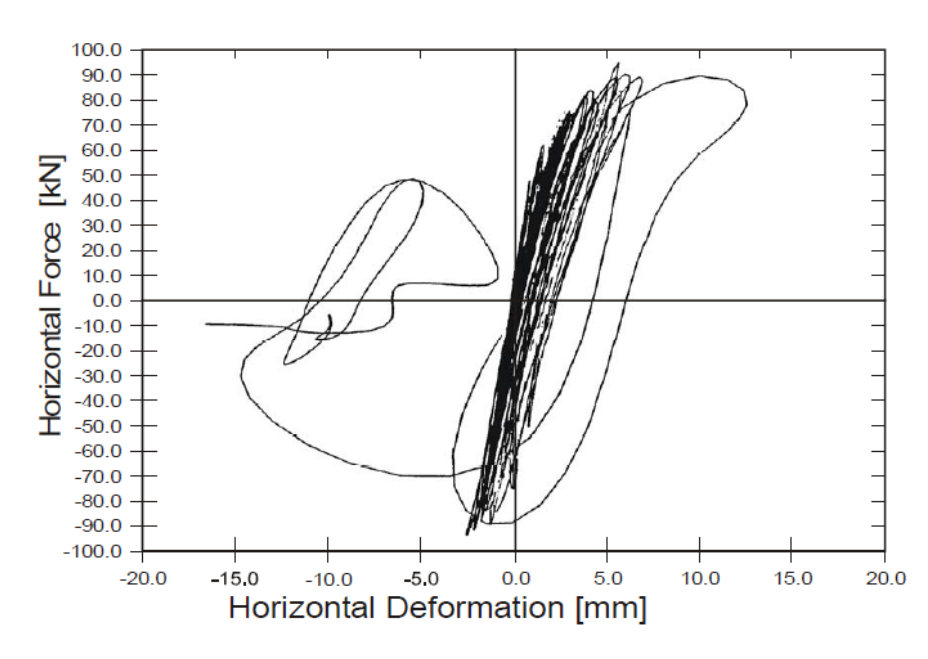


Figure 2.17 Horizontal force versus horizontal deformation in case of mortar-brick failure [37]

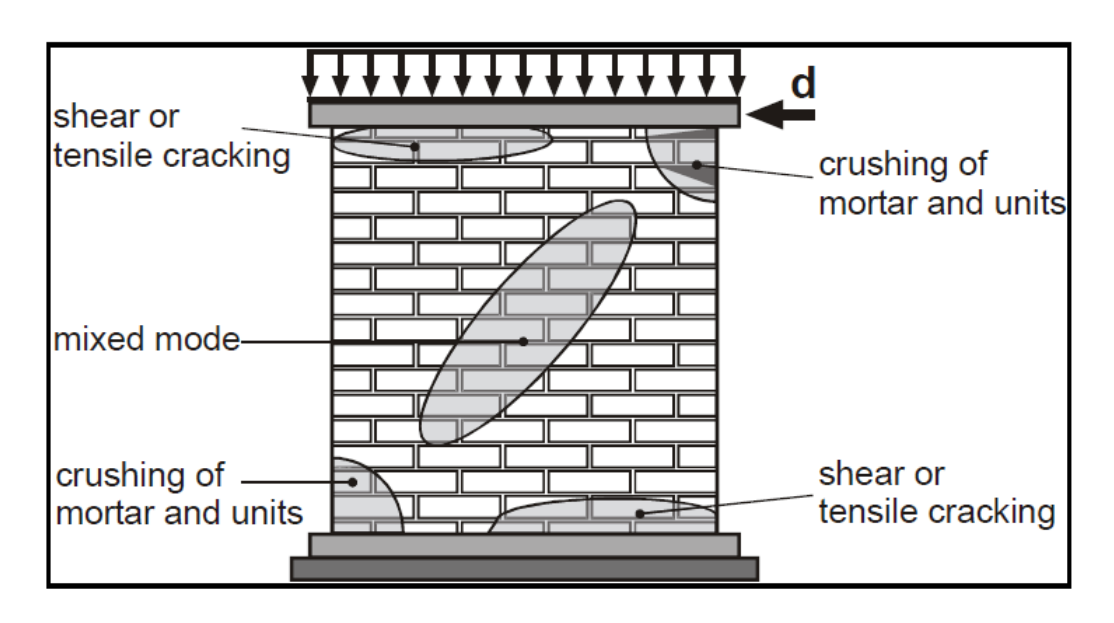


Figure 2.18 Local failure patterns of URM wall $^{[25]}$

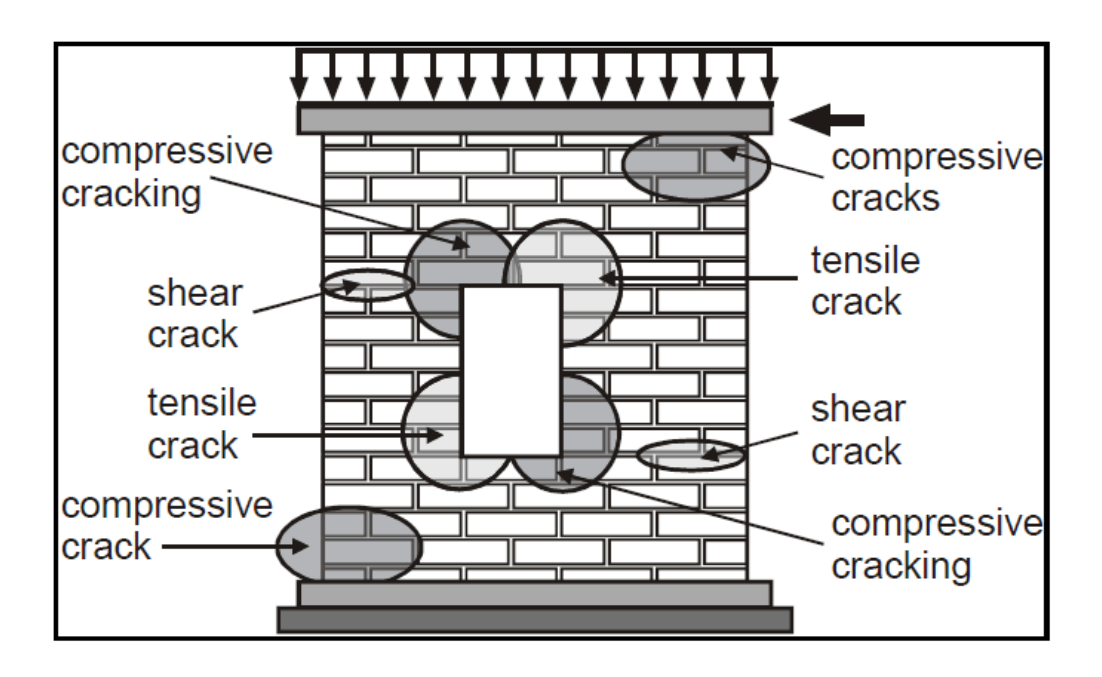


Figure 2.19 Local failure patterns URM wall with opening [25]

The amount and direction of the principal tensile stress is influenced primarily by the ratio of vertical load to the horizontal rocking load and high amounts of vertical load lead to a considerably high shear strength of the wall.

It must be mentioned that during the seismic loading, due to stiffness degradation, some or all of the above mentioned failure modes at various parts of the wall may occur.

In order to evaluate the possible failure modes of URM wall, some seismic evaluation methods have been suggested by design codes which are mainly in a performance-based basis. Since the retrofit design process starts necessarily from seismic evaluation and determining the structural requirements for desired performance, evaluation process of the Federal Emergency Management Agency (FEMA) will be briefly presented as follows.

In "Pre-standard and Commentary for the Seismic Rehabilitation of Buildings," FEMA 356 (2000) [38], acceptance criteria of URM walls for different performance levels is based on the lateral force-deformation relationship of the wall as shown in Figure 2.20. The same approach has been followed by ASCE 41 (2006) standard [39].

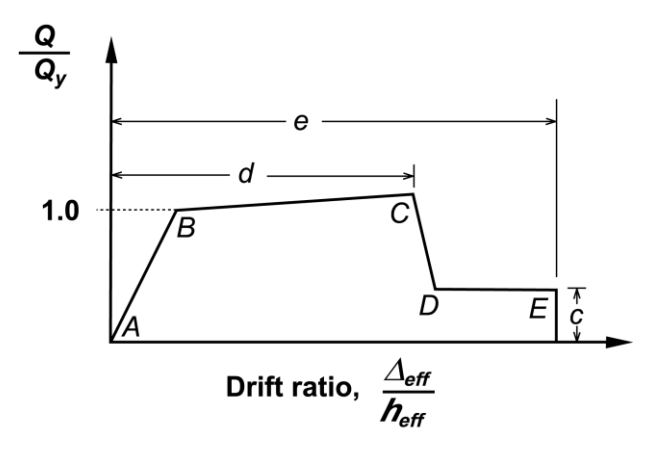


Figure 2.20 Generalized force-deformation relation for masonry elements [38]

Typical load and stress state in URM wall subjected to lateral loading is shown in Figure 2.21^[40].

As it can be seen from Figure 2.20, the lateral response of a URM wall prior to yielding is linear-elastic, and can be identified as the initial straight-line portion of the load-deflection

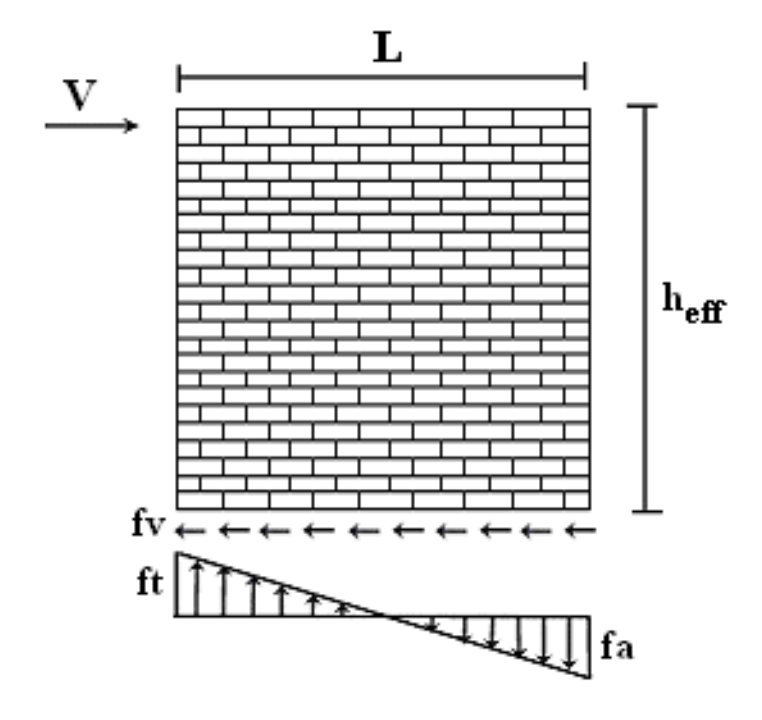


Figure 2.21 URM wall under horizontal lateral loading [40]

curve. At yield point due to failure mechanism, deflections are increased and strength is decreased. The elastic stiffness of URM wall is the slope of the load-deflection curve in the linear-elastic zone of the diagram. Two relations are used to determine the stiffness of the wall as relations (2.17) and (2.18) which are presented for cantilevered walls and the walls that have full restraint against rotation at the top and bottom, respectively.

$$k_{pier} = \frac{1}{\frac{h_{eff}^{3}}{3E_{m}I_{g}} + \frac{h_{eff}}{A_{v}G_{m}}}$$

$$(2.17)$$

$$k_{pier} = \frac{1}{\frac{h_{eff}^{3}}{12E_{m}I_{g}} + \frac{h_{eff}}{A_{v}G_{m}}}$$
(2.18)

where

h_{eff} wall height to the point of lateral load,

E_m elastic modulus of URM,

 A_v effective shear area (assumed to be 5/6 of the gross area),

I_g the moment of inertia of the uncracked wall cross section,

 G_m the shear modulus (assumed to be $0.4E_m$)

As it was mentioned before, the lateral strength of URM walls depends on the mode of failure. Four different possible types of in-plane failure modes were introduced by FEMA 356 as bed-joint sliding, rocking, diagonal tension, and toe crushing. The calculations method of wall strength for each mode is presented as follows.

When the shear stress in the base of the wall (f_v in Figure 2.21) reaches the shear strength, bed-joint sliding failure (Figure 2.15 (b)) occurs and a straight crack forms along the length of the bed joint leads to the wall sliding. The bed-joint sliding strength, V_{bjs} , is calculated by relation (2.19), where v_{me} is the expected bed-joint sliding shear strength and A_n is the net area of the mortared/grouted section. In the other words, V_{bjs} is the lateral load which results in sliding.

$$V_{bjs} = V_{me} A_n \tag{2.19}$$

The rocking failure mode (Figure 2.15(c)) occurs when a crack forms at the bottom of the wall and results in in-plane rocking.

The rocking strength of the wall, Vr, can be calculated by equation (2.20).

$$V_r = 0.9 \alpha P_E \left(\frac{L}{h_{eff}} \right)$$
 where, (2.20)

P_E expected axial compressive force

L length of the wall

h_{eff} effective height of the wall

 α 0.5 for a fixed-free cantilevered wall and for a fixed-fixed pier

Diagonal tension failure (Figure 2.15 (a)) occurs when diagonal (X) shape cracks form through the wall. If the cracks form in a step-wise manner, the strength of the wall can be calculated similar to the bed-joint sliding strength. But if these cracks pass through both bed joint mortar and brick, corresponding strength can be calculated by the following relation,

$$V_{dt} = f'_{dt} {}^{A}_{n} \left(\frac{L}{h_{eff}}\right) \sqrt{1 + \frac{f_{a}}{f'_{dt}}}$$
(2.21)

where f'_{dt} is the lower bound diagonal tension strength of URM and f_a is the lower bound axial compressive stress.

In case of excessive compressive stresses in the corners of the wall due to rocking, toe crushing failure mode occurs (Figure 2.15 (d)). Toe crushing strength can be calculated by the following relation,

$$V_{tc} = \alpha P_L \left(\frac{L}{h_{eff}} \right) \left(1 - \frac{f_a}{0.7f_m'} \right)$$
 (2.22)

where f_m is the lower bound compressive strength of URM. The L/h_{eff} ratio shall not be taken less than 0.67.

The above mentioned in-plane failure modes can be categorized as the deformation-controlled (ductile) and force-controlled (brittle) ones. They were shown for both FEMA 356 and ASCE41 codes in Table 2.1.

Table 2.1 Failure types of URM wall in FEMA 356 and ASCE 41

Failure Type	Deformation-controlled	Force-controlled
Bed-joint sliding	× (FEMA356)	× (ASCE41)
Rocking	× (FEMA356, ASCE41)	
Toe compression		× (FEMA356, ASCE41)
Diagonal cracking		× (FEMA356, ASCE41)

There is a difference on the bed joint sliding failure for two codes. In recent ASCE 41 code this failure mode is considered as force-controlled unlike FEMA 356.

The possible failure modes for different wall aspect ratios are as follows,

H/L>1 Flexural Failure (Ductile and high energy dissipation)

H/L≤1 Shear Failure (Brittle and low energy dissipation)

In which the flexural and shear failure can be described as,

1. Flexure failure: Rocking and Toe crushing

2. Shear failure: Sliding and Diagonal tension

However, as it was mentioned above, still there is not an agreement on the characteristics of sliding failure mode. The lowest energy dissipation and most brittle behavior are belonged to the shear mode and diagonal tension failure in particular.

The possible failure modes in different magnitudes of axial loading can be summarized as,

a) Under lower loads: Rocking and Sliding or combination of both

b) Under higher loads: Diagonal tension

References

36

- [1] Zhuge, Y. (1996). Nonlinear Dynamic Response of Unreinforced Masonry under In-Plane Lateral Loads. PhD Thesis, Queensland University of Technology.
- [2] Chuang, S.W. (2004). Seismic Retrofitting Techniques for Existing Unreinforced Masonry, PhD Thesis, University of South Australia.
- [3] Mann, W., Betzler, M. (1994). Investigations on the effect of different forms of test samples to test the compressive strength of masonry. In: Proc 10th Intl. Brick/Block Masonry Conf. Calgary, Canada, pp. 1305-1313.
- [4] Binda, L., Fontana, A. and Frigerio, G. (1995). Mechanical behavior of brick masonries derived from unit and mortar characteristics. Proc. Mt. Brick and Block Masonry Conf. J.W. de Courcy, Elsevier Applied Science, London, UK, pp. 378-402.
- [5] Hilsdorf, H.K. (1969) Investigation into Failure Mechanism of Brick Masonry Loaded in Axial Compression. Proc. of Int. Conf. on Masonry Structural Systems, Gulf Pub. Col., Houston, Texas, pp.34-41.
- [6] Hofmann, G., Schubert, P. (1994). Compressive strength of masonry parallel to the bed joints, Proc. 10th Int. Brick and Block Masonry Conf., Ed. N.G. Shrive and A. Huizer, Calgary, Alberta, pp.1453-1462.
- [7] ENV 1996-1-1. Eurocode No.6. (1998). Design of masonry structures, Part 1-1: general rules for buildings rules for reinforced and un-reinforced masonry.
- [8] ACI committee 530. (1999). Building code requirements for masonry structure. American Concrete Institute, Farmington Hills, MI.
- [9] Department of transport. (1993). The assessment of highway bridges and structures. British Standard BD 21/93, Her Majesty's Stationery Office, London.
- [10] Francis, A.J., Horman, C.B., Jerrems, L.E. (1971). The effect of joint thickness and other factors on the compressive strength of brickwork. In: West HWH, Speed KH, editors. Proc. of the 2nd int. brick masonry conf. Stoke-on-Trent, UK: British Ceramic Research Association, pp. 31-37.
- [11]Khoo, C.L., Hendry, A.W. (1973). A failure criterion for brickwork in axial compression. Proc. 3rd intl. brick masonry conference. pp.139-145.
- [12] Hilsdorf, H.K. (1969). Investigation into the failure mechanism of brick masonry loaded

- in axial compression. Designing, engineering and constructing with masonry products. Gulf Publishing Company. pp. 34-41.
- [13] Binda, L., Fontana, A., Frigerio, G. (1988). Mechanical behavior of brick masonries derived from unit and mortar characteristics. Proc. of the 8th international brick/block masonry conf, Dublin, pp. 205-216.
- [14] Atkinson, R.H., Noland, J.L., Abrams, D.P. (1982). A deformation theory for stack bonded masonry prisms in compression. Proc. of 7th intl. brick masonry conf., Melbourne University, Melbourne, pp. 565-576.
- [15] Roca, J.G., Marco, C.O., Adam, J.M. (2013). Compressive strength of masonry made of clay bricks and cement mortar: Estimation based on Neural Networks and Fuzzy Logic. Engineering Structures, Vol. 48, pp. 21-27.
- [16] Abdelkrim, B. (2009). Shear Capacity Prediction of Confined Masonry Walls Subjected to Cyclic Lateral Loading. PhD Thesis, Kanazawa University.
- [17] D'Ayala, D.F. (1997). Numerical Modeling of Masonry Structures Reinforced or Repaired. Proc. of Computer Methods in Structural Masonry-4, Italy, pp.161-168.
- [18] Mehlmann, M., Oppermann, B. (1994). The Role of Masonry and Rendering Mortar in Modern Masonry Construction. In: International Brick and Block Masonry Conference, Calgary, Canada, pp.139-149.
- [19] Powell, B., Hodgkinson, H.R. (1976). The Determination of Stress/Strain Relationship of Brickwork. Masonry Conference, Brugge.
- [20] Brain, H., Humerto, R. (1988). Shear behavior of mortar joints in Brickwork subjected to non-uniform compressive stress. Proc. of the 8th International Brick/Block Masonry Conference, Dublin.
- [21]Schubert, P. (1988). Compressive and Tensile Strength of Masonry. Proc.8th International Brick and Block Masonry Conference, Ireland, pp. 406-419.
- [22] Backes, H. P. (1985). On the behavior of masonry under tension in the direction of the bed joins. PhD Thesis, Aachen University of Technology.
- [23] Page, A.W. (1981). The biaxial Compression Strength of Brick Masonry. Proc. Instn. Civ. Engrs., Part 2, 71, pp. 893-906.

- [24]Page, A.W. (1983). The Strength of Brick Masonry under Biaxial Tension- Compression. The International Journal of Masonry Construction, 3, No. 1.
- [25] Mohamed, A.S.O. (2004).Behaviour of Retrofitted Masonry Shear Walls Subjected to Cyclic Loading. PhD Thesis, University of Karlsruhe.
- [26] Ganz, H.R. and Thurlimann, B. (1982). Tests on the Strength of Masonry Walls under Biaxial loads. Zurich, Swiss Federal Technical University, Institute for Structural Statics and Construction. Report Y/OLS-93/7.
- [27] Guggisberg, R., Thurlimann, B. (1987). Experimental determination of masonry strength parameters. Report No. 7502-5, Institute of Structural Engineering, ETH Zurich, Switzerland.
- [28] Lurati, F., Thurlimann, B. (1987). Test in concrete masonry walls. Report No. 8401-3, Institute of Structural Engineering, ETH Zurich, Zurich, Switzerland
- [29] Hordijk, D. A. (1991). Local Approach to Fatigue of Concrete. PhD Thesis, Delft University of Technology.
- [30] Van Mier, J.G.M. (1984). Strain-softening of concrete under multiaxial loading conditions, PhD Thesis, Eindhoven University of Technology, The Netherlands.
- [31] Borri, A., Sorace, S. (1993). FE analysis strategies for structural materials with small tensile strength. J. Press. Vessel Technol. 115, pp.156–163.
- [32] Dhanasekar, M. (1985). The performance of brick masonry subjected to in-plane loading. PhD Thesis, The University of Newcastle.
- [33] Zhuge, Y., Thambiratnam, D., Corderof, J. (1998). Nonlinear dynamic analysis of unreinforced masonry. Journal of Structural Engineering, Vol.124, No.3.
- [34] Page, A. (1982). An experimental investigation of the biaxial strength of brick masonry. Proc. of 6th Int. Brick/Block Masonry Conf, Associazionne Nazionale Degli Industriale dei Laterizi, Rome, Italy, pp.3-15.
- [35] Page, A.W. (2002). Un-reinforced Masonry Structures-An Australian Overview. Research Paper 15, Published in PDF (Acrobat) Format.
- [36] ElGawady, M.A., Lestuzzi, P. & Badoux, M. (2006). Retrofitting of masonry walls using shotcrete. NZSEE conference.

- [37] Mann, W., König, G., Ötes, A. (1988). Tests of Masonry Walls Subjected to Seismic Forces. Proc. of 8th International Brick and Block Masonry Conference, Ireland.
- [38] Federal Emergency Management Agency (FEMA). (2000). Prestandard and Commentary for the Seismic Rehabilitation of Buildings, FEMA 356, Washington, D.C.
- [39] American Society of Civil Engineers (ASCE). (2006). Standard ASCE/SEI 41-06. Seismic Rehabilitation of Existing Buildings.
- [40]Sweeney, S.C., Horney, M.A., Orton, S.L. (2004). Tri-Directional Seismic Analysis of an Unreinforced Masonry Building with Flexible Diaphragms. US Army Corps of Engineers, Engineer Research and Development Center.

Chapter 3

SEISMIC RETROFITTING OF UNREINFORCED MASONRY WALLS

6.1 Retrofit Strategies of Masonry

As it was mentioned in Chapter 1, there is a vital need for seismic strengthening of masonry structures. From a general rehabilitation point of view, the concept of preservation of masonry buildings can be categorized as the following actions [1]:

- a) Stabilization
- b) Repair
- c) Strengthening
- d) Seismic retrofit

Stabilization is generally applied to historical monuments which are partially collapsed during the time and mainly deals with improvement in masonry materials subjected to gradual quality decay or failures caused by past earthquakes or human-made damages. In the other words, stabilizing saves the structural integrity of the existing buildings.

Repair deals with recovering of the initial mechanical or strength properties of the materials or structural components of URM structure. The purpose of repair is not to correct the deteriorations of structure and in this sense it is different from stabilization.

Since it is not clear if the initial structural performance of a URM structure meets the required seismic requirements, there is a need to provide additional strength to building. Strengthening is aimed to respond to a more demanding level of structural safety.

Due to the earthquake-induced nature of the inertia lateral forces, sometimes strengthening is not the proper response and some other modifications in structural behavior are needed. In the other words, retrofit process may not necessarily contribute to the strengthening of URM structure. Even sometimes partial weakening (or adding ductility) of the structure may provide an adequate seismic performance. Therefore, retrofitting can be a better solution to respond the seismic demands of a URM building than only strengthening.

As the objective of this research work, retrofitting of URM wall is considered. From a structural point of view, an appropriate seismic retrofit strategy should comply with the condition below,

Seismic demand ≤ Capacity

which may be fulfilled by taking the following actions ^[2]:

- 1) Reducing seismic requirements
- 2) Improving the mechanical behavior
- 3) Combination of above modalities

Reduction of seismic requirement can be generally achieved by changing the building functionality to the one with lower seismic demand. Although in some cases it may be considered as the final solution, it is not possible in general.

Among the above mentioned actions, improving the mechanical behavior or retrofitting would be considered in most of the cases.

Also, the retrofit policies of URM structures may be categorized as partial and global retrofitting which includes the following features [3]:

- a) Improving structural connections
- b) Increasing the rigidity of floor slabs
- c) Increasing the strength/deformability of load bearing walls

As a global retrofit plan, all seismic acceptance criteria - including both partial and global behavior - should be fulfilled.

A proper rehabilitation process involves two steps such as seismic evaluation of existing building and retrofit design. These steps are shown as a simple flowchart in Figure 3.1. The efficiency of a certain retrofit strategy must be controlled through appropriate experimental or analytical process.

The most important factor that should be considered in the retrofit design of a URM structure, - whether a global or partial method - is the expected failure modes. Due to the complex seismic response of the components of a URM building and different study requirements, the failure causes of the structure should be prioritized. As it was mentioned

before, in-plane and out-of-plan failure mechanisms of the load bearing walls play key role in the URM collapse. Therefore, retrofitting of URM walls is the most important part of a global retrofit plan.

The basic strategies for retrofitting of URM walls can be described as follows:

- 1) Surface treatment
- 2) Element addition
- 3) Combination of both

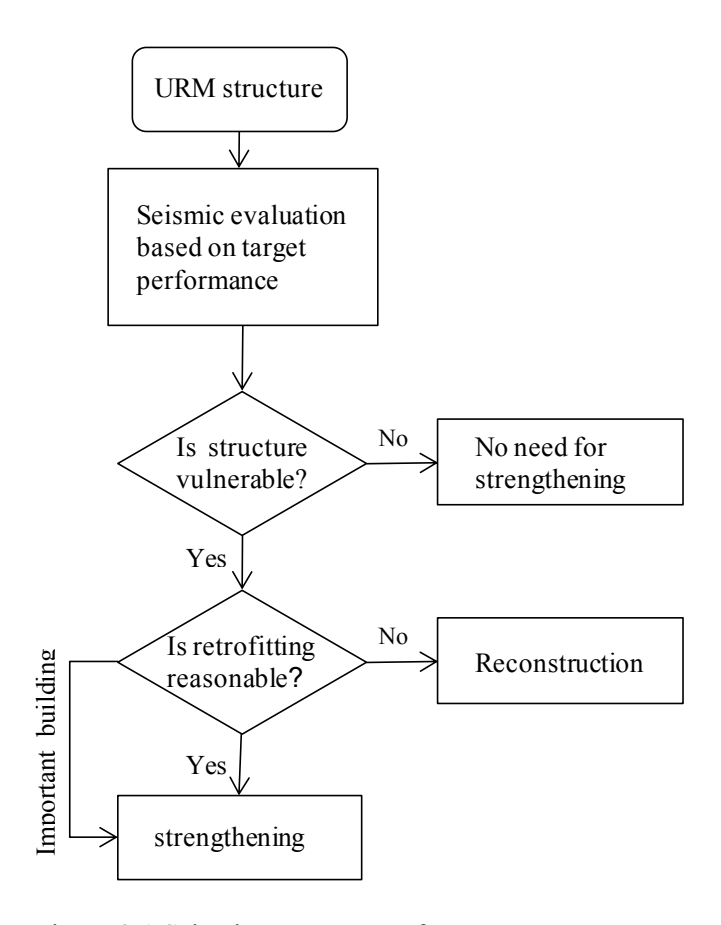


Figure 3.1 Seismic assessment of URM structures

These strategies may include the following practical actions:

- Prestressing
- Reinforcement

- Structural substitution
- Tying
- Anchoring
- Material substitution
- Propping
- Confinement
- Improvement
- Enlargement

A URM retrofit technique may involve all or some of these actions. The conventional retrofit techniques of URM are described briefly as the following part of this chapter.

6.2 Conventional Retrofit Techniques of URM

There are various methods of URM retrofitting in different categories, and some of them are under research process ^[4,5,6,7,8]. Application of these methods to URM structures is expected to increase the strength and/or ductility of the structure.

A summary of the URM retrofitting methods with a brief review on the related literature comes below.

3.2.1 Surface Treatment

Surface treatment is a common strategy for URM, which has largely developed through practical application experiences. Since in this approach, retrofitting covers the surface of masonry walls, it is not suitable for historical structures with architectural values. Recent methods in this category are introduced below.

1) Shotcrete

Shotcrete is a covering method of masonry walls with sprayed concrete reinforced by the mesh of steel bars. This technique consists of:

- -Shrinkage control reinforcement
- -Shear dowels
- -A cleaned surface, watered and grinded

- Sprayed wall surface [9]

Several experiments have shown that the application of shotcrete increases the lateral strength of the specimens by a factor of approximately 3.6 and using it on both sides of the wall (generally 20 mm thick layers) makes the wall more ductile. This type of retrofitting improves the energy dissipation by a factor of 4.2. Also the stiffness of the retrofitted specimens at the peak lateral force is approximately 3 times the stiffness of the unretrofitted one at the same force [10]. Moreover, shotcrete increases the flexural strength of URM walls [11]



Figure 3.2 Externally retrofitted wall in shotcrete method [11]

2) Textile Reinforced Mortar (TRM)

Textile Reinforced Mortar (TRM) layers are made of carbon fiber textile meshes roving in two orthogonal directions with a mortar containing polymeric additives ^[12]. TRM jacketing improves both the strength and ductility of the URM wall and it is a strongly recommended retrofitting method for unreinforced masonry walls subjected to in-plane loading (improvement by a factor of 5-6.5) ^[9]. A comparative experimental study showed that TRM jackets are at least 65–70% and 15–30% as effective as fiber reinforced polymers (FRP) jackets for shear strength and deformation capacity with identical fiber configurations ^[13].

3) Ferrocement

The ferrocement overlay rehabilitation is the fixing of a galvanized iron mesh to a wall via nails or other connectors and covering it with a rich mix of cement-sand mortar with the ratio of 1:3 [14]. Some experimental works showed that this method increases the strength of the wall slightly. It was shown that the ferrocement surface coating added little flexural strength over rocking because the tensile strength of the steel hardware cloth was very small. Also, the effectiveness of ferrocement overlay as indicated with the product of strength times ductility, was roughly equal to one of the non-rehabilitated specimens [15].

4) Polypropylene (PP) Meshing

This method uses polypropylene bands in a mesh form embedded in a cement layer cover. This method extremely improves the shear behavior and deformability of URM wall. Moreover, the retrofitted walls exhibit a 60% residual strength after peak strength, which is sustained even for larger deformations. However, since PP-bands have a relatively low stiffness compared to the masonry walls, they do not contribute to increase the wall peak strength. [16]. PP bands are cheap and therefore this retrofitting method is simple and suitable for developing countries as it was used in Nepal, Pakistan, and Kathmandu [17].

5) Re-Pointing

If the bricks of a wall are in good quality but the mortar is weak, this method can be used. The mortar is replaced with the mortar of a higher strength. Some studies showed that although minimal amount of material is required in this technique, no noticeable improvement was observed in the dynamic behavior of the retrofitted specimens [18].

6) Bamboo Reinforcement

The retrofitting system in this technique consists of vertical and horizontal bamboo used as internal reinforcing and buttresses, and a ring beam. Experiments have shown a significant increase like 400% in ultimate displacement. However, bricks surrounding the bamboo cannot provide proper protection of bamboo [18]. Moreover, due to various environmental conditions of earthquake-prone regions of world, this material is not generally available.

7) Steel Wire Mesh Reinforcement

Steel wire mesh reinforcement consists of two horizontal and vertical strips. Vertical strips are applied at the intersection of walls, the centre of long walls and at free ends. The horizontal strips applied at the top of the walls connect all of the vertical strips. These strips are covered with a cement cover to protect them from corrosion. Retrofitted houses in Peru with this method showed no damage during the 2001 and 2007 earthquakes (south Peru, Magnitude=8.4 Richter). Even retrofitted walls without covering mortar showed an appropriate seismic behavior [17].



Figure 3.3 Steel wire mesh applied to the surface of URM wall

8) Fiber Reinforced Polymer (FRP)

Fiber Reinforced Polymers (FRP) composites are made of fibers in a polymeric matrix. FRP materials are lightweight and non-corrosive. They exhibit high tensile strength and impact resistance, and are available in several forms like mesh strips, reinforcing bars, and prestressing tendons ^[19]. Applying FRP to a URM wall increases both the in-plane and out-of-plane characteristics of the wall ^[20].

Some studies showed that FRP overlays improve the shear resistance of the wall by a factor of 1.3 to 2.9. Ultimate drift of the retrofitted specimen was about 1.2 times of the one

for unretrofitted specimen and the extent of this improvement depends on fiber characteristics and applying position and direction.

Under static cyclic loading test, application of FRP improved the lateral resistance by a factor of 1.7 to 5.9. However, as it reported in several experimental research works available in literature, debonding occurred at lateral load levels ranging from 50% to 80% of the ultimate load resistance ^[21]. Debonding of FRP highly limits the performance of this method.

Glass fiber reinforced polymer (GFRP) strips have been used for retrofitting of concrete members for many years with great success. Easy application and good ductility of this method have made it suitable for URM structures.

Some experiments showed that the application of GFRP strips in a horizontal configuration improves both in-plane and out-of-plane flexural and shear behavior. However, using only vertical strips can improve the in-plane performance [22].

Carbon fiber reinforced polymer (CFRP) is a kind of FRP which is made of high strength fibers (carbon) embedded in a polymeric resin matrix. The fibers resist tension while the resin transfers the loads among the fibers [23].

Experiments showed that on average, the maximum lateral force resisted by the CFRP reinforced wall specimens was 1,500% greater than the capacity of unreinforced reference specimens [24].

Aramid fiber reinforced polymer (AFRP) is characterized by light weight and high tensile strength. AFRP have been successfully used for retrofitting of concrete members.

9) Steel Strip Meshing

In this method steel strips in different arrangements are applied to the surface of URM wall. Numerous experiments proved that by using steel strips the compressive strength of the wall was increased from 12 to 26 percent and the shear strength was increased from 30 to 87 percent, as well as a considerable increase in the elastic limit of the wall ^[25].

Application of steel strips is effective in increasing in-plane strength, ductility, and energy dissipation capacity of the wall too ^[26].



Figure 3.4 Vertical and diagonal steel bracing [11]

10) Cement-Based Matrix-Grid (CMG)

This system consists of an alkali resistant (AR) glass coated grid, SRG 45 (structural reinforcing grid), and a polymer modified AR-glass fiber reinforced mortar. Experiments showed that applying various arrangements of the CMG system improves the strength and ductility of a URM wall significantly. It improves the shear strength by a factor of 1.7or 2. However it does not affect the initial stiffness of the wall [27].

11) Post Tensioned Cables

In this method, cables consist of prestressed strands of high-tension steel protected from corrosion by grouted steel tubes. The diagonal cables are applied like a bracing system of a steel structure, and are anchored at the foundation and roof. Special mats are made for the anchoring cables at the roof and foundation ^[28].

Adding cables as a very good tensile element to walls makes them ductile and able to dissipate higher seismic energy. Experiments showed that this method can improve the lateral strength of URM wall by a factor of 2 [29].

12) Post-Tensioning Using Rubber Tyres

In this method, released compressive force from the stretched rubber produces the post tensioning effect on URM walls. Scrap rubber tyres assembled by wooden and metal connectors are used. Experiments showed that this technique improves the ductility of walls and prevents its sudden collapse caused by an earthquake. However, the efficiency of this method depends on the direction of reinforcement. Using horizontal and vertical reinforcements causes increase in failure acceleration by 70% and 40%, respectively. However, application of them in both directions causes only 10% increase [18].

13) Glass Grid Reinforced Polymers (GGRP)

GGRP system consists of a glass unidirectional reinforcement grid and polyurea resin to create a composite laminate. GGRP has many desirable properties such as rapid cure and insensitivity to humidity along with good physical properties, including a high degree of hardness, flexibility, and tensile strength. Studies showed that using the GGRP system increases in-plane and out-of-plane strengths and the stiffness of URM walls. It increases the lateral strength of the URM wall by a factor of 5 [30].

3.2.2 Injection

In this method grout or epoxy injection is used to fill voids or cracks. Since this method does not affect the surface of the wall, it is popular for historical buildings with special architectural features. This technique is very useful for the purposes of improving compressive and shear strength of URM walls by restoring the initial stiffness of it. However, when injection was applied to some parts of the building, it must be proved that any partial increase of structure strength is not dangerous for other parts or the whole building [11].



Figure 3.5 Grout injection [11]

3.2.3 Confinement

In this method, tie columns confine the URM wall at corners, intersections, and the border of openings. In some countries like China and Iran, this method applies to new masonry construction as the confined masonry structure [31]. However, because of the minor effects of using columns alone for the confinement of walls, it is necessary to apply a horizontal element like a beam to the system. This method improves the ductility and energy dissipation of a masonry structure. Also it improves the structural integrity of URM considerably. The intensity of this improvement depends on the relative rigidity between the masonry and the surrounding frame and also material properties [11,18].

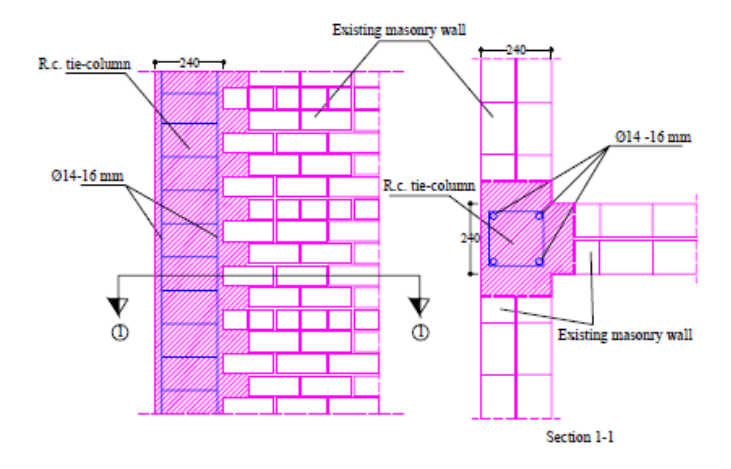


Figure 3.6 Confinement of URM wall by tie column [11]

3.2.4 Center Core

The center core system consists of a reinforced, filled core placed in the center of an existing URM wall. Reinforcing bars are anchored to the roof and foundation. The filler material itself consists of a binder material (e.g. epoxy, cement, and polyester) and a filler material (e.g. sand). However, improvement in shear resistance in the case of using epoxy and polyester with sand is more than cement grout while the energy dissipation during loading is limited [11]. Retrofitted structures resist both in-plane and out-of-plane loadings, and in a static cyclic test, its ultimate load resistance may be doubled [18].

Experiments showed that the ductility and out-of-plane behavior of the wall retrofitted with this technique was improved [32].

3.2.5 Base Isolation

In this method, URM building is isolated from ground excitation by using isolators. Sometimes because of the structural weakness of a superstructure or its historical value, it is impossible to retrofit it by other methods and base isolation can be considered as a proper solution. However, the process of a base isolation technique can be very difficult.

At first, loads carried by a superstructure must be transmitted gradually to the temporary supports. Then by casting needle-beams under masonry walls and installing some under the beams, loads can be transmitted to the foundation or base [33].

There are some base isolators that are being used nowadays, but applying these systems to URM structures is unreasonable especially in developing countries. Among the base isolators, friction seismic isolation (FSI) is the most suitable method for masonry structures. In the FSI technique there is no need for any spring or complicated device [34].

6.3 Retrofitting with Engineered Cementitious Composites

Engineered Cementitious Composite (ECC) – also refers to as High Performance Fiber Reinforced Cement Composite (HPFRCC) in Japan, Strain-Hardening Cement-based Composite (SHCC) and bendable concrete – with multiple fine cracks is a cement-based composite material with a strain-hardening tensile behavior and an excellent capability to control the width of crack [35, 36]. This composite material has shown a high strain capacity and can absorb and dissipate high amounts of energy [37]. Improving the low tensile strength, strain-softening and brittle behavior of URM walls by surface retrofitting with such a ductile strain-hardening material was the main motivation of retrofitting with this material.

Kyriakides and Billington [38] studied ECC retrofitting for concrete frame-infill masonry walls. They conducted a series of experiments in order to examine the impact of a thin layer of ECC applied to masonry infill wall as well as when it is applied on a masonry wall bounded by a non- ductile reinforced concrete frame. The study results showed that ECC can help keep unreinforced masonry walls in tact to large lateral drifts, adding significant

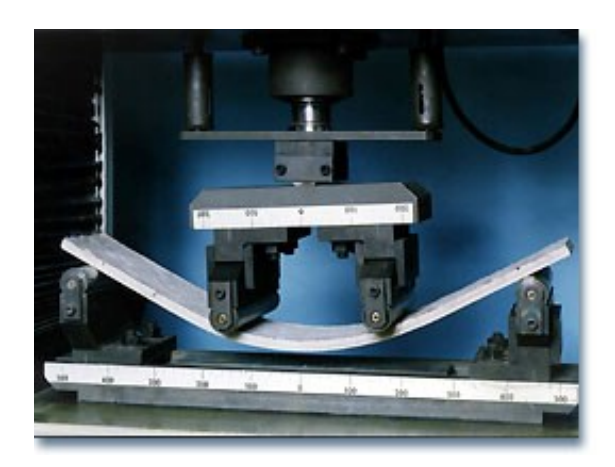


Figure 3.7 High deformability of ECC composite [36]

ductility to the entire structural system under cyclic loading.

The effect of ECC mixture components on its retrofit functionality for masonry walls was studied by Bruedern et al.^[39]. The test results showed that the shear load bearing capacity and the energy absorption capacity of masonry increased by the application of a thin ECC layer.

Maalej et al.^[40] studied the ECC retrofitting for URM walls under impact loading. The quasi-static loading test results showed that the ECC-strengthening system improves the out-of-plane resistance of masonry walls significantly. Moreover with the use of ECC overlay, fragmentations due to impact were also reduced significantly.

Also Lin et al.^[41] conducted some in-plane and out-of-plane tests on the ECC retrofitted masonry specimens and examined a two story URM building shotcreted with ECC in New Zealand. As a result of out-of-plane tests, an increase in maximum load of 1.6 times the strength of the bare wall was observed when ECC retrofitting was applied on the compression surface and an increase of 13.2 times when it was applied on the tension side.

6.4 Effectiveness of the URM Retrofitting Methods

Considering the contents of part 3.2 and 3.3, advantages and disadvantages of the retrofitting methods were summarized in Table 3.1.

Table 3.1 Advantages and disadvantages of URM retrofitting methods

Method	Advantages	Disadvantages
Shotcrete	Available materials, Improves shear and flexural strength of in-plane behavior, Improves ductility and energy dissipation, Improves out-of-plane stability	High mass, Requires trained workers, Space reduction, High disturbance, Requires finishing, Affects architecture
TRM	Low mass, Improves in-plane behavior, Improves strength and ductility, Low space reduction, Low disturbance	Requires trained workers, High cost, Affects architecture, Requires finishing
Ferrocement	Low cost, Low technology, Low mass, Available materials	Low efficiency, Space reduction, Requires finishing, Low energy dissipation, Affects architecture
PP Meshing	Low cost, Low technology, Improves shear behavior and ductility, Low mass	Affects architecture, Requires finishing
Re-Pointing	Low technology, Low cost, Low mass, Available materials, Low space reduction	Low efficiency, Affects architecture, Required finishing
Steel Wire Mesh Reinforcement	Low technology, Low mass, Improves shear behavior, Improves out-of-plane stability, Available materials	Corrosion potential, Requires trained workers, Requires finishing, Affects architecture, Space reduction

Table 3.1 Advantages and disadvantages of URM retrofitting methods - continue

Method	Advantages	Disadvantages
FRP	Low mass, Improves shear and flexural strength of in & out-plane behavior, Low disturbance	High cost, Requires finishing, Affects architecture, Requires trained workers
Steel Strip Meshing	Improves shear and compressive strength of in-plane behavior, Improves ductility and energy dissipation, Available materials	High cost, Corrosion potential, Requires finishing, Affects architecture, Requires trained workers
CMG	Improves strength and ductility, Low mass, Low space reduction	No effect on stiffness, High cost, Requires trained workers, Affects architecture
Post Tensioned Cables	Low mass, Low disturbance, Minimal effect on architecture, Improves ductility and energy dissipation	Advanced technology, Hard to anchor, Corrosion potential, Requires trained workers, Requires finishing
Post- Tensioning Using Rubber Tyres	Low mass, Low disturbance, Improves shear strength, Improves ductility, Available materials, Low cost	Hard to anchor, Affects architecture, Space reduction, Requires finishing
GGRP	Improves shear and flexural strength of in & out-of-plane behavior, Improves stiffness, Low mass	High cost, Requires trained workers, Affects architecture

Table 3.1 Advantages and disadvantages of URM retrofitting methods - continue

Method	Advantages	Disadvantages
	Low mass, Minimal effect on architecture,	High cost, Creating of zones with different
T	No space reduction, Low disturbance,	stiffness and strength,
Injection	Available materials, Improves compressive	Requires trained
	and shear strength	workers, Advanced
		technology
		Hard to apply,
		Required finishing,
	Improves ductility and energy dissipation,	High disturbance,
Confining	Available materials,	Limited effect on
	Available materials,	shear strength, Low
		effect on out-of-plane
		behavior
	No space reduction, Minimal effect on	Low energy
	architecture, Low disturbance, Available	dissipation,
Center Core	materials, Improves in & out-of-plane	Creation of zones with
Center Core	stability, Improves shear and flexural	different stiffness and
	strength	strength, Requires
	Strongth	trained workers
Base Isolation	No need to retrofit superstructure, No	Advanced technology,
Base Isolation	effect on the architecture	High cost
		High cost, Requires
	Improves shear strength, Improves out-of-	trained workers, Space
ECC	plane stability, Improves ductility and	reduction, High
	energy dissipation	disturbance, Affects
		architecture

As a result of comparison between these techniques, it was revealed that the surface treatment is the most suitable method from both applicability and cost-performance viewpoints in the case that the covering of the wall surface is acceptable due to architectural reasons. Among the materials which have been examined in the surface treatment category, ones with higher deformation and tensile capacity exhibit better in-plane retrofit performance in terms of the shear resistance and deformability. This fact was taken as a basis for selection of appropriate materials for retrofit purpose in this research work.

Newly developed Engineered Cementitious Composite (ECC) exhibits high tensile and deformability and was utilized in current study for URM wall retrofitting.

Fiber reinforced polymer (FRP) products are well-known for their retrofitting potential in the variety of structure types. However as it was mentioned earlier, pre-mature debonding of FRP limits its efficiency. In present study, in order to eliminate this undesirable behavior, confining bands which has previously been applied to the retrofitting of RC columns with wall [42], was utilized.

Among FRP products, aramid fiber reinforced polymer (AFRP) with light weight and good workability was selected and in this study, AFRP sheet with confining band system has been utilized as a retrofit solution for URM walls.

References

- [1]EU-INDIA economic cross cultural programme. (2006). Guidelines for the conservation of historical masonry structures in seismic
- [2] Lungu, D., Arion, C. FP6 PROHITECH project: Volume 1: Intervention strategies for the seismic protection of historical building heritage in the Mediterranean basin, chapter 5, ISBN: 978-88-7699-169-1.
- [3] ASCE/SEI 41-06 Standard. (2006). Seismic rehabilitation of existing buildings. American Society of Civil Engineers.
- [4] Macabuag, J., Bhattacharya, S. (2009). Extending the collapse time of non-engineered masonry buildings under seismic loading. EWB-UK Research Conference.
- [5] Ismail, N., Ingham, J. State-of-the-art retrofit interventions for unreinforced masonry walls. Seismic Retrofit Solutions Website (http://www.retrofitsolutions.org.nz/).
- [6] Macabuag, J. (2010). Dissemination of seismic retrofitting techniques to rural communities. EWB-UK National Research Conference.
- [7] Abrams, D.P. (2000). Seismic rehabilitation methods for unreinforced walls. 3nd EQTAP workshop, Manila, Philippines.
- [8] GooDWin, C., Tonks, G., Ingham, J. (2011). Retrofit techniques for seismic improvement of URM buildings. Journal of the Structural Engineering Society, New Zealand Inc., Volume 24 No. 1. pp.30-45.
- [9] Ismail, N., Ingham, J.M. State-of-the-art retrofit interventions for unreinforced masonry walls. Department of civil and environmental engineering, University of Auckland, New Zealand.
- [10] ElGawady, M.A., Lestuzzi, P. & Badoux, M. (2006). Retrofitting of masonry walls using shotcrete. NZSEE conference.
- [11] ElGawady, M., Lestuzzi, P., Badoux, M. (2004). A review of conventional seismic retrofitting techniques for URM. 13th International Brick and Block Masonry Conference Amsterdam

- [12] Papanicolaou, C. G., Triantafillou, T. C., Karlos, K., Papathanasiou, M. (2006). Seismic retrofitting of unreinforced masonry structures with TRM. ICTRC'2006-1st international RILEM conference on textile reinforced concrete.
- [13] Papanicolaou, C.G., Triantafillou, T.C., Karlos, K., Papathanasiou, M. (2007). Textile-reinforced mortar (TRM) versus FRP as strengthening material of URM walls: in-plane cyclic loading. Materials and Structures, Vol.40, pp.1081–1097.
- [14] Arya, A.S., Agarwal, A. Simple retrofitting details for improving earthquake resistance of brick masonry buildings in NCT of Delhi and the NCR. GOI–UNDP, Disaster risk management program, National disaster management division, Ministry of home affairs, North block, New Delhi.
- [15] Abrams, D., Smith, T., Lynch, J. and Franklin, S. (2007). Effectiveness of rehabilitation on seismic behavior of masonry piers. Journal of structural engineering © ASCE, 32-43.
- [16]Mayorca, P. and Meguro, K. Proposal of a new economic retrofitting method for masonry structures, JSCE journal of earthquake engineering
- [17] Macabuag, J. (2010). Dissemination of Seismic Retrofitting Techniques to Rural Communities. EWB-UK national research conference.
- [18] Smith, A. & Redman, T. (2009). A critical review of retrofitting methods for unreinforced masonry structures. EWB-UK research conference hosted by the royal academy of engineering
- [19] Galati, N., Garbin, E., Nanni, A. (2005). Design guidelines for the strengthening of unreinforced masonry structures using fiber reinforced polymer (FRP) systems. University of Missouri –Rolla.
- [20] FEMA 547. (2006). Chapter 21-building type URM: unreinforced masonry bearing walls, techniques for the seismic rehabilitation of existing buildings.
- [21] Elgawady, M. (2004). Seismic in-plane behavior of URM walls upgraded with composites. Phd thesis, École polytechnique federale de lausanne.
- [22] Turek, M., Ventura, C.E. and Kuanb, S. (2007). In-plane shake-table testing of GFRP strengthened concrete masonry walls. *Earthquake Spectra*, Vol. 23, No. 1, pages 223–237.

- [23] Santa Maria, H., Alcaino, P., Luders, C. (2006). Experimental response of masonry walls externally reinforced with carbon fiber fabrics. Proceedings of the 8th U.S. National conference on earthquake engineering, April 18-22, San Francisco, California, USA.
- [24] Hoeppner, C. R., Sparling, B. F., Wegner, L. D., Sakr, K. (2002). CFRP reinforced masonry walls subjected to out-of plane loading. 4th structural specialty conference of the Canadian society for civil engineerin, Montréal, Québec, Canada, June 5-8.
- [25] Farooq, S.H., Ilyas, M. and Ghaffar, A. (2006). Technique for strengthening of masonry wall panels using steel strips. Asian journal of civil engineering (Building and Housing), Vol.7, No.6, pp.621-638.
- [26] Taghdi, M., Bruneau, M. and Saatcioglu, M. (2000). Seismic retrofitting of low-rise masonry and concrete walls using steel strips. Journal of structural engineering, pp.1017-1025.
- [27] Prota, A., Marcari, G., Fabbrocino, G., Manfredi, G. and Aldea, C. (2006). Experimental in-plane behavior of tuff masonry strengthened with cementitious matrix-grid composites, Journal of composites for construction © ASCE, pp.223-233.
- [28] Tena-colunga, A. (1996). Some retrofit options for the seismic upgrading of old low-rise school building in Mexico. Earthquake spectra, Vol. 12, No.4.
- [29] Chuang, S.W. (1995). Seismic retrofitting techniques for existing unreinforced masonry structures, Phd Thesis, M.E., Cornell University, U.S.A.
- [30] Garbin, E., Galati, N., Nanni, A. (2005). Design guidelines for the strengthening of unreinforced masonry structures using glass grid reinforced polymer (GGRP) systems. University of Missouri Rolla.
- [31] Building and Housing Research Center. (2005). Iranian code of practice for seismic resistant design of buildings Standard No. 2800 3rd edition.
- [32] Ismail, N., Mahmood, H., Derakhshan, H., Clark, W. and Ingham, J. M. (2009). Case study and development of seismic retrofit solution for a heritage URM building. 11th Canadian Masonry Symposium, Toronto, Ontario.
- [33] Gemme, M.C. (2009). Seismic retrofitting of deficient Canadian buildings. Master thesis, Massachusetts Institute of Technology.

- [34] Qamaruddin, M. (1998). A state-of-the-art review of seismic isolation scheme for masonry buildings. ISET Journal of earthquake engineering, Paper No.376, Vol. 35, No.4, pp.77-93.
- [35] Victor C. Li. (2003). On engineered cementitious composites (ECC) A review of the material and its applications. Journal of Advanced Concrete Technology Vol. 1, No. 3, pp. 215-230, Japan Concrete Institute.
- [36] Japan Society of Civil Engineers (JSCE). (2008). JSCE recommendation for design and construction of high performance fiber reinforced cement composite with multiple fine cracks.
- [37] V. Mechtcherine, J. Schulze. (2005). Ultra-ductile concrete material design concept and testing. CPI concrete Plant International, No.5, pp.88-98.
- [38] M. Kyriakides, S. Billington. (2008). A seismic retrofit for masonry infill walls using ductile concrete. Creating and Renewing Urban Structures Tall Buildings, Bridges and Infrastructure, 17th Congress Report of IABSE Chicago, USA.
- [39] Bruedern, A.-E., Abecasis, D., Mechtcherine, V. (2009). Development of strain-hardening cement- based composites for the strengthening of masonry. Concrete Repair, Rehabilitation and Retrofitting II, London, England, pp. 887-893.
- [40] Maalej, M., Lin, W.V.J., Nguyen, M.P., Quek, S.T. (2010). Engineered cementitious composites for effective strengthening of unreinforced masonry walls. Engineering Structures, Vol. 32, pp. 2432-2439.
- [41] Lin, Y.-W., Lawley, D., Ingham, J.M. (2010). Seismic strengthening of an unreinforced masonry building using ECC shotcrete. 8th International Masonry Conference, Dresden, Germany, pp. 1461-1470.
- [42] Hanai, N., Kosugi, K., Ichinose, T., Shirakawa, T. (2011). Experiments on aramid fiber retrofit for RC columns with walls, Journal of Structural and Construction Engineering (Transaction of AIJ), Vol. 76, No. 659.

Chapter 4

MODELING OF MASONRY

Since the numerical modeling was utilized in this research work for evaluation of the in-plane behavior of the retrofitted masonry wall, available modeling strategies for URM walls and proposed approaches for retrofitted wall are introduced and discussed in this chapter.

Even though masonry is an old construction technique, research in this field and analytical study in particular is very young and arose only in the recent decades.

Up to now several strategies and computational methods have been proposed or adopted for the analysis and assessment of masonry structures. These methods are based on different theories and approaches, resulting in different levels of complexity which extends from simple empirical methods to complex mathematical formulations of non-linear static and dynamic equations. It should be expected that the results of different approaches might be also different. However, more complexity in analysis process does not necessarily mean better results and validation of these analytical results by experimental data should be considered. Since the final purpose of the development of such computational methods is to be applied to actual practice by engineers, the analysis time and cost are also important factors in proposing of such analytical techniques.

In order to model any structural behavior, there should be enough knowledge on the constitute law and failure criteria of the material. Unfortunately, a reliable constitute law for masonry is not available yet. Although some closed-form models have been proposed for masonry behavior, their ability in prediction of masonry behavior under multi-axial loading states is questionable. As a result, there is a common tendency among researchers to numerical modeling in which different loading and material specification can be considered.

Up to now, various analysis methods have been applied to masonry analysis such as finite element (FEM) [1-10], discrete element (DEM) [11-18], applied element (AEM) [19-21] and limit analysis [22-25] methods. Also some simplified method which are mainly based on equivalent frame simulations, have been proposed for URM analysis.

Among these methods, finite element method has been considered as a method with relatively adequate accuracy. Although finite element method is a powerful numerical method for the analysis of structures, there are difficulties in modeling of discrete structural systems like masonry and some researchers prefer discrete analysis (DEM) rather than continuum model defined in finite element method. Recently, a combination of FEM and DEM methods has been considered for masonry analysis.

Here, the major strategies for URM modeling and their capabilities are introduced. Then, homogenization theory as a recent development in URM modeling field is briefly described.

Modeling of the retrofitted masonry consists of two processes such as unreinforced and retrofit modeling. In this study, for unreinforced part, simple micro-model method from heterogeneous modeling category was employed. The modeling procedure and the contributing features in this technique are described in this chapter.

The retrofit modeling process is highly dependent on the retrofit strategy. As mentioned in previous chapter, surface treatment using ECC and AFRP materials was intended in this study. Therefore, the retrofit part of the numerical modeling was targeted toward the specific requirements of external application and the characteristics of retrofit material in particular.

Although the properties and retrofit mechanisms of ECC and AFRP materials are very different, due to the existence of fiber and binder in both of them, their mechanical behavior has some similarities. So, each material was modeled considering its inherent behavioral features. New approaches for modeling of each material were proposed and adopted in this research work which explained as the last part of this chapter. An experimental study was conducted on the masonry specimens retrofitted by ECC overlay and AFRP sheet and the reliability of the proposed analytical models was validated as explained in Chapters 5 and 6, respectively.

4.1 Modeling Approaches for URM

Masonry is a non-linear anisotropic composite material that consists of brick units and joint mortar and exhibits directional behavior. Two major approaches in masonry modeling field namely heterogeneous and homogeneous modeling are described as follows.

4.1.1 Heterogeneous Modeling

In this approach unit bricks and mortar are considered separately which suits for small size models. Many factors such as material properties of bricks and mortar, shape and hollow distribution of bricks, arrangement of bed and head joints and joint thickness are considered in this strategy. Because of the complexity of modeling, this approach may not be considered as an economical option for actual structure analysis due to the high required analysis time and cost [26]. Two techniques are used in this approach, micro-modeling and interface modeling. Also micro-modeling is divided into two subparts as detailed micro-modeling and simplified micro-modeling [27] which are explained as follows.

1) Micro-Modeling

In this method, brick unit and the joint mortar shall be modeled as separate members. Almost all failure modes can be considered in this approach. Interface elements for simulation of the bed joint mortar – bricks locking must be defined well. In standard finite element methods and programs, the interface element can be treated with contact elements. However the normal and tangent stiffness of contact and other related parameters must be well determined in order to overcome the convergence problems. This approach is suited for small structural elements with heterogeneous states of stress and strain. The main purpose of micro modeling is the prediction of the local structural behavior of URM based on the mechanical properties of each constitute such as brick and mortar. In order to have an accurate model, all required mechanical properties of the elements should be determined experimentally. As it was mentioned before, numerous parameters are needed to reach accurate results in this method and some experiments are practically difficult to conduct. In lack of such experimental data, calibration with reference specimens can be considered as another solution but with limited accuracy. Moreover, in calibration process, high deviation of masonry specifications should be considered.

Due to the complexity issues, two techniques are used in this field as detailed and simplified micro-modeling.

a) Detailed micro-modeling

In this technique, units and bed joint mortar are represented by continuum elements whereas

the mortar-brick interface is represented by discontinuous elements as shown in Figure 4.1 (b) [28].

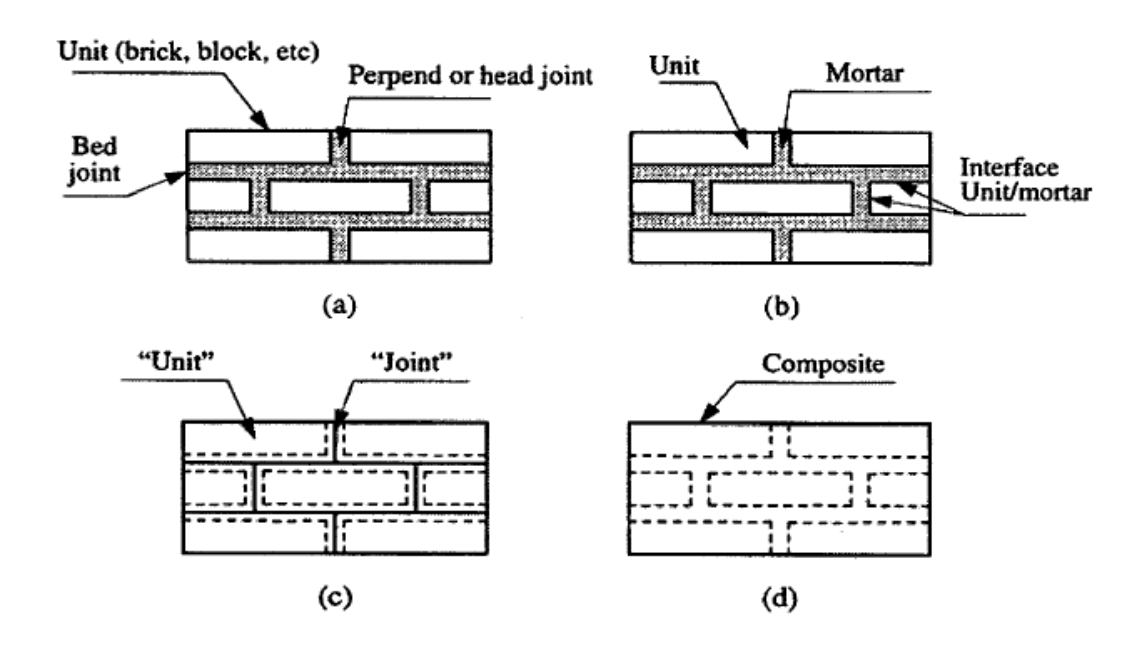


Figure 4.1 Modeling approaches for masonry [28]

- (a) URM sample
- (b) detailed micro-modeling
- (c) simplified micro-modeling (d) macro-modeling

b) Simplified micro-modeling

In this method, expanded units are represented by continuum elements whereas the behavior of the mortar joints and unit-mortar interface is lumped in discontinuous elements. These interface elements represent the preferential crack locations where tensile and shear cracking may occur. This method is shown as a schematic illustration in Figure 4.1 (c).

4.1.2 Homogeneous Modeling

In this approach the masonry units and mortar are assumed to be smeared to an isotropic and anisotropic composite material representing the consisting elements which can be applied for large size models. Two techniques are used in this approach as macro-modeling and micro/macro-modeling.

1) Macro-Modeling

In this method one composite material representative of both units and mortar (and their interface) is modeled as shown in Figure 4.1 (d). The mechanical properties of this material must be determined by experiments or by calibration to some approved behavioral models. Macro models are applicable when the structure is composed of solid walls with sufficiently large dimensions so that the stresses across or along a macro size will be fairly uniform. Clearly, macro modeling is more practice oriented due to the reduced time and memory requirements as well as a user friendly mesh generation. This type of modeling is the most valuable technique when a balance between accuracy and cost is desired.

Due to simplicity of the modeling, some failure modes cannot be captured in this approach. For example this method is not capable to determine the failure pattern at mortar and units connection points or other localized effects. Moreover, still there is not a completely proved yield surface models for anisotropic and isotropic masonry macro models. It needs comprehensive test results to determine the property of masonry assemblage under different loading conditions.

2) Micro/Macro-Modeling

Unit and mortar material properties modified with specific formulations and simulated with concrete/rock criteria.

A homogeneous approach also can be utilized to model the larger-size specimens under cyclic loading.

In present study, simple micro-model approach was employed to simulate the behavior of the URM part of the ECC and AFRP retrofitted wall. Modeling and analysis procedure are explained in Chapter 6. Also validation of analysis results with test data is shown there.

4.1.3 Homogenization Theory

Homogenization can be defined as the modeling technique of a heterogeneous medium by means a unique continuous medium. Its goal is to determine the mechanical parameters of the unique fictitious material that best represents the real heterogeneous material or composite material. However homogenization for elasto-plastic materials has some problems in plastic range but since masonry is a brittle material, only elastic range can be considered [29].

In masonry homogenization approach, two techniques are commonly used:

- a) Homogenization based on the fundamental behavior of constitutes which is in the format of closed-form equations.
- b) Numerical homogenization which is mainly based on the calibration of test samples using a proved constitute law and performing numerical analysis such as finite element method.

The first method requires some simplifying assumptions and based on complicated equations representing the mechanical properties of brick, mortar and interface. The results of this method is not necessarily in a well-agreement with test results especially when the direction of loads or geometry changes. Moreover, size effect issue alters the accuracy of the obtained results.

As numerical homogenization, since the behavior of the masonry is non-linear brittle, constitute law of a brittle material can be adopted for masonry as a preliminary assumption. Then, based on the test results, this behavioral model modified in order to fit the real mechanical characteristics of masonry. As instance, plain concrete as a brittle non-linear material has shown a behavior similar to masonry in terms of stress-strain relation, failure criteria and stiffness degradation and can be used as a preliminary model.

However it should be mentioned that the there might be some differences between the results of the final modified model and test results because of the difference in principal behavior of masonry and concrete. Concrete exhibits a relatively isotropic behavior while masonry is an anisotropic material which exhibits a directional behavior.

Despite of the above mentioned disadvantage of the numerical homogenization, easy application and low cost analysis procedure makes it a suitable macro-model for prediction of the masonry behavior in large scales and consequently for actual practice.

Some constitute models for plain concrete and brittle materials in general have been proposed. To select the one which is appropriate for masonry behavior, the most important factor is the anisotropy of masonry. This behavioral characteristic has been considered in some of the concrete models such as "smear cracking" and "damage plasticity" models.

4.2 Modeling Procedure in Simple Micro-Model Technique

Simple micro-model technique from heterogeneous modeling category was employed for modeling of the unreinforced part of the retrofitted masonry wall. In this method, brick and mortar are smeared in each other and their interface as the most possible failure plane of the masonry assemblage is taken into account. Obviously, the most important modeling process in this technique is the determination of the interface characteristics.

The interface characteristics in this method are represented by the surface contact behavioral features such as tangential and normal behaviors. Also, the cohesive behavior and damage criterion are taken into account. These behavioral aspects are explained briefly as follows. Details about the application of this method are explained in Chapter 6.

4.2.1 Tangential Behavior

Shear stress in contact is transmitted between the attached surfaces by tangential behavior. The relationship between the stresses can be described by a friction model based on the Coulomb theory. The contact can resist shear stresses up to a certain magnitude before its surfaces start sliding relatively.

In a three dimensional model, there are two orthogonal components of shear stress, which act in two perpendicular slip directions of the contact plane. Taking an isotropic behavior assumption, these two shear stress components can be taken as equal.

4.2.2 Normal Behavior

In order to consider the over closure or interpenetration of the attached surfaces of the contact, normal stiffness of interface is defined.

The normal stiffness of the contact is originated from the uniaxial compressive/tensile behavior of bed joint mortar.

4.2.3 Cohesive Behavior

Cohesive behavior can be described by a traction-separation law between surfaces as shown in Figure 4.2. The model assumes a linear elastic traction-separation law prior to damage. Failure of the cohesive behavior occurred by a degradation of cohesive stiffness, derived from damage process. Once the cohesive behavior is damaged, the friction model

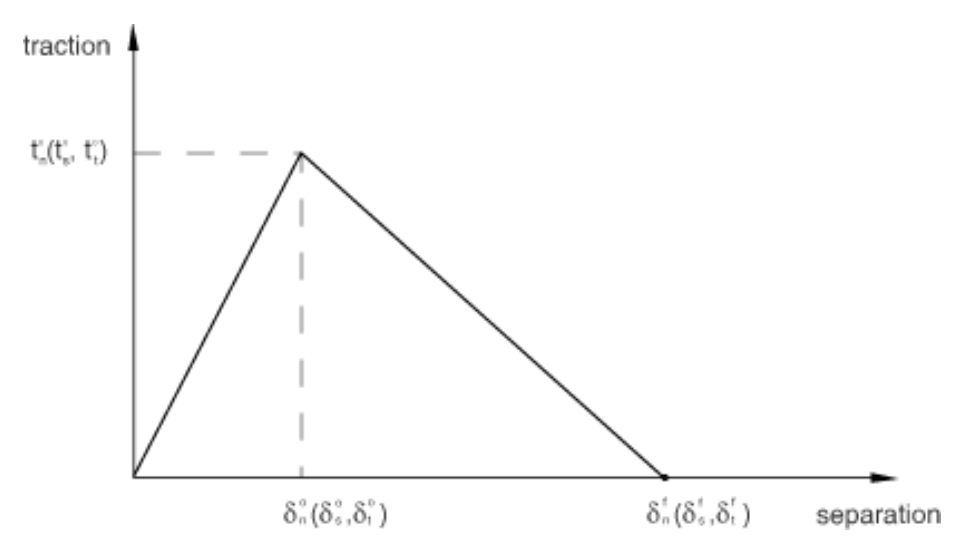


Figure 4.2 Typical linear traction-separation model [30]

becomes active and contributes to the shear strength. When the cohesive behavior is completely damaged, the shear strength is just provided by friction model.

Traction-separation law assumes an initial linear elastic behavior followed by the initiation and evolution of damage for general cohesive materials.

In case of brick-mortar cohesive behavior, the tangential and normal stiffness of the traction-separation law is originated from the elastic and shear modulus of mortar.

4.2.4 Damage Criterion

The beginning of the degradation of the cohesive response is assumed to happen when the maximum stress criterion is accomplished. In the other words, damage in interface begins when the traction in one of the planar or normal directions reaches the peak value which could be resisted by the contact. In case of brick-mortar contact, these peak values are the normal tensile strength of mortar and shear bond strength between brick and mortar in two planar directions. The required parameters for URM in simplified modeling are summarized in Table 4.1. These parameters are explained in detail at part 6.3 of Chapter 6.

4.3 Modeling of ECC and AFRP Retrofitted Masonry

New modeling approaches were proposed and adopted in this study for both of ECC and

Table 4.1 Required parameters for URM in simplified modeling technique

Model part		Required parameters		Determination method		
Cmaara	Smeared brick and mortar E		Young's modulus	Compressive test results of		
Silleared	a office and mortal	ν	Poisson's ratio	unit brick		
	Tangential	μ	Friction coefficient			
	Normal	K _n	Normal stiffness			
	Cohesive	K _{nn}	K _{nn}	Normal cohesive stiffness	From calibration of URM model to test results	
			Planar cohesive stiffnesses	model to test results		
T . C		K _{tt}	Planar conesive stiffnesses			
Interface		t_n^{0}	Tensile strength of mortar	Taken as low as 0.1 MPa		
				t_s^0	Shear bond strength	Shear test results of
Damage	Damage	t_t^{0}	of brick-motar	URM triplet		
		δ^0	Displacement at failure	From calibration of URM model to test results		

AFRP retrofitting methods. Also, in order to validate these models, experimental study was carried out as explained in detail at Chapter 5. These approaches are explained as follows.

4.3.1 ECC Retrofitting Model

As mentioned in Chapter 3, unlike usual cementitious materials, due to existence of fibers in ECC mortar, it exhibits a ductile behavior as well as a high tensile capacity. The studies have been conducted on ECC are mainly focused on the behavior of the structural members made by this material such as beam or column usually reinforced by steel bars. Also, some compressive and tensile constitute laws were proposed for ECC.

In this study, ECC was intended to apply as an external overlay with a small thickness compare to the one of URM wall. Considering the characteristics of ECC, it was assumed that the shear capacity of thin ECC overlay is provided by its tensile behavior and the effect of compressive behavior is neglected. As a result, ECC layer was considered as a membrane structural member.

Kanakubo et al ^[31] proposed a general compressive-tensile model for ECC including a bilinear constitute law for tensile behavior in a reinforced beam which is based on a perfect elasto-plastic material assumption as shown in Figure 4.3.

Also, in their general model, it is assumed that the principal tensile stress of ECC keeps tensile strength at shear failure.

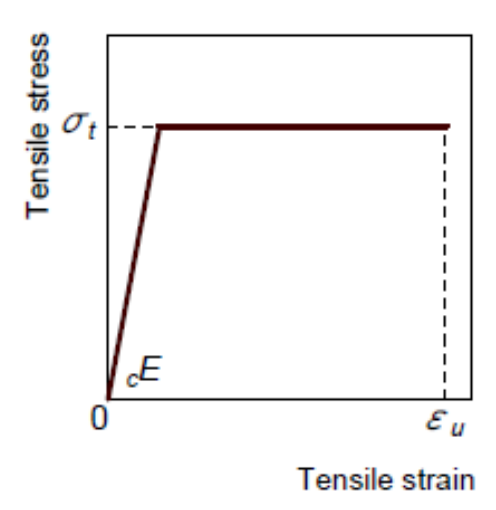


Figure 4.3 Perfect elasto-plastic tensile stress-strain relation of ECC [31]

The ultimate tensile strain of the model (ϵ_u) is given by $0.85\epsilon_{tu,b}$ and the tensile strength (σ_t) is given by $0.82f_{tu,b}$. $\epsilon_{tu,b}$ and $f_{tu,b}$ are the ultimate tensile strain and stress of ECC obtained from bending test on the material prism samples. Elastic modulus for tension is regarded as same as the elastic modulus obtained from compression test ($_cE$).

This model was adopted in numerical analysis. Application of the model is described in part 6.3 of Chapter 6.

The required parameters for ECC modeling are summarized in Table 4.2. These parameters are explained in detail at part 6.3 of Chapter 6.

Table 4.2 Required parameters for ECC modeling

Model part	Requ	ired parameters	Determination method
ECC avaday	$\sigma_{ m t}$ $\epsilon_{ m u}$	Yield stress Ultimate strain	Results of bending test on prism samples
ECC overlay	cЕ	Young's modulus	Results of compressive test on cylinder samples

4.3.2 AFRP Retrofitting Model

AFRP and FRP products in general, exhibit high tensile capability in the fiber orientation and their behavior is linear elastic with a brittle tensile rupture at the ultimate strain. The high ultimate tensile strain of AFRP has made this material as a suitable choice for retrofit applications. AFRP sheets are usually applied to surfaces by epoxy resin cohesive materials. However, due to pre-mature debonding of AFRP sheet from the substrate, only a fraction of its ultimate tensile strain contributes to the retrofit performance. In this study, in order to eliminate the debonding effect, confining band system was decided to apply.

A new modeling approach was proposed in which the AFRP retrofit sheet and the cohesive resin were regarded as a homogenized material with a bilinear tensile constitute law. This model is shown in Figure 4.4. The yield and ultimate tensile strains of this model are assumed as the effective and ultimate strains of AFRP, respectively. The effective strain was defined in part 6.4 of Chapter 6. In this model, the debonding behavior of AFRP sheet from masonry substrate is represented by the plastic phase of the AFRP-resin material.

The required parameters for AFRP modeling are summarized in Table 4.3. These parameters are explained in detail at part 6.5 of Chapter 6.

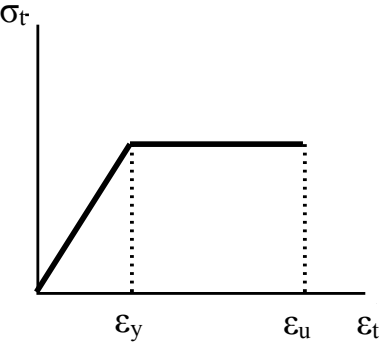


Figure 4.4 Elasto-plastic tensile stress-strain diagram for AFRP-resin

Table 4.3 Required parameters for AFRP modeling

Model part	Requ	ired parameters	Determination method
AFDD 1	$\epsilon_{ m y}$	Yield strain	Effective strain (part 6.4 of Chapter 6)
AFRP sheet	ϵ_{u}	Ultimate strain	Taken from literature [32]
	Е	Young's modulus	Data from producing company

References

- [1] Mengi, Y., Sucuoclu, H., Mcnive, H.D. (1984). A linear mathematical model for the seismic inplane behavior of brick masonry walls part 1: Theoretical consideration. Earthquake Engineering and Structural Dynamics, 12, pp.313-326.
- [2] Tzamtzis, A.D., Asteris, P.G. (2003). Finite element analysis of masonry structures: Part II- proposed 3-D nonlinear microscopic model. Ninth North American Masonry Conference, Clemson, South Carolina, USA.
- [3] Mengi, Y., Mcnive, H.D. (1989). A mathematical model for the in-plane non-linear earthquake behavior of unreinforced masonry walls. Part1: experiments and proposed model. Earthquake Engineering and Structural Dynamics, 18, pp.233-247.
- [4] Del Piero, G. (1989). Constitutive equation and compatibility of the external loads for linear elastic masonry-like materials. MECCANICA, 24, pp. 150-162.
- [5] Lotfi, H. R., Shinc, P. B. (1991). An appraisal of smeared crack model for masonry shear wall analysis. Computers & Structures, 41, No. 3, pp. 413-425.
- [6] Pietrijszczak , S., Niu, X. (1992). A mathematical description of macroscopical behavior of brick masonry. International journal of solid structures, 29, No. 5, pp. 531-546.
- [7] Lourenço, P.B. (1995). An orthotropic continuum model for the analysis of masonry structures. TNO Building and Construction Research, report no. 95-NM-R0712.
- [8] Papa, E., Nappi, A. (1997). Numerical modeling of masonry: A material model accounting for damage effects and plastic strains. Applied Mathematical Modeling, 21, pp.319-335.
- [9] Lourenço, P. B. (1997). An anisotropic macro-model for masonry plates and shells: implementation and validation. TNO Building and Construction Research, report no. 97-NM-R0564.
- [10] De Buhant, P., De Felice, G. (1997). A homogenization approach to the ultimate strength of brick masonry. J. Mech. Phys. Solids, 45. No. 7. pp. 1085-1104.
- [11] Maier, G., Nappi, A. (1990). A theory of no-tension discretized structural systems. Engineering Structures, 12, pp. 227-234.
- [12] Alfaiate, J., De Almeida, J.R. (2000). Discrete cracking of masonry walls. European

- Congress on Computational Methods in Applied Sciences and Engineering ECCOMAS 2000, Barcelona, Spain.
- [13] Formica, G., Sansalone, V., Casciaro, R. (2002). A mixed solution strategy for the nonlinear analysis of brick masonry walls. Computer Methods in Applied Mechanics and Engineering, 191, pp.5847–5876.
- [14] Cecchi, A.,Sab, K. (2004). A comparison between a 3D discrete model and two homogenised plate models for periodic elastic brickwork. International Journal of Solids and Structures, 41, pp.2259–2276.
- [15] Chetouane, B., Dubois, F., Vinches, M., Bohatier, C. (2005). NSCD discrete element method for modeling masonry structures. International Journal for Numerical Methods in Engineering, 64, pp.65–94.
- [16]Casolo, S., Pena, F. (2007). Rigid element model for in-plane dynamics of masonry walls considering hysteretic behavior and damage. Earthquake Engineering and Structural Dynamics, 36, pp.1029–1048.
- [17] Augenti, N., Parisi, F. (2009). Non-linear static analysis of masonry structures. ANIDIS2009, Bologna.
- [18] Casolo, S., Milani, G. (2010). A simplified homogenization-discrete element model for the non-linear static analysis of masonry walls out-of-plane loaded. Engineering Structures, 32, pp. 2352-2366.
- [19] Gambarotta, L., Lagomarsino, S. (1997). Damage models for the seismic response of brick masonry shear walls. Part II: The continuum model and its applications. Earthquake Engineering and Structural Dynamics, 26, pp.441-462.
- [20] Mayorca, P., Meguro, K. (2003). Modeling Masonry Structures using the Applied Element Method. SEISAN-KENKYU, 55, pp. 581-584.
- [21] Worakanchana, K., Mayorca, P., Guragain, R., Navaratnanaj, S., Meguro, K. (2008). 3-D Applied element method for PP-band retrofitted masonry. 14th World Conference on Earthquake Engineering, Beijing, China.
- [22] Livesley, K. (1992). A computational model for the limit analysis of three-dimensional masonry structures. Meccanica (Netherlands), 27, pp.161-172.

- [23] Orduna, A., Lourenço, P. B. (2002). Cap Model for Limit Analysis and Strengthening of Masonry Structures. Journal of Structural Engineering, 129, No. 10.
- [24] Milani, G., Lourenço, P.B., Tralli, A. (2007). 3D homogenized limit analysis of masonry buildings under horizontal loads. Engineering Structures, 29, pp.3134–3148.
- [25] Gilbert, M., Casapulla, C., Ahmed, H.M. (2006). Limit analysis of masonry block structures with non-associative frictional joints using linear programming. Computers and Structures, 84, pp. 873–887.
- [26] Lourenço, P. B. (1995). Two approaches for the analysis of the masonry structures: micro and macro-modeling. HERON, 40, No.4.
- [27] Görgülü, Ü. (2002). Computational modeling of masonry. European Union SAFERR project, Kassel University, Germany.
- [28] Lourenco, P. B. (1996). Computational strategies for masonry structure, Delft University Press, The Netherlands.
- [29] Rivieccio, P.G. (2006). Homogenization strategies and computational analyses for masonry structures via micro-mechanical approach. PhD thesis, University of Napoli Federico II.
- [30] Hibbit, D., Karlson, B., Sorensen, P. (2002). ABAQUS/Standard theory manual. HKS.
- [31] Kanakubo, T., Shimizu, K., Kanda, T., Nagai, S. (2007). EVALUATION OF BENDING AND SHEAR CAPACITIES OF HPFRCC MEMBERS TOWARD THE STRUCTURAL APPLICATION. Proceedings of the Hokkaido University COE Workshop on High Performance Fiber Reinforced Composites for Sustainable Infrastructure System material modeling, structural design and application, Sapporo, Japan.
- [32] Triantafillou, T. C., Antonopoulos, C. (2000). Design of concrete flexural members strengthened in shear with FRP. Journal of Composites for Construction, Vol.4, pp.198–205.

Chapter 5

EXPERIMENTAL PROGRAM

15.1 Objective and Scope of Experiments

As it was explained in Chapter 3, ECC and AFRP sheet were selected as retrofit material options for URM wall in this research work. In order to evaluate the efficiency of them as well as to validate the analytical models proposed for each retrofitting technique, two series of experiments were conducted on the bare and retrofitted specimens. In-plane tests were performed on the small-size specimens such as shear triplet and diagonal compression tests. Also, in order to catch the compressive effect of ECC retrofitting, uniaxial compression test was conducted on the prism specimens.

The URM wall specimens were treated on surface with ECC overlay and AFRP sheet in both sides. In case of AFRP retrofitting, in order to avoid pre-mature debonding of the retrofit sheet, confining bands were applied to the specimens.

The test results of the retrofitted and bare specimens were compared to each other and the performance of each retrofitting method was evaluated. Also, the failure pattern and load-deflection behavior of both bare and retrofitted specimens were studied. Experimental procedure and the obtained results are described as follows.

15.2 ECC Retrofitting

5.2.1 Outline of Experiment

In order to catch the retrofit capability of ECC on URM wall, uniaxial compression and shear triplet tests were conducted on the small-size specimens. Two types of specimens were constructed and tested such as unretrofitted (refers to as U specimens) and retrofitted (refers to as R specimens). Comparison between the test results of these two series was used to evaluate the retrofit efficiency. Mechanical characteristics of materials such as the strength and stress-strain relation of masonry unit bricks, bed joint mortar and ECC mortar were obtained through testing and are discussed in the following parts.

5.2.2 Characterization of ECC

The components of ECC mortar - based on the mixture plan provided by the producing company- is shown in Table 5.1 ^[1]. The binder was consisted of cement and fly ash (type II specified in JIS A 6201), with a weight ratio of 7:3. The cement type was ordinary Portland cement (OPC) and the design air content was 15%.

In addition to above mentioned contents, the ECC mortar mixture contained some additives such as air entraining agent (AE) for adjustment of air content, calcium sulfoaluminate (CSA)-type expansive additive for reduction of drying shrinkage, low alcohol-type shrinkage reducing agent for reduction in the drying shrinkage, bio-saccharide-type thickening agent for flowability, fiber dispersibility and air entraining and high-range water reducing agent for flowability. The fiber type of the used ECC was poly vinyl alcohol (PVA) which its properties are shown in Table 5.2 [1]. More information about the effect of ECC components on its overall performance could be found on other research works [1,2,3].

Tests were conducted on ECC mortar to find the specific weight, mortar flow, compressive and flexural strength, ultimate tensile strain, modulus of elasticity and Poisson's ratio which are shown in Figures 5.1-5.6. Due to the relatively low workability of ECC mortar, for retrofitting purpose, the amount of super plasticizer (SP) in the mixture was increased up to 1.5 times (as shown in Tables 5.3 and 5.4 as CECP1-3 and BECP1-3 samples).

Information about the tested samples and mechanical properties of ECC mortar are shown in Tables 5.3 and 5.4. Compressive stress-strain diagram of ECC mortar (samples CEC7-9 & CECP1-2) is shown in Figure 5.7. Also, extreme fiber stress-strain diagram of ECC (samples BEC1-3 & BECP1-3) is shown in Figure 5.8 which is the result of three point bending test on prism samples. Tensile strain in Figure 5.8 is the strain measured at the bottom side of the specimen center. This strain was shown until the detachment of strain gauge from the ECC surface.

The compressive strain range of ECC was close to the one of ordinary concrete or mortar as shown in Figure 5.7. Also as it can be seen from Figure 5.8, tensile strains more than 1% for the most of the bending test samples were recorded.

The average flexural strength of samples BEC1-3 and BECP1-3 is indicated in Table 5.4. Due to the existence of fiber in ECC mortar, a very slow flexural failure mode along with a high ultimate tensile strain was observed.

The average compressive strength versus time diagram of ECC is shown in Figure 5.9.

Table 5.1 ECC mix proportion [1]

Water by Binder ratio W/B	Sand by binder ratio S/B	Water content W (kg/m³)	Fiber volume fraction $V_f(\%)$
0.32	0.41	382	2.1

Table 5.2 Properties of PVA fiber [1]

Fiber length L _f (mm)	Fiber diameter d _f (mm)	Fiber elastic modulus E _f (kN/mm ²)	Fiber Strength in standard test (N/mm²)	Specific gravity (g/cm ³)	Elongation (%)
12	0.039	43	1620	1.3	6

Table 5.3 ECC test sample properties

Sample	Test	Dimension (mm)	Age (days)
CEC1, CEC2, CEC3			7
CEC4, CEC5, CEC6	Compression	50 x 100	14
CEC7, CEC8, CEC9	Compression	30 X 100	28
CECP1, CECP2, CECP3			28
BEC1, BEC2, BEC3	Danding	40 x 40 x 160	28
BECP1, BECP2, BECP3	Bending	40 X 40 X 100	28



Figure 5.1 ECC mortar mixture



Figure 5.2 Flow test on ECC mortar



Figure 5.3 Compressive test on ECC



Figure 5.4 Compressive failure of ECC



Figure 5.5 Bending test on ECC



Figure 5.6 Flexural failure of ECC

Table 5.4 Mechanical properties of ECC mortar

Property	Amount	Sample	Age (days)
C: C. W: -1.4 (-/3)	1.53	CEC1-9 & BEC1-3	Fresh
Specific Weight (g/cm ³)	1.64	CECP1-3 & BECP1-3	1/10/511
Mortor Floyy (mm)	130	CEC1-9 & BEC1-3	Eragh
Mortar Flow (mm)	134	CECP1-3 & BECP1-3	Fresh
	12.07	Average of CEC7-9	20
Elastic Modulus (kN/mm ²)	15.8	Average of CECP1-2	28
Poisson's Ratio	0.210	Average of CEC7-9	28
Poisson's Ratio	0.203	Average of CECP1-2	28
	18.8	Average of CEC7-9	28
Compressive Strength (N/mm ²)	24.6	Average of CECP1-2	28
FI 1.6: (1.0)(2)	8.41	Average of BEC1-3	28
Flexural Strength (N/mm ²)	9.87	Average of BECP1-3	28

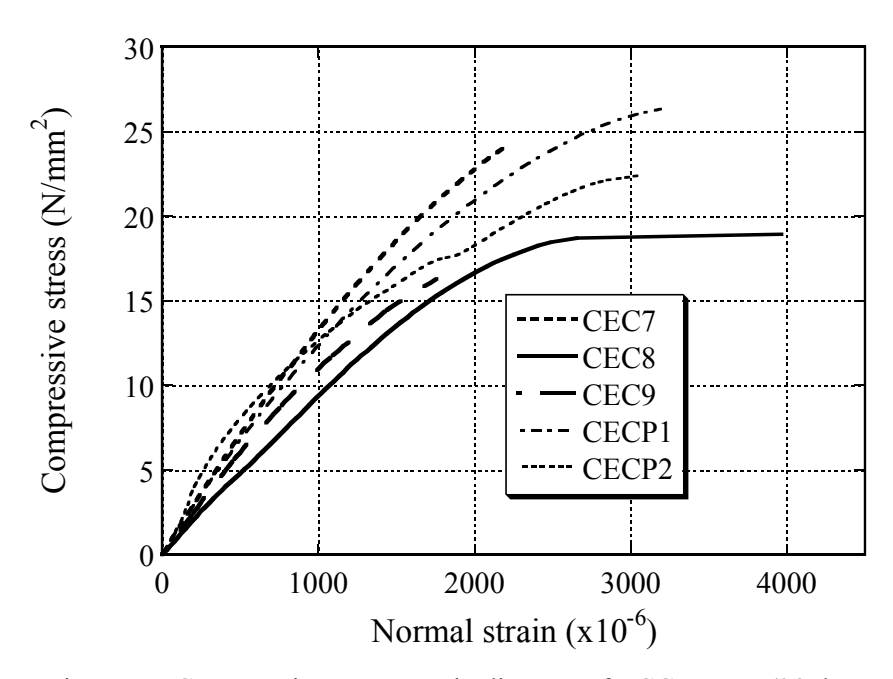


Figure 5.7 Compressive stress-strain diagram of ECC mortar (28 days age)

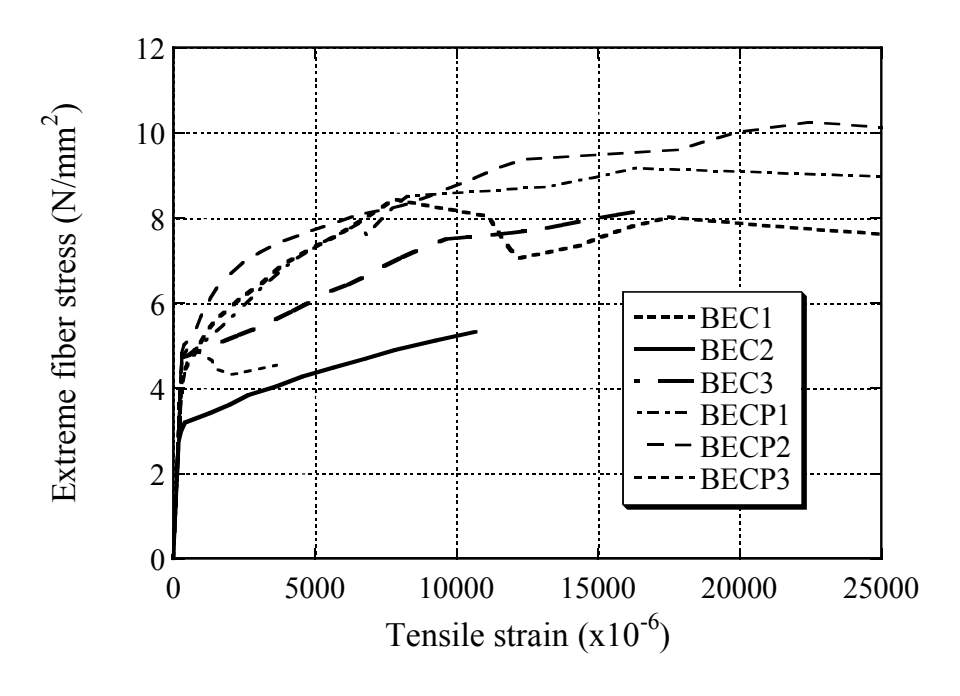


Figure 5.8 Extreme fiber stress-strain diagram of ECC mortar (28 days age)

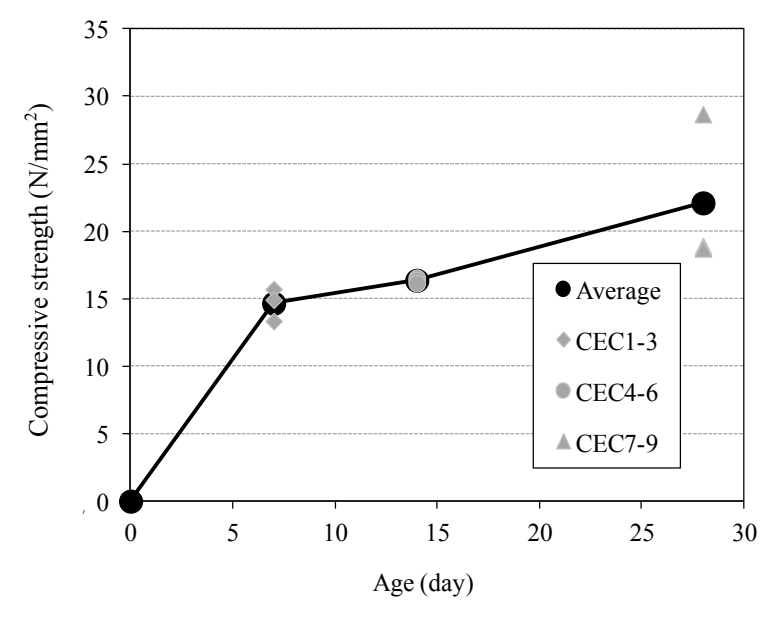


Figure 5.9 Compressive strength versus time diagram of ECC mortar

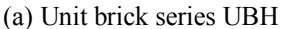
It must be mentioned that the mixing process of ECC mortar, its workability and treatment method are different from usual cement mortars and there is a need to special application system especially in case of shotcrete on the wall surface as it was reported by Lin et al. [4].

5.2.3 Properties of Masonry Brick

In order to find out the mechanical parameters of masonry unit brick such as modulus of elasticity, compressive and flexural strength, six masonry unit bricks were tested. The unit brick which was used in this study was a plain one (without holes) with average size of 210 mm x 110 mm x 60 mm. Three units out of them were tested under uniaxial compression (namely UBH1-UBH3) and three unit bricks were tested under three-point bending (namely UBB1-UBB3).

The loading sides of bricks were capped using a rapid-hardening cement mortar in order to provide a uniform force application surface. Two strain gauges were pasted on the both sides of each compressive specimen to obtain the deformational data, and in case of the bending specimens; strain gauge was pasted on the bottom tension surface of brick as shown in Figures 5.10(a) and 5.10(b), respectively. The average modulus of elasticity of the bricks (UBH series) was obtained as 17.7 kN/mm² and the average compressive and flexural strength of bricks were found as about 64.5 N/mm² and 9.0 N/mm², respectively.







(b) Unit brick series UBB

Figure 5.10 Masonry unit brick specimens

Table 5.5 Properties of masonry unit brick series UBH and RBH

Comple no	Aga (daya)	Dimensions (mm		Dimensions (mm)		- (NI/mm²)	A (N/2)
Sample no.	Age (days)	Length	Width	Height	$P_{max}(kN)$	$\sigma_{\rm max}({ m N/mm}^2)$	Ave. σ_{max} (N/mm ²)
UBH1	1	209.9	99.06	59.83	1262	59.541	
UBH2		209.01	98.42	59.14	1452	69.244	64.53
UBH3	1	210.49	99.69	59.86	1386	64.796	
RBH1	52	209.82	112.84	59.21	2434	100.851	
RBH2	52	210.61	120.23	59.17	2234	86.549	88.98
RBH3	52	210.14	114.7	58.6	1954	79.528	

Table 5.6 Properties of masonry unit brick series UBB

Commissions	Dir	mensions (m	 nm)	D (1:~f)	- 21/ 20	A (2)
Sample no.	Length	Width	Height	P _{max} (Kg1)	$\sigma_{bmax}(N/mm^2)$	Ave. σ_{bmax} (N/mm ²)
UBB1	209.35	98.76	59.45	1544	9.113	
UBB2	209.65	99.18	59.57	1220	7.141	8.97
UBB3	209.1	99.14	59.23	1800.5	10.665	

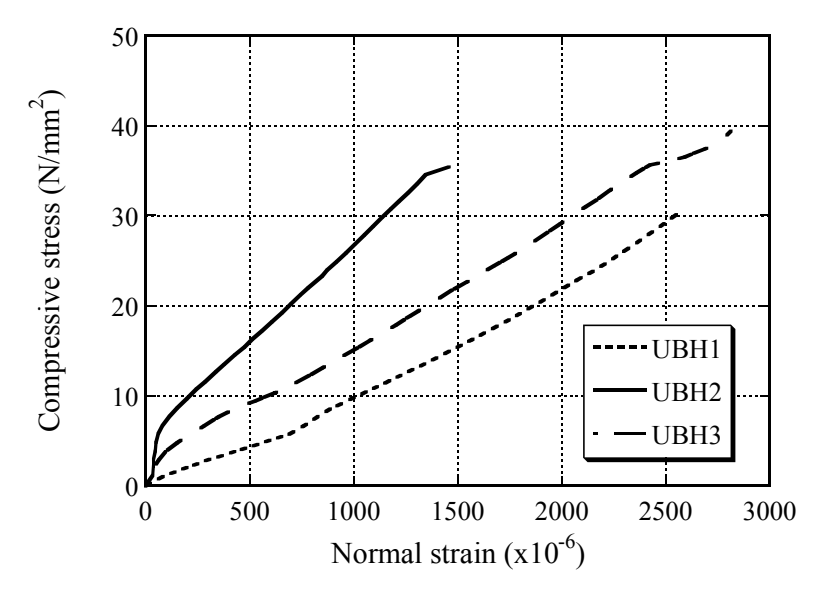


Figure 5.11 Compressive stress-strain diagram of masonry unit brick (UBH series)

The properties and compressive stress-strain diagram of unit brick specimen series UBH are shown in Table 5.5 and Figure 5.11, respectively. Also properties and flexural strength of UBB specimen series are shown in Table 5.6.

5.2.4 Properties of Bed Joint Mortar

In order to reach more realistic results from the study, bed joint mortar was prepared with a 28 days compressive strength as low as the one being used in common masonry construction in earthquake-prone regions.

This mortar was prepared by mixing of cement, sand, light weight silica powder blended with proportion of 1:6.5:1, respectively. Also w/c ratio was chosen equal to 130%. In order to measure the material constants of bed joint mortar such as compressive and flexural strength, compression and three-point bending tests were conducted on the cylindrical and prism samples, respectively (CBJ1-3 and BBJ1-3 samples in Table 5.7).

Deformational data was obtained by using two strain gauges for each cylindrical sample in both horizontal and vertical directions as shown in Figure 5.12. In case of the flexural specimens, strain gauge was pasted on the tension side of the prism.

Table 5.7 Bed joint mortar test sample properties

Sample	Test	Dimension (mm)	Age (days)
CBJ1, CBJ2, CBJ3	Compression	50 X 100	28
BBJ1, BBJ2, BBJ3	Bending	40 x 40 x 160	28

Table 5.8 Mechanical properties of bed joint mortar

Flow (mm)	157	
Specific Weight (g/cm ³)	1.96	
Elastic Modulus (kN/mm ²)	12.3	
Poisson's Ratio	0.158	
Compressive Strength (N/mm ²)	10.0	



Figure 5.12 Compressive test on bed joint mortar

Specific weight and compressive strength of bed joint mortar was calculated as 1.96 g/cm³ and 10.0 N/mm², respectively. Mechanical properties of bed joint mortar are shown in Table 5.8. Compressive and extreme fiber stress-strain diagrams of bed joint mortar are shown in Figures 5.13 and 5.14, respectively.

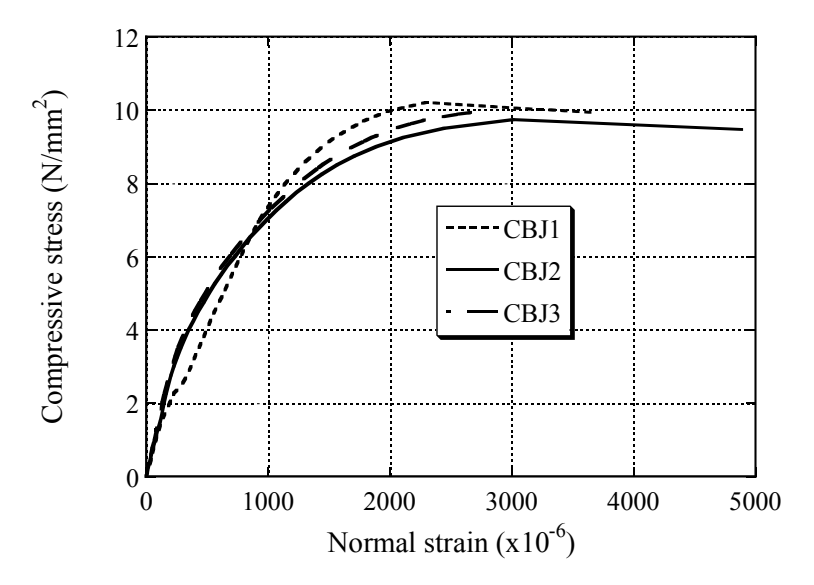


Figure 5.13 Compressive stress-strain diagram of bed joint mortar

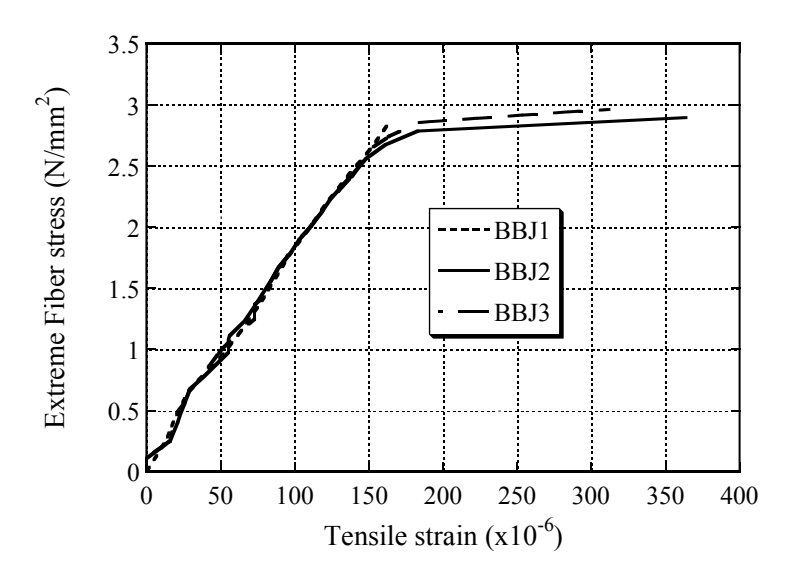


Figure 5.14 Extreme fiber stress-strain diagram of bed joint mortar

5.2.5 Masonry Test Specimens

The masonry specimen types which tests were conducted on and the corresponding test results are shown in Figure 5.15 and Table 5.9. Two series of masonry specimens were constructed such as triplet and prism. The construction process is shown in Figures 5.17-21.

Each series consists of both unretrofitted and retrofitted specimens. Also in order to grasp the effect of ECC overlay on the unit masonry brick, retrofitted unit bricks were also tested.

Due to the following reasons, thin layers of ECC mortar such as 10 mm and 20 mm were examined in the experiments:

- (a) Existence of fibers in ECC mixture makes it as a material with high capability in stress redistribution during the cracking process and thin layer of it can resist considerable deformations.
- (b) Considering the added mass in actual application and its seismic disadvantages, thin layer is desirable.
- (c) Using thicker layers makes it necessary to provide an appropriate shear transfer mechanism like shear keys between ECC and URM substrate. Application of shear keys to URM due to weak bed joint mortar and possible pre-loading damages, poses to numerous difficulties. These kind of damages can greatly affect the in-plane and out-of-plane behavior of URM wall and should be avoided.

Nine triplet specimens were constructed to obtain the shear effect of ECC retrofit. Three out of them (namely 10RT1-10RT3) were retrofitted by ECC mortar in both sides with thickness of 10 mm and other three ones (namely 20RT1-20RT3) were retrofitted in a similar way but with thickness of 20 mm. Three specimens (namely UT1-UT3) were left unretrofitted as control ones.

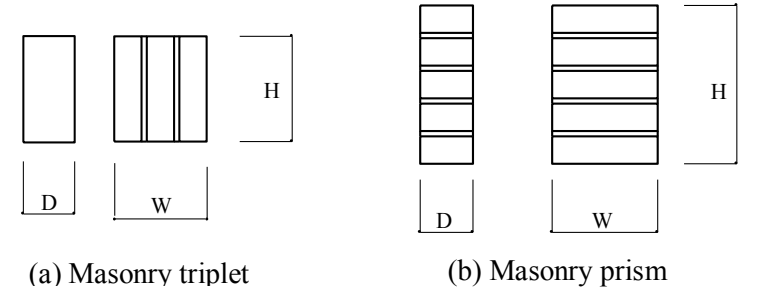


Figure 5.15 Masonry specimen forms





(a) RBH specimens

(b) RBB specimens

Figure 5.16 Retrofitted masonry unit bricks

Table 5.9 Masonry specimen types (ECC retrofitting)

Туре	Name	Dimensions (mm)		ECC Thickness			
		Width (W)	Depth (D)	Height (H)	(mm)	Age (day)	Pmax(kN)
Brick	UBH1	209.90	99.06	59.83	0	-	1262
	UBH2	209.00	98.42	59.14	0	-	1452
	UBH3	210.50	99.69	59.86	0	-	1386
	RBH1	209.80	112.80	59.21	10	49	2434
	RBH2	210.60	120.20	59.17	10	49	2234
	RBH3	210.10	114.70	58.60	10	49	1954
	UBB1	209.35	98.76	59.45	0	-	15.15
	UBB2	209.65	99.18	59.57	0	-	12
	UBB3	209.1	99.14	59.23	0	-	17.66
	RBB1	210.31	120.02	60.17	10	30	17.26
	RBB2	209.97	120.07	59.55	10	30	16
	RBB3	210.9	120.64	61.01	10	30	16.4
	UT1	191.00	99.12	209.70	0	378	39.6
Triplet	UT2	191.30	98.49	210.60	0	42	19.45
	UT3	189.00	99.72	212.40	0	378	19
	10RT1	192.00	120.30	212.50	10	378	72.5
	10RT2	194.00	117.70	211.20	10	378	72.9
	10RT3	191.60	119.60	212.20	10	42	72.4
	20RT1	191.80	136.00	213.20	20	42	95.6
	20RT2	195.00	138.80	212.90	20	378	109.6
	20RT3	195.00	137.50	212.90	20	378	119.8
Prism	UP1	210.00	98.65	337.70	0	378	820.5
	UP2	209.50	99.32	344.00	0	378	703
	UP3	210.30	100.20	340.50	0	42	634.5
	10RP1	210.40	121.70	338.20	10	42	688
	10RP2	209.80	119.30	336.00	10	378	730
	10RP3	210.60	119.90	337.30	10	378	760
	20RP1	210.90	138.40	341.00	20	42	664
	20RP2	210.80	138.30	341.70	20	378	795
	20RP3	210.50	137.60	340.30	20	378	738



Figure 5.17 Construction of UT specimens



Figure 5.18 Construction of UP specimens



Figure 5.19 Molding of RT specimens



Figure 5.20 Molding of RP specimens



Figure 5.21 Retrofitting of RT specimens

Nine masonry prism specimens were made with the height to length ratio about 1.6 to find out the compressive effect of ECC treatment. Three of these specimens (namely 10RP1-10RP3) were retrofitted by ECC mortar in both sides with thickness of 10 mm and other three ones (namely 20RP1-20RP3) were retrofitted with 20 mm thick mortar. Three specimens (namely UP1-UP3) were left bare.

Also six retrofitted unit brick specimens were provided. Three specimens (namely RBH1-RBH3) and the other three ones (namely RBB1-RBB3) were retrofitted for compressive and three-point flexural tests, as shown in Figures 5.16(a) and 5.16(b), respectively.

In all masonry specimens, the thickness of bed joint mortar was kept as about 10 mm. All specimens were cured after construction for at least 28 days. Then, they were retrofitted in both sides and cured again.

In order to provide an adequate cohesion between ECC overlay and URM, polymer dispersion primer liquid (ethylene vinyl acetate copolymer emulsion) was applied to masonry surface. This primer prevents the mortar water to be absorbed by the masonry substrate as well. Also in the all retrofitted specimens, load was applied on both masonry and ECC layer during the tests.

5.2.6 Test Procedure

5.2.6.1 Masonry Unit Bricks Tests

Two series of masonry unit bricks were provided such as bare and retrofitted. The arrangement of strain-gauges in retrofitted unit bricks is shown in Figure 5.16.

5.2.6.2 Shear Triplet Tests

Four displacement transducers were used to catch the deformational response of triplet specimens under a force control loading manner. A 19 mm thick steel plate and two 35 mm thick steel plates were used as the force application surface and base supports, respectively. Their arrangement is shown in the Figure 5.22(a).

5.2.6.3 Prism Tests

Masonry prism specimens were tested under compression normal to bed joints. To ensure a uniform pressure, steel plates are set on the top and bottom sides of the prisms. The strain

along the axis of the loading was measured using two displacement transducers on both shorter sides of the specimens as shown in Figure 5.22(b).





(a) Triplet specimen (specimen type 10RT3)





(b) Prism specimen (specimen type 10RP1)

Figure 5.22 ECC retrofitted masonry specimens

5.2.7 Test Results and Discussion

Test results are discussed in three parts such as masonry unit brick, shear triplet and prism tests. Failure mode and ultimate load, behavioral data such as stress-strain diagram and other mechanical characteristics were used as a basis to evaluate the effectiveness of the retrofitting method.

5.2.7.1 Masonry Unit Brick Tests

Both bare and retrofitted unit brick specimens were failed in a vertical splitting mode of brick along with the departing of ECC overlay in the retrofitted ones. However as it was observed, buckling of ECC overlay was occurred prior to brick failure. The failure mode of both retrofitted and bare unit bricks were shown in Figure 5.23. An increase about 38% in compressive strength of the retrofitted bricks (RBH) was observed as shown in Figure 5.24.

In case of UBB and RBB specimen series, flexural strength was not changed due to retrofitting.



(a) Specimen type UBH1

(b) Specimen type RBH3

Figure 5.23 Failure mode of masonry unit bricks

5.2.7.2 Shear Triplet Tests

The failure modes of triplet specimens are shown in Figure 5.25. Bare triplet specimen was failed through departing of brick and bed joint mortar at a very low displacement as shown in Figure 5.25(a). It can be explained as a result of weak bed joint mortar and low

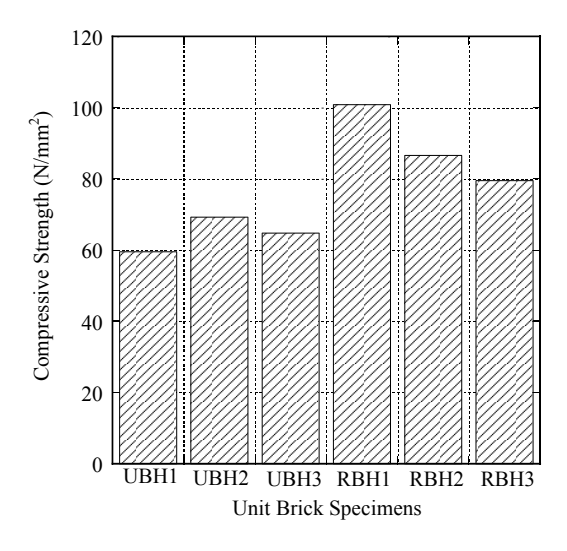


Figure 5.24 Compressive strength of masonry unit bricks

bond strength -calculated as about 0.46 N/mm²- between brick and mortar interface. Symmetrically developing cracks were observed in failure mode of the retrofitted triplet specimens as shown in Figure 5.25(b). Also, ECC overlay decreased the local weakness by preventing unsymmetrical failure mode.

Shear stress-strain diagram of both bare and retrofitted specimens are shown in Figure 5.27. Shear strength was considered as the maximum shear stress which specimens were





(a) Specimen type UT2

(b) Specimen type 10RT3

Figure 5.25 Failure mode of masonry triplet specimens

subjected to during the test. Also shear stress was calculated simply using maximum vertical load recorded during the experiment and the corresponding sectional area which is subjected to shear stress.

Shear strain induced by vertical compressive test load is shown by a schematic drawing in Figure 5.26, where γ shear strain, δ average relative displacement of the two adjacent brick center points, d is the distance between the brick centers and P is the compressive load. H and D are height and depth of specimen, respectively as indicated in Table 5.9.

Shear strain is calculated using following relation,

$$\gamma \cong \tan \gamma = \frac{\delta}{d} \tag{5.1}$$

Shear stress is simply calculated as follows,

$$\tau = \frac{P}{2A} \tag{5.2}$$

Figure 5.26 Shear strain in masonry triplet specimens

in which, the cross sectional area A is,

$$A = H \times D \tag{5.3}$$

For ECC retrofit overlay of thickness 10 mm, increase in shear strength was about 203% for specimens aged 42 days and 106% for 378 days. In case of ECC thickness of 20 mm, the

corresponding increase was about 251% for specimens aged 42 days and 179% for 378 days as shown in Figures 5.28 and 5.29.

Also deformation capacity of the retrofitted specimens was increased significantly as shown in Figure 5.27. The average deformation capacity – in this study refers to the deformation at 80% of maximum strength – of ECC overlay of thickness 10 and 20 mm at age of 378 days was about 33 and 28 times the one of deformation capacity at maximum strength of reference (bare) specimen, respectively.

The lower bound of this deformation capacity for the retrofitted specimens with 10 and 20 mm thick ECC overlay was obtained as about 20 and 27 times of the unretrofitted ones. The position of the above mentioned 80% strength was shown as point marks in all diagrams of Figure 5.27.

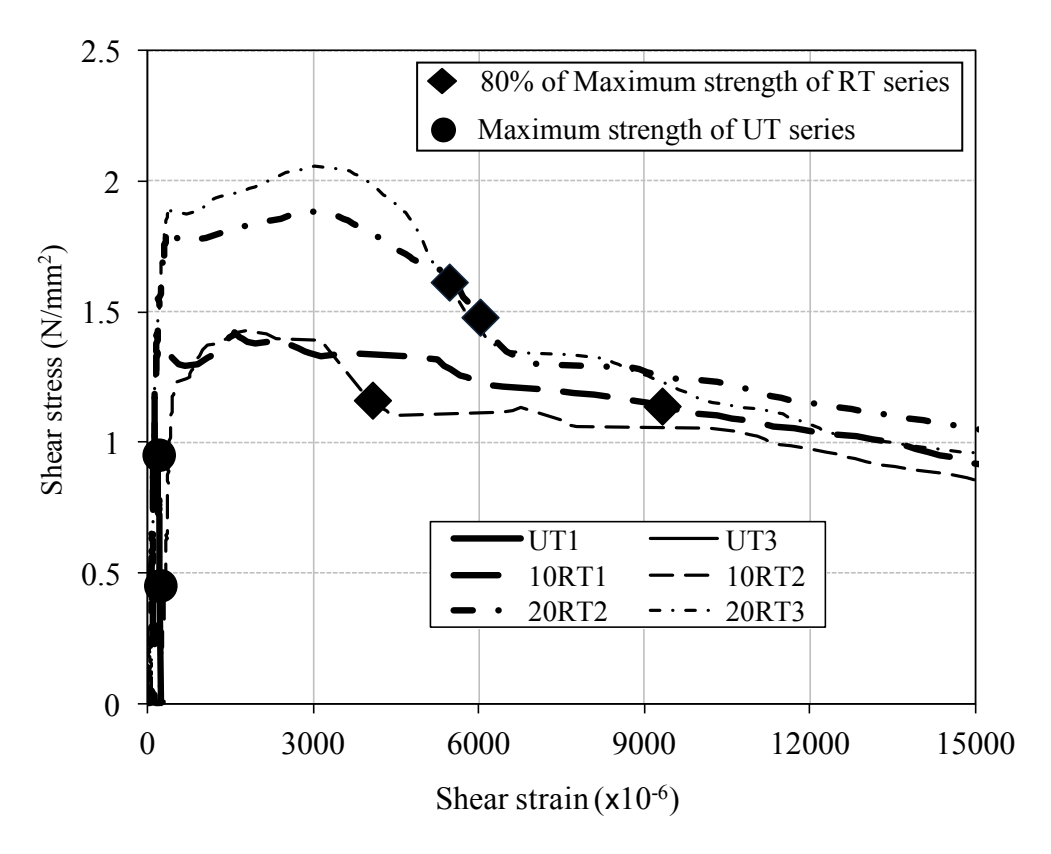


Figure 5.27 Shear stress-strain diagram of masonry triplet specimens aged 378 days

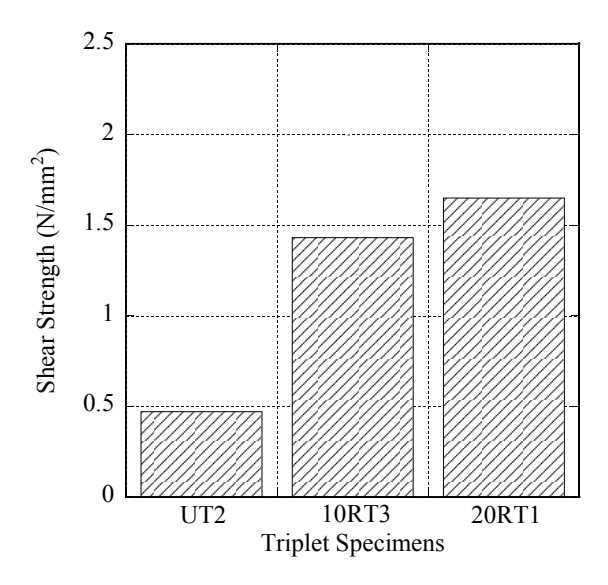


Figure 5.28 Shear strength of masonry triplet specimens aged 42 days

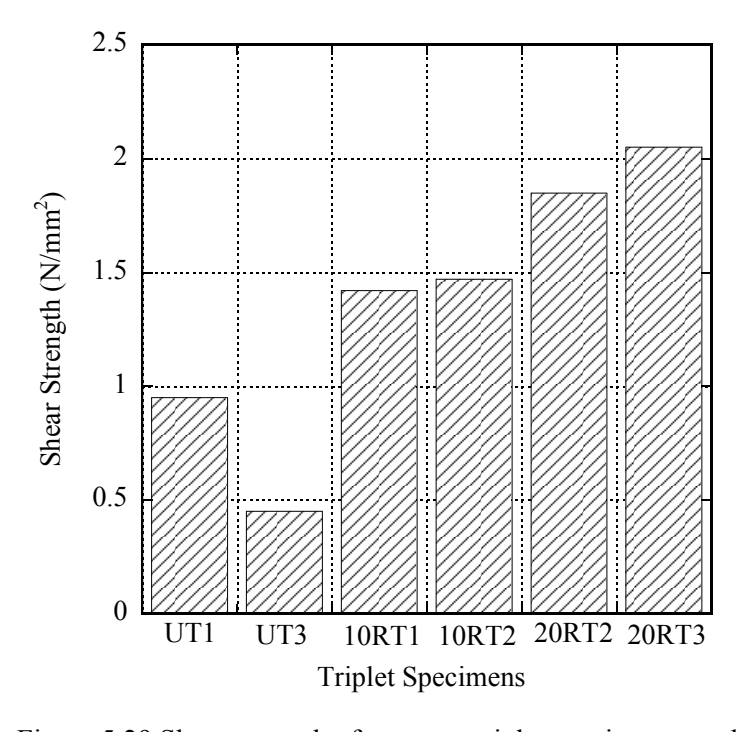


Figure 5.29 Shear strength of masonry triplet specimens aged 378 days

As it can be seen in Figure 5.27, higher shear strength and deformability of the retrofitted specimens can improve the energy dissipation capability of the URM specimens.

In some retrofitted specimens with ECC thickness of 20mm, detachment of ECC overlay from brick surface was observed. However in some of them, vertical tensile cracks were observed in side bricks prior to the detachment and resulted in their splitting.

5.2.7.3 Prism Tests

Failure mode of bare prism specimen was represented by vertical tensile cracks parallel to the loading direction. They appeared mostly on the longer sides of prism as shown in Figure 5.30(a). In case of the retrofitted specimens, due to the confining effect of ECC overlay, failure condition was similar to buckling behavior as shown in Figure 5.30(b).

Moreover, it was observed that in case of ECC overlay of 20 mm thick, detachment of ECC overlay from brick surface was started before the above mentioned buckling behavior.

Compressive stress-strain diagram of both bare and retrofitted prism specimens at age of 42 days are shown in Figure 5.31. The comparison between compressive strength and maximum compressive load bearing of the bare and retrofitted prisms are shown in Figures 5.32-5.35. The test results were shown in Figure 5.31 until the detachment of the displacement meters from the specimen but since the compressive force was still rising, the compressive strength shown in Figure 5.32 and the corresponding value in Figure 5.31 are different (for example in case of specimen type 10RP1).



(a) Specimen type UP3



(b) Specimen type 10RP1

Figure 5.30 Failure mode of masonry prism specimens

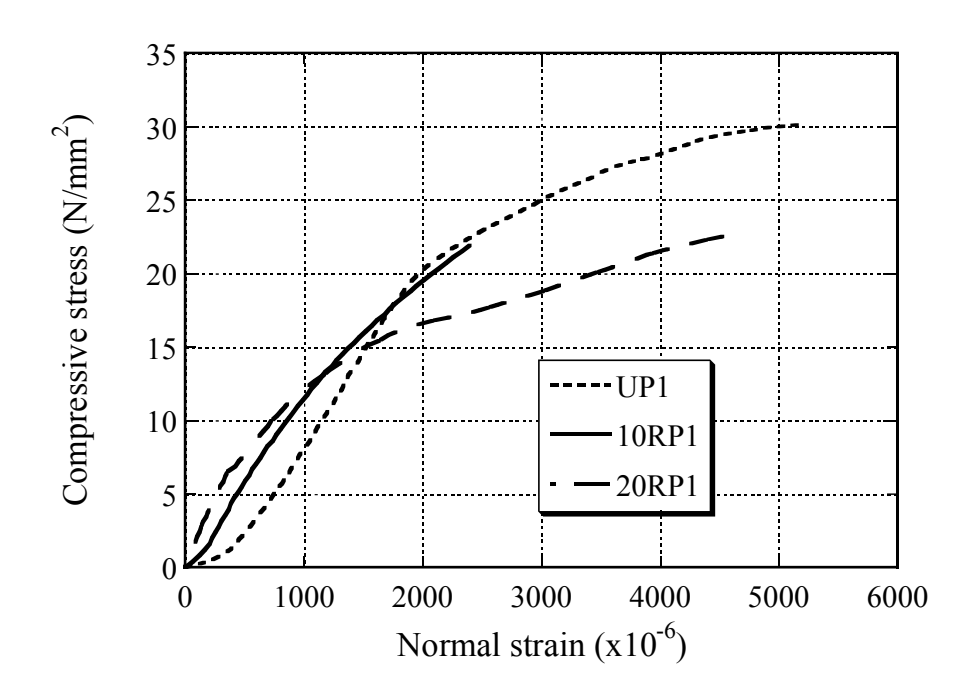


Figure 5.31 Compressive stress-strain diagram of masonry prism specimens aged 42 days

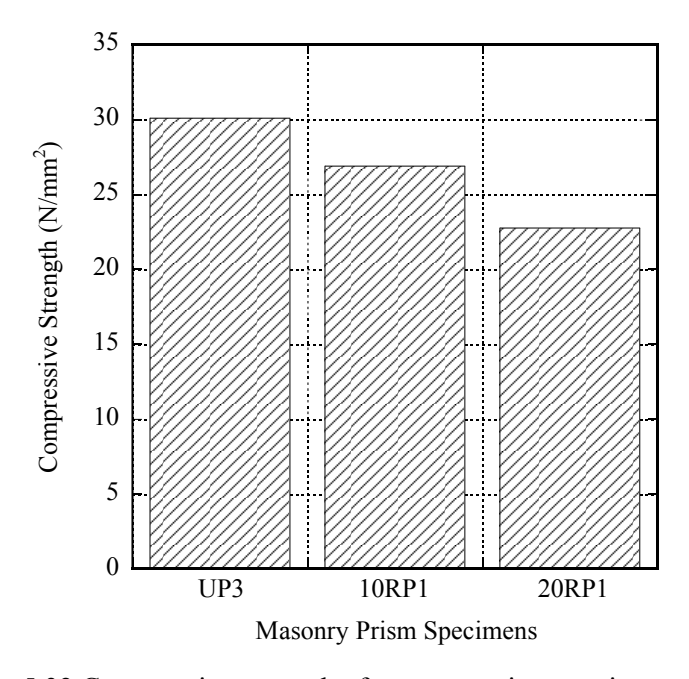


Figure 5.32 Compressive strength of masonry prism specimens aged 42 days

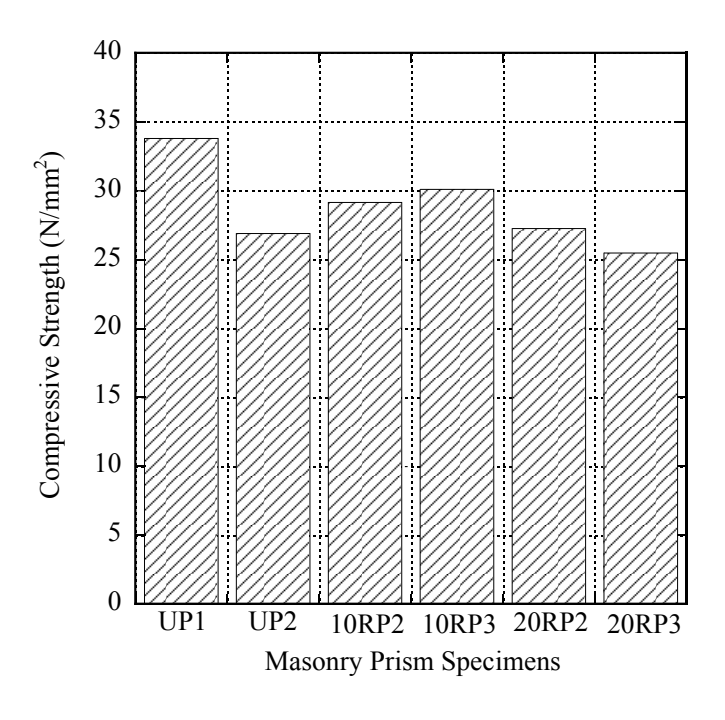


Figure 5.33 Compressive strength of masonry prism specimens aged 378 days

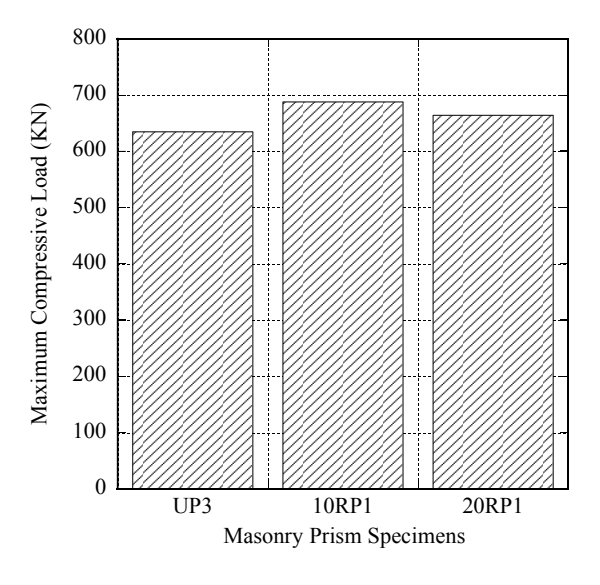


Figure 5.34 Maximum compressive load carried by masonry prism specimens aged 42 days

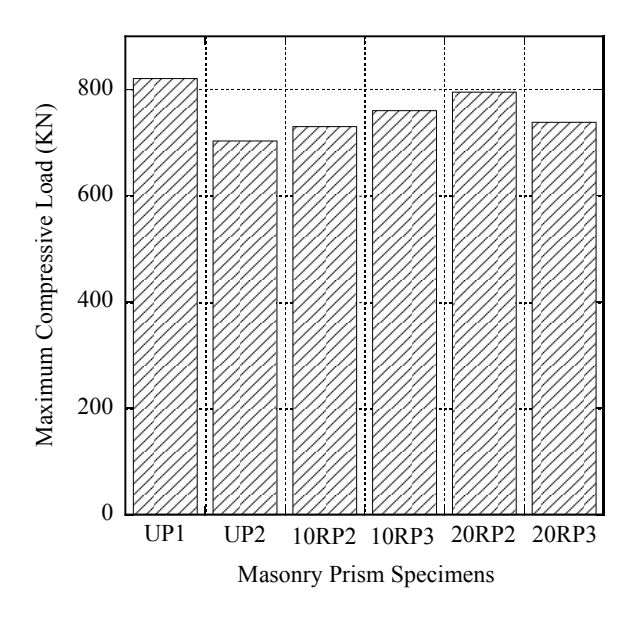


Figure 5.35 Maximum compressive load carried by masonry prism specimens aged 378 days

An improvement in initial stiffness of the retrofitted prism specimens was observed and it seems that the compressive strength of the retrofitted specimens was decreased compare to bare ones as shown in Figure 5.32. Based on the observation during the failure of the retrofitted prisms, part of compressive load was resisted by ECC overlay which buckled before the failure of the whole specimen and resulted in a lower compressive strength of the specimen. Therefore, ECC retrofitting did not have considerable effect on the compressive load bearing capacity of the specimens and the mechanical behavior of prism specimens under compression before and after retrofitting was almost the same.

In prism specimens, normal strain (ϵ) was calculated based on the average vertical displacements (δ) recorded by two side displacement meters as shown in Figure 5.36 by the following relation,

$$\varepsilon = \frac{\delta}{L} \tag{5.4}$$

in which L is the distance between centers of the second and fourth bricks. Also compressive stress is simply calculated by dividing the vertical force by the application area.

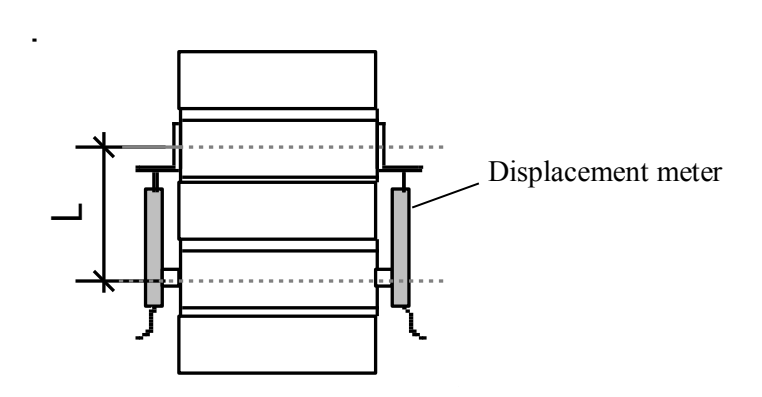


Figure 5.36 Configuration of prism test

5.2.8 Conclusion Remarks for ECC Retrofitting

By comparing the test results and the failure modes of unretrofitted and retrofitted URM specimens, the findings for ECC retrofitting techniques are summarized as follows:

- (1) Shear resistance of triplet specimens increased significantly. For ECC retrofit overlay of thickness 10 mm, increase in shear strength was about 203% for specimens aged 42 days and 106% for 378 days. In case of ECC thickness of 20 mm, the corresponding increases were about 251% for specimens aged 42 days and 179% for 378 days.
- (2) Deformation capacity of the retrofitted triplet specimens increased significantly. The deformation capacity (in 80% of maximum capacity) of ECC retrofit of thickness 10 and 20 mm at age of 378 days was about 33 and 28 times the one of reference (bare) specimens, respectively.
- (3) ECC retrofitting changed the brittle failure mode of the URM to a ductile and developing failure which means a better energy dissipation behavior.
- (4) Symmetric developing cracks in the failure mode of shear triplet test showed a considerable improvement in brittle behavior of URM.

(5) ECC retrofitting does not have considerable effect on the compressive load bearing capacity.

Due to significant improving effect of ECC on shear behavior of specimens, it can be considered as a suitable in-plane retrofitting method for URM walls.

5.3 AFRP Retrofitting

5.3.1 Outline of Experiment

In order to grasp the shear effect of AFRP sheet retrofitting on the URM wall specimens, diagonal compression tests were conducted on the small-size wall specimens. The results of such an experimental study can be used for evaluating the behavior of the retrofitted masonry wall.

5.3.2 Material and Specimen Specification

Inclination degree (θ) of specimens was about 48° as shown in Figure 5.37. The specimen types which tests were conducted on are shown in Figure 5.38. The specifications of specimens, aramid sheet - which was suggested by producing company [5] – and test results, are shown in Tables 5.10-12. The construction process is shown in Figures 5.39-5.44.

The brick used for the construction of specimens was the same as the one used in ECC retrofitting with approximate dimensions of 210 mm x 110 mm x 60 mm with an average compressive strength of 64.5 N/mm². The compressive strength of the bed joint mortar - with similar mixture as ECC retrofitting phase - used in the construction of specimens series A and B were measured as 14.6 N/mm² (63 days age) and 17.3 N/mm² (119 days age), respectively.

In order to avoid pre-mature debonding of AFRP sheet, aramid bands were applied to the top and bottom of the specimens. This method has previously been applied to the retrofitting of RC columns with wall ^[6].

Two bands at top and bottom of specimens were considered as the minimum requirements to ensure proper confining efficiency. They were wrapped around the specimens and were fixed using adhesive. In application of the band to actual building, a sewing like method can be used in which the aramid band passes through the holes created in URM wall and confines the sheet in both side of URM wall. This method is shown as a schematic illustration in

Figure 5.45.

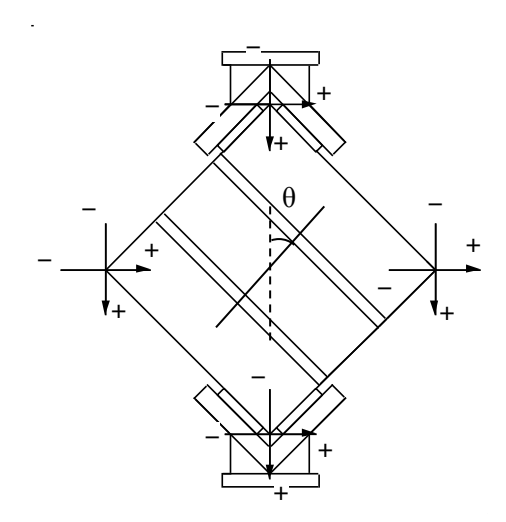


Figure 5.37 Configuration of diagonal compression test

Table 5.10 Specimen specifications (AFRP Retrofitting)

Cracinan	Dimension (mm)			Datrafitting gahama	D (leN)
Specimen	Width (W)	Depth (D)	Height (H)	Retrofitting scheme	$P_{\text{max}}(kN)$
A12	209.65	100.09	189.03	Unretrofitted	150.2
A21	209.01	102.08	192.59	Sheet A	139.1
A22	209.51	102.12	190.80	Sheet A	137
A31	209.64	102.58	191.34	Sheet A + Band A	196.4
A32	210.74	102.52	194.45	Sheet A + Band A	174.6
B11	331	99.4	271.5	Unretrofitted	60.0
B12	324	100.4	272.6	Unretrofitted	36.2
B21	328	103.3	298.4	Sheet B1 + Band B	127.6
B22	329	101.9	299.6	Sheet B1 + Band B	114.8
B31	329	103.9	274.1	Sheet B2 + Band B	120.8
B32	328	104.5	278.2	Sheet B2 + Band B	127.9

Table 5.11 Aramid sheet specifications

Sheet type	Material	Dimension (mm)	Thickness
A	AK-10/10	190 x 180	1 layer
B1	AK-10/10	310 x 250	1 layer
B2	AK-20/20	310 x 250	1 layer
Band A	AK-90	20 x (640 + 250 overlap)	3 layers
Band B	AK-90	20 x (900 + 250 overlap)	3 layers

Table 5.12 Aramid sheet material specifications

Material	Weight (g/m ²)	Tensile capacity (kN/m)	Thickness (mm)	Tensile Strength (N/mm ²)	Young's Modulus (kN/mm2)
AK- 10/10	180	98/98	0.048		
AK- 20/20	325	196/196	0.096	2060	118
AK-90	623	882	0.430		

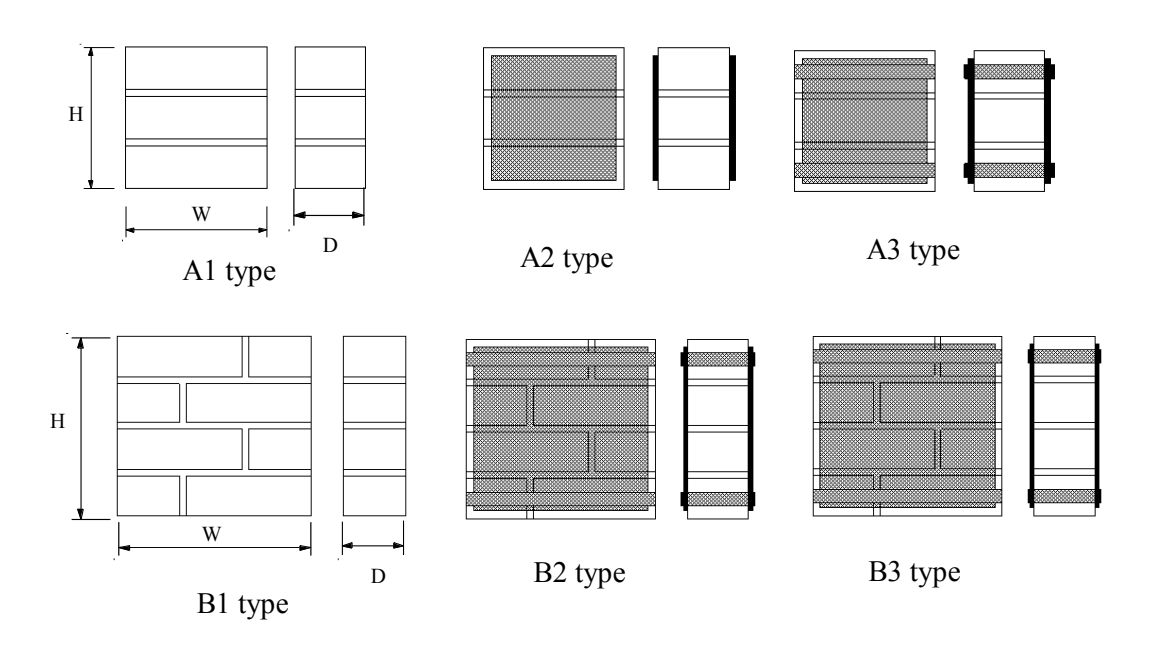


Figure 5.38 Specimen types (AFRP Retrofitting)



Figure 5.39 Application of primer



Figure 5.40 Surface treatment using putty



Figure 5.41 Application of adhesive



Figure 5.42 Removing air with roller



Figure 5.43 Coating with adhesive



Figure 5.44 Wrapping confining bands

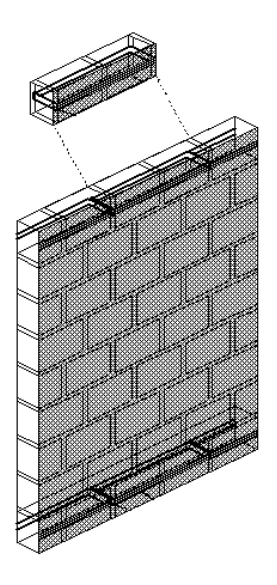


Figure 5.45 Application of AFRP band to URM wall

Width of the aramid band was decided in the way that it covers sheet without being in touch with bed joint mortar. Also the application of the band to actual URM wall was considered in which creating holes in wall for wide bands is almost impossible. As a result, considering the average height of a unit brick (about 60 mm), 20 mm was decided as the width of the aramid band. Also in order to eliminate pre-mature debonding of aramid sheet and ensure the maximum possible efficiency of it, three layers of band were applied. The application of aramid sheet consisted of the following five steps as shown in Figures 5.39-44:

- 1) Cleaning of specimen surface and application of primer
- 2) Surface treatment using putty to make a flat surface
- 3) Application of adhesive
- 4) Wrapping sheet and removing air with roller
- 5) Coating with adhesive

Three types of material for primer, putty and adhesive were used which all were mainly based on epoxy resin adhesive and each of them consisted of two parts as main and hardening components.

5.3.3 Shear stress and strain in diagonal specimens

Shear strain induced by vertical compressive load is shown by schematic drawings in Figure 5.46, where γ shear strain, δ displacement of the specimen edge, δ_H relative diagonal deformation of specimen in horizontal direction, δ_V relative diagonal deformation of specimen in vertical direction, L diagonal length, θ inclination degree and P is the compressive load. W, H and D are width, height and depth of specimen, respectively.

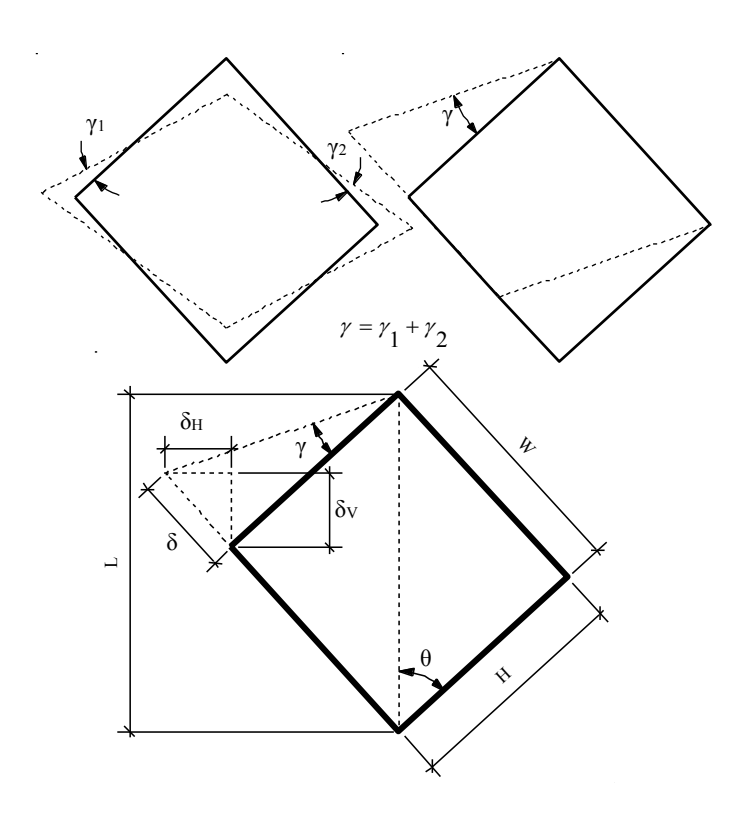


Figure 5.46 Shear strain in diagonal specimen

Shear strain is calculated based on the following relation,

$$\gamma \cong \tan \gamma = \frac{\delta}{H}$$
 in which,

$$\delta = \delta_H \cos \theta + \delta_V \sin \theta \tag{5.6}$$

In the case of $\theta = 45^{\circ}$, relation (5.5) can be written as:

$$\gamma = \frac{\delta_H + \delta_V}{L} \tag{5.7}$$

which is recommended by ASTM [7].

Shear stress is simply calculated by the following relation,

$$\tau = \frac{P\sin\theta}{A} \tag{5.8}$$

in which, the cross sectional area A is:

$$A = W \times D \tag{5.9}$$

5.3.4 Test Results and Discussion

Failure of unretrofitted specimens (A1and B1 types) was represented by departing of brick and bed joint mortar in a very low displacement. Also, splitting of bricks was observed in some specimens. In the case of specimens type A2, departing of aramid sheet from brick surface was followed by brick sliding and rupture of sheet along the adjacent bed joint. In the case of A3, B2 and B3 specimen types, failure was started by debonding of sheet and its rupture at a place close to the confining band located in top and bottom of specimens and followed by diagonal cracks passing both brick and bed joint mortar (Figures 5.47 and 5.48).

Shear stress-strain diagram of specimens A and B are shown in Figure 5.49 and Figure 5.50, respectively. As it is shown in Figure 5.51, shear strength of specimens A31 and A32 compare to specimen A12 increased about 28% and 13%, respectively. In case of series B, compare to specimen B1 type, shear strength of specimen types B2 and B3 increased about 146% and 149%, respectively as shown in Figure 5.52.

Higher shear strength obtained from the retrofitted specimens with aramid sheet and band compare to ones retrofitted with sheet only shows the confining effect of it on specimen strength and ductility as observed during the failure of specimens.

Through the same method used for evaluation of deformability in ECC test results, A2 type showed ductility about 4.5 times bare A1 type. Also B2 and B3 types showed ductility about 4 and 5.5 times bare B1 type.

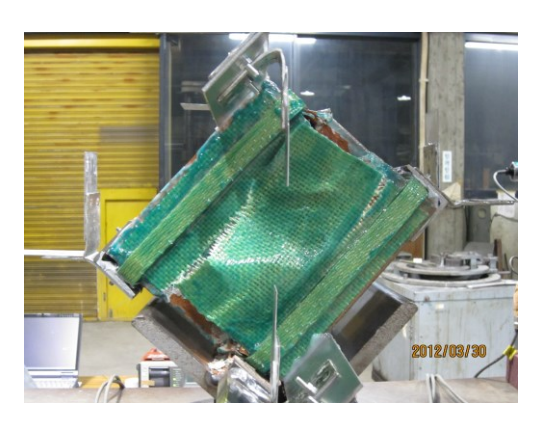
There is a difference between the results of A and B series for both bare and retrofitted specimens. This can be attributed to the size effect of the specimens.

The bond characteristics between brick and aramid sheet (FRP sheet in general) play the key role in the debonding behavior of the sheet and consequently governs the performance of AFRP-URM retrofit technique.

This bond behavior was not studied at present stage of study. However, this fact has been investigated in some research works recently [8].

Also some retrofitting codes [9] introduced slip-shear strength models which are mainly based on the bond studies of concrete- FRP and further investigations are needed in order to propose a rational model for FRP-URM bond behavior.





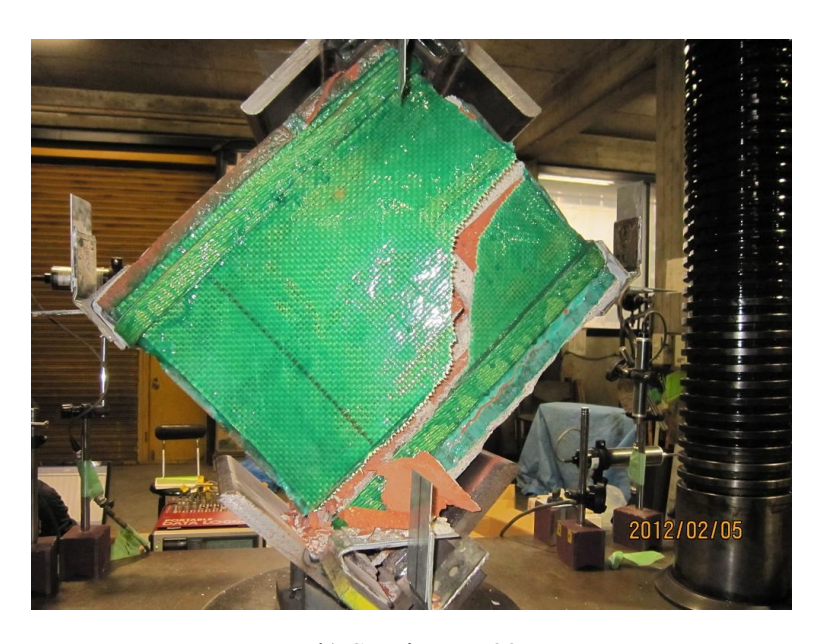
a) Specimen A21

b) Specimen A32

Figure 5.47 Failure mode of retrofitted specimens type A



a) Specimen B12



b) Specimen B22

Figure 5.48 Failure mode of bare and retrofitted specimens type B

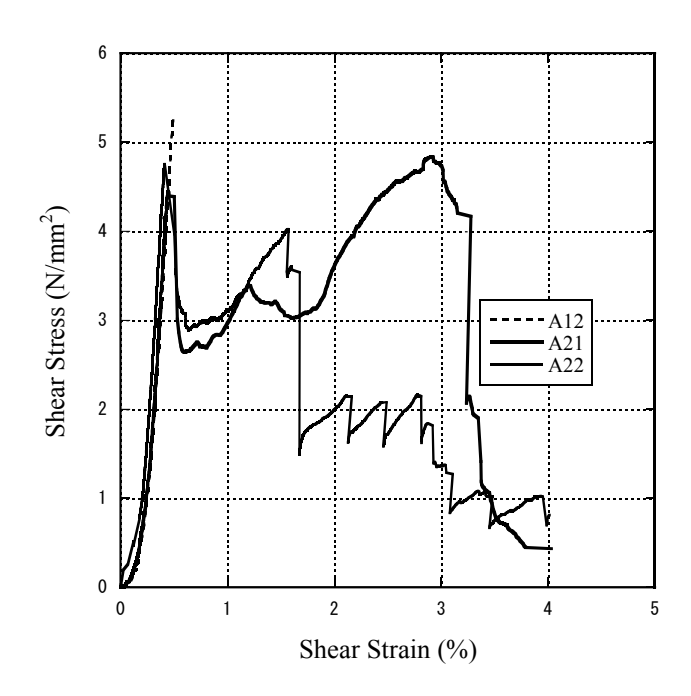


Figure 5.49 Shear stress-strain diagram of specimens type A

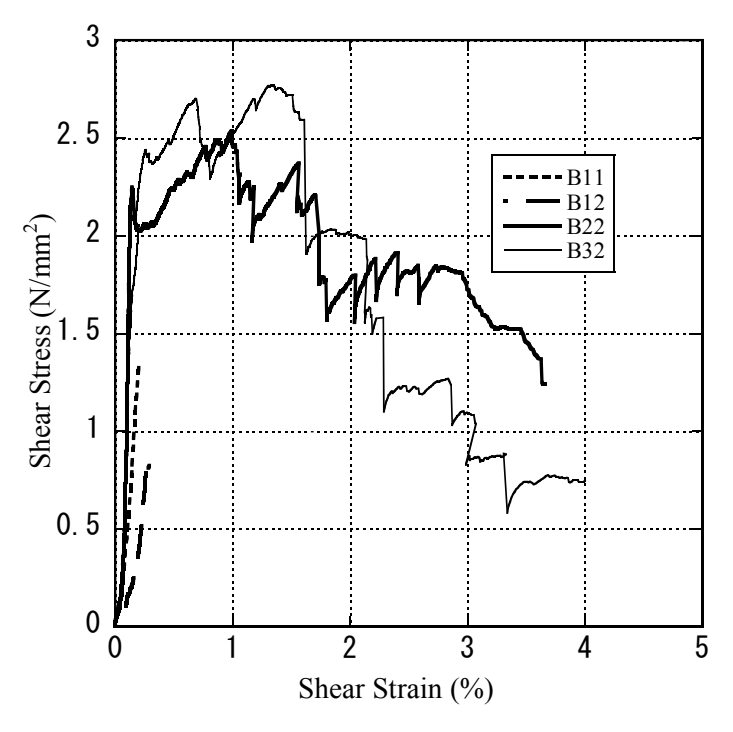


Figure 5.50 Shear stress-strain diagram of specimens type B

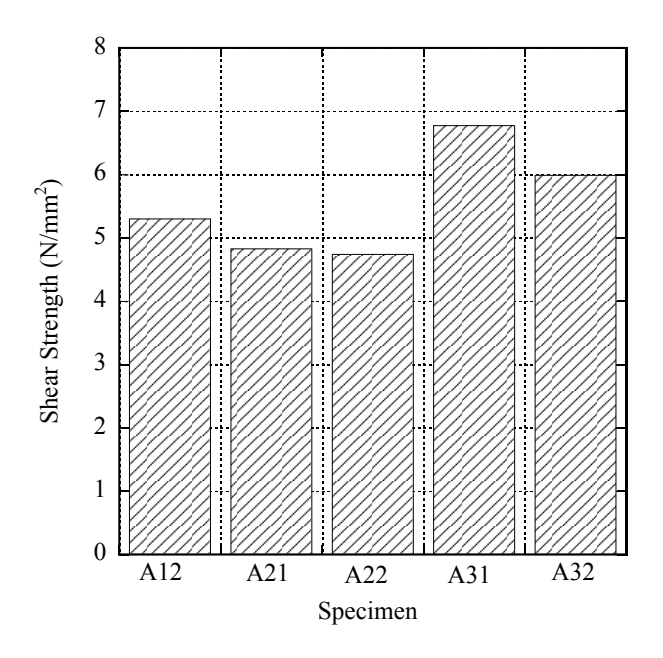


Figure 5.51 Shear strength of specimen series A

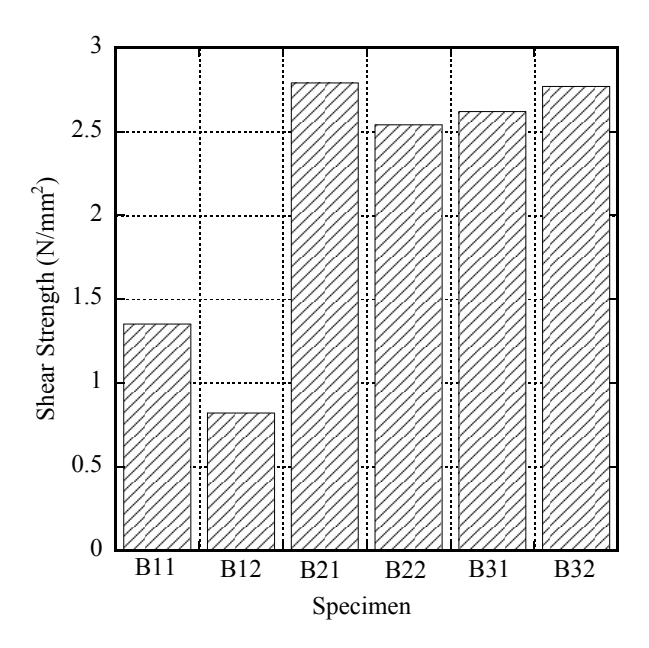


Figure 5.52 Shear strength of specimen series B

5.3.5 Comparison to Other Retrofitting Methods

Here, results of AFRP retrofit study in terms of shear and deformation capacity were compared to some other retrofitting methods which are available in literature [10].

The comparison is shown in Table 5.13. V_{URM} and V_{RM} are referred to shear capacity of unreinforced and retrofitted masonry, respectively. Also D_{URM} and D_{RM} are the deformability of URM and retrofitted ones. The average test results of the specimens type B were shown in this table.

Comparison revealed that AFRP retrofitting compare to other methods shows a relatively fine balance between shear capacity and deformability enhancement.

Progressive cracking is mostly responsible for brittle in-plane failure which is originated from the low deformation capacity and leads to low energy dissipation capability of unreinforced masonry walls. In-plane failure mode is mainly governed by the first cracks generally occur in weak interface between brick and mortar during the application of lateral loads. Also the failure pattern and geometrical non linear behavior of the URM wall are greatly influenced by cracking. Therefore, although improving of the shear strength of the wall is vital, in order to avoid brittle failure and dissipating seismic energy, deformation capacity should be enhanced as well. In order to reach such deformability, the non-ductile debonding of AFRP overlay - in case of this study - must be prevented which was achieved by utilizing confining band.

Also it should be mentioned that some other factors influence the evaluation of the efficiency of strengthening techniques. Parameters such as added mass to structure, alteration

Table 5.13 Comparison of AFRP retrofitting to other methods

Retrofitting method	V_{RM}/V_{URM}	D_{RM}/D_{URM}
Shotecrete	3	1
Polymer band	1	2.5
Steel strip	1.9	_
Polymer grids	1.2	2
Ferrocement	1.5	1.7
AFRP (this study)	1.48	4.75

to the shear stiffness, corrosion potential, anchorage problem to wall substrate, creation of zones with different stiffness.

AFRP sheet and FRP laminates in general have a very low alteration to the original mass and stiffness of the wall.

Moreover, there are some non-technical advantages and disadvantages of different retrofitting methods such as cost, space reduction and alteration to the original architectural features of URM structure [11]. As a result, due to numerous affecting parameters when it comes to the efficiency evaluation of a retrofit method, decisions should be made carefully.

5.3.6 Conclusion Remarks for AFRP Retrofitting

Comparing the test results and the failure modes of unretrofitted and AFRP retrofitted masonry specimens, the following conclusion remarks were found out:

- (1) Shear strength of specimens A31 and A32 compare to bare specimen A12 were increased about 28% and 13%, respectively.
- (2) Compare to bare specimen B1, shear strength of specimens B2 and B3 were increased about 146% and 149%, respectively.
- (3) A2 type showed ductility about 4.5 times of bare A1type specimen.
- (4) B2 and B3 types showed ductility about 4 and 5.5 times of bare B1type.
- (5) Beneficial effect of confining band on strength and ductility was observed.

Considering the beneficial effect of AFRP sheet on the shear strength and deformation capacity of URM specimens, it can be considered as a suitable retrofitting method.

References

- [1] Kanda, T., Saito, T., Sakata, N., Hiraishi, M. (2003). Tensile and anti-spalling properties of direct sprayed ECC, Journal of Advanced Concrete Technology, Japan, Concrete Institute, Vol.1, No.3, pp.269-282.
- [2] Li, V. C. (2003). On engineered cementitious composites (ECC) A review of the material and its applications, Journal of Advanced Concrete Technology, Japan Concrete Institute, Vol.1, No. 3, 215-230.
- [3] Li, V. C. (2008). Engineered cementitious composites (ECC) Material, structural, and durability performance, Concrete Construction Engineering Handbook, Chapter 24, Ed. E. Nawy.
- [4] Lin, Y.-W., Lawley, D., Ingham, J.M. (2010). Seismic strengthening of an unreinforced masonry building using ECC shotcrete, 8th International Masonry Conference, Dresden, Germany, pp.1461-1470.
- [5] FIBEX Co. Ltd. http://www.fibex.co.jp/index.html
- [6] Hanai, N., Kosugi, K., Ichinose, T., Shirakawa, T. (2011). Experiments on aramid fiber retrofit for RC columns with walls, Journal of Structural and Construction Engineering (Transaction of AIJ), Vol. 76, No. 659.
- [7] American Society for Testing and Materials (ASTM). (2002). Standard test method for diagonal tension (shear) in masonry assemblages.
- [8] Ghiassi, B., Marcari, G., Oliveira, D.V., Lourenco, P.B. (2012). Numerical analysis of bond behavior between masonry bricks and composite materials, Engineering Structures, Vol. 43, pp. 210-220.
- [9] National Research Council of Italy (CNR). (2009). CNR-DT200. Guide for the design and construction of externally bonded FRP systems for strengthening existing structures.
- [10] ElGawady, M., Lestuzzi, P., Badoux, M. (2004). A review of conventional seismic retrofitting techniques for URM. 13th International Brick and Block Masonry Conference, Amsterdam.
- [11] Zamani Ahari, G., Yamaguchi, K. (2010). A Proposal of the Most Suitable Retrofitting Methods for URM Structures in Iran An Extensive Review of Recent Techniques.

Journal of Habitat Engineering , Volume 2, Number 2, pp.105 - 114.

Chapter 6

ANALYTICAL STUDY

6.1 Analysis Procedure

In order to predict the in-plane behavior of the ECC and AFRP retrofitted URM wall, analytical study was carried out. A simple shear model was proposed for prediction of the shear strength of ECC-URM and the obtained results were validated by experimental data. Efficient strain approach -which has originally been developed for design of the FRP retrofitted concrete members-, is adopted for URM. The effect of confining band system and its contribution to the efficient strain of AFRP sheet was evaluated and discussed.

Finite element analysis was conducted for both of ECC and AFRP retrofitted URM specimens employing simple micro-modeling technique. An elasto-plastic tensile model was adopted for ECC. Also a new approach was proposed for AFRP retrofit model using a bilinear constitute law for AFRP-resin homogenized material. Calibration of the models was done by adjustment of the behavior of modeled unreinforced specimens to the corresponding experimental data. Then the results of numerical analysis for the retrofitted specimens were validated with experimental data in terms of load resistance and deformability. As a result, good agreement was achieved for both ECC and AFRP retrofit models.

6.2 Simple Shear Model for ECC Retrofitted Triplet Specimens

From the shear experiment conducted on triplet specimens, it was observed that the shear cracks in ECC layer formed along the vertical bed joints between bricks. Also, the propagation of cracks was symmetrical in both sides of the specimens as shown in Figure 6.1.

From experimental observation, shear failure of the bare triplet specimens occurred in a very small displacement while the corresponding deformation in the retrofitted ones was much larger. So as it was expected, since both triplet and ECC were under vertical load, middle brick was departed from the side ones at early stage of loading and the ECC layer provided shear load resistance up to the failure of specimen. Therefore, the final shear



Figure 6.1 Crack propagation in ECC retrofitted triplet specimens

strength of ECC retrofitted triplet is equal to the shear resistance provided by ECC overlay.

As shown in Figure 6.2, assuming a perfect bond between ECC layer and masonry substrate, will result in a equal displacement in masonry and the attached ECC overlay (δ_m = δ_{ecc}). Shear strength of the retrofitted triplet can be calculated by the following relations where V, V_m , V_{ecc} are the provided shear load resistance by the retrofitted assemblage, unreinforced masonry and ECC layer, respectively.

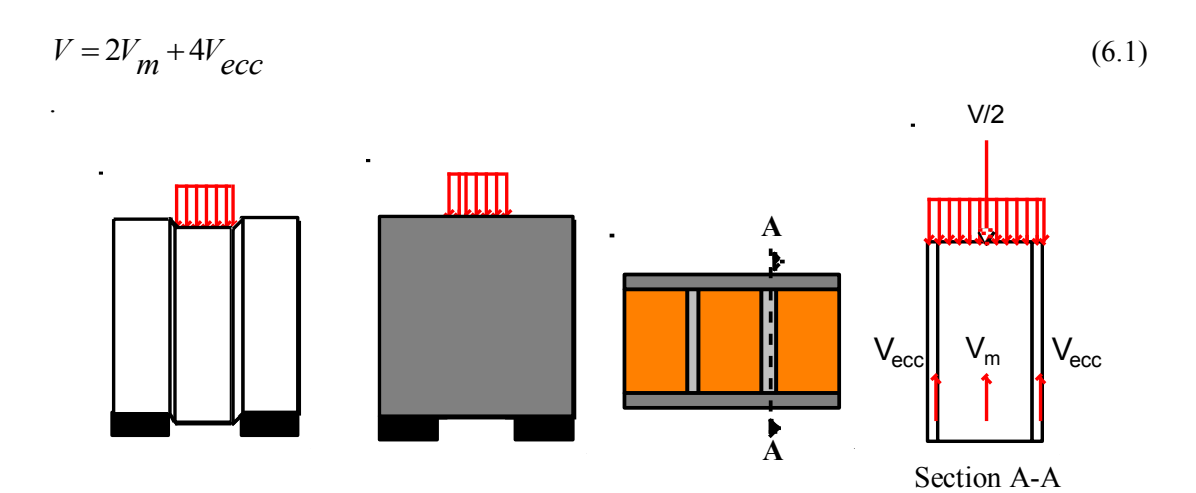


Figure 6.2 Shear force equilibrium in ECC retrofitted triplet specimens

In case of bare masonry, according to classic Coulomb law,

$$V_m = c + \mu N \tag{6.2}$$

where c, bond strength between brick and bed joint mortar, μ , friction coefficient and N is the applied force normal to brick-mortar interface plane.

Since no confining load was applied in triplet tests,
$$N=0$$
 and then, $V_m=c$ (6.3)

In case of ECC overlay,

$$V_{ecc} = f_{vecc} A_{ecc} \tag{6.4}$$

$$A_{ecc} = t_{ecc}h_b \tag{6.5}$$

where f_{vecc} is the characteristic shear strength of ECC and A_{ecc} is the sectional area which is subjected to shear loading. t_{ecc} and h_b are thickness of ECC layer and height of brick or triplet specimen, respectively. According to Li et al [1], shear strength of ECC mortar is about 1.5 times of its ultimate tensile strength obtained from uniaxail tensile test (f_{tu}). Then,

$$f_{Vecc} = 1.5 f_{tu} \tag{6.6}$$

In the experimental program of this research work, three-point bending test has been conducted on ECC prism samples. As it was studied by Kanakubo et al $^{[2]}$, it was found out that the uniaxial tensile strength of ECC (with the same properties used in current experiments) is about 0.7 times of the corresponding result of bending test (f_{tb}),

$$f_{tu} = 0.7 f_{tb} \tag{6.7}$$

Combining the relations (6.6) and (6.7), the relation (6.4) can be rewritten as,

$$V_{ecc} = 1.05 f_{tb} A_{ecc} \tag{6.8}$$

Once slip occurred in brick-mortar interface, $V_m = 0$ and relation (6.1) will be as follows,

$$V = 4V_{ecc} (6.9)$$

Combination of relations (6.8) and (6.9) will result,

$$V = 4.2 f_{tb} A_{ecc} \tag{6.10}$$

The experimental data and the shear strength predicted by the above simple model are shown in Table 6.1.

Table 6.1 Experimental and analytical shear strength of ECC retrofitted triplet specimens

Specimen	h _b (mm)	$A_{\rm ecc}({\rm mm}^2)$	V analysis (kN)	V experiment (kN)
10RT1	212.50	2125	81.57	72.5
10RT2	211.20	2112	81.07	72.9
10RT3	212.20	2122	81.46	72.4
20RT1	213.20	4264	163.69	95.6
20RT2	212.90	4258	163.46	109.6
20RT3	212.90	4258	163.46	119.8

As it can be seen from Table 6.1, shear strength of triplet specimens retrofitted by 10 mm thick ECC overlay (10RT series) can be predicted by just a 12% difference while the results for the specimens with 20 mm thick ECC retrofit (20RT series) are overestimated. This fact can be explained by the failure mechanism of 20RT specimen series in which the departing of ECC layer from masonry surface was occurred before reaching the ECC layer to its ultimate shear capacity as described in Chapter 5. In the other words, without providing adequate shear transfer system between masonry and thick ECC layer, the retrofit overlay would not

fully contribute to the shear strength of the specimen. So the assumption of perfect bond between ECC and masonry is not valid for layers with higher thickness. In case of thick ECC layer, debonding of ECC overlay from middle brick was occurred prior to the shear cracking of layer. This debonding behavior along with eccentricity of the applied load to the side bricks gradually leads to the total departing of ECC layer from the masonry substrate.

6.3 Numerical Micro-Model Analysis of ECC Retrofitted Triplet Specimens

As described in Chapter 4, micro-modeling is a suitable method for prediction of URM behavior in small sizes. Here, finite element analysis was conducted on the triplet specimen micro-model via ABAQUS non-linear code [3].

Simple micro-modeling approach, in which the unit bricks are modeled separately through their respective constitutive law considering the interaction between them, was utilized. In the other words, in this type of modeling, brick and mortar are smeared in each other and the characteristics of interface as the most possible failure plane of the masonry assemblage are taken into account.

The objective of the numerical analysis is to catch the shear behavior of the retrofitted masonry specimen from bare one by an appropriate finite element model. Such a model can be useful for the retrofit design and the evaluation of retrofit efficiency. Calibration of the model was done by adjustment of the unreinforced model behavior to the corresponding experimental data of URM specimens. The results of analysis on the retrofitted specimens with different thickness of ECC overlay were validated with experimental data and discussed.

6.3.1 Material Properties

The material properties of brick and ECC were obtained from the tests conducted on the materials as described in Chapter 5. The unit brick and ECC were taken as linear elastic and perfect elasto-plastic materials, respectively. The average Young's modulus of the brick was found to be 17.7 kN/mm² and the Poisson's ratio was taken as 0.2. In case of ECC, the average Young's modulus and Poisson's ratio was obtained as 13.94 kN/mm² and 0.207, respectively. Considering the dictated shear cracking pattern in ECC layer during the triplet tests, the failure of ECC is governed by its shear behavior which is originated from the tensile

behavior. In the other words, in the case of triplet specimens, the effect of compressive stress in ECC can be neglected. Kanakubo et al ^[2] proposed a bilinear constitute law for tensile behavior of ECC which is based on a perfect elasto-plastic material assumption and shown in Figure 6.3. Also, in their general model, it is assumed that the principal tensile stress of ECC keeps tensile strength at shear failure. The model is adopted in this numerical analysis.

The ultimate tensile strain of the model (ϵ_u) is given by $0.85\epsilon_{tu,b}$ and the tensile strength (σ_t) is given by $0.82f_{tu,b}$. $\epsilon_{tu,b}$ and $f_{tu,b}$ are the ultimate tensile strain and stress of ECC obtained from bending test on the material prism samples. Elastic modulus for tension is regarded as same as the elastic modulus obtained from compression test ($_cE$).

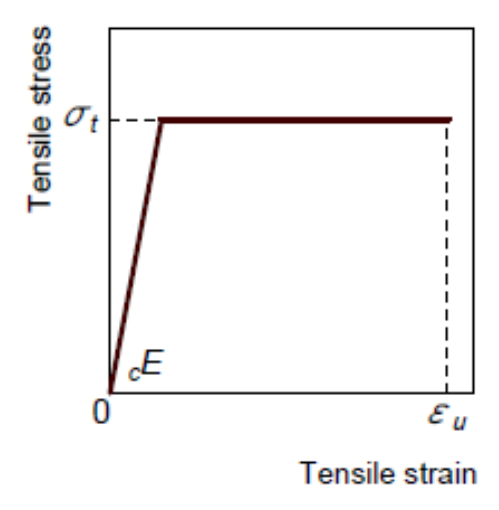


Figure 6.3 Perfect elasto-plastic tensile stress-strain relation of ECC [2]

The parameters used in the modeling of retrofitted triplet, based on the average of experimental data introduced in Table 5.4 and Figure 5.8 of Chapter 5, are shown in Table 6.2.

Table 6.2 Parameters of bilinear tensile constitute law for ECC model

$\sigma_{\rm t} ({\rm N/mm}^2)$	$\varepsilon_{\mathrm{u}}(\%)$	$_{c}E\left(kN/mm^{2}\right)$
7.49	2.25	13.94

6.3.2 Discretization of Model

The brick units were modeled as eight node 3D continuum solid elements with three translation degrees of freedom at each node (C3D8R). ECC overlay was modeled as four node quadrilateral membrane element (M3D4R). Mesh size dependency and result convergence study was performed and as a result, a coarse mesh with element size in the order of 25 mm was applied. The interface between brick and mortar was modeled using surface to surface contact algorithm which is explained in detail as the next part. A perfect bond between ECC and masonry substrate was assumed and in the FEM model, it was applied utilizing Tie contact which constraints all translational and rotational degrees of freedom of two attached surfaces. The bottom face of the side bricks were assumed to be fixed with all the degrees of freedom arrested. The incremental compressive load was applied on the top surface of the middle brick in terms of displacement. The model of URM and retrofitted triplet specimens are shown in Figures 6.4 and 6.5.

6.3.3 Characteristics of Interface

One of the most important aspects in a masonry micro-model is the interaction between its elements which is determined by the characteristics of the mortar-brick bond. Here, as a simple micro-model, the interaction between bricks was modeled by using surface contact algorithm which includes two kind of formulations such as small-sliding, in which surfaces can undergo relatively small sliding but arbitrary rotation and finite-sliding, where separation and sliding of finite amplitude and arbitrary rotation of the surfaces are allowed. The small-sliding formulation was utilized in current model.

In order to model the brick-mortar interface in masonry, contact behavioral features such as tangential and normal behavior of the contact should be defined. Also, the cohesive behavior and damage criterion are needed. These behavioral aspects and their application to triplet model are explained as follows.

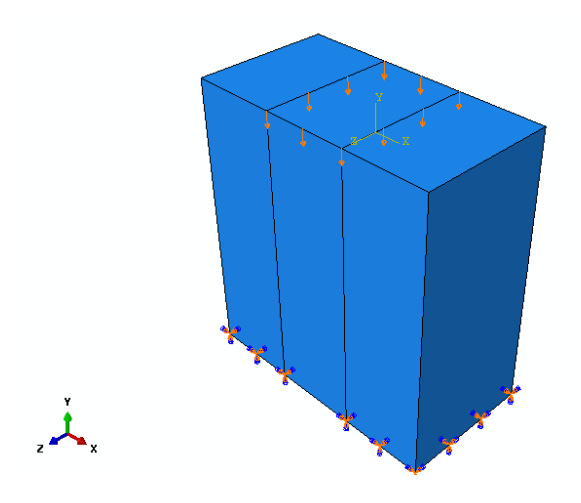


Figure 6.4 Model of unreinforced triplet specimens

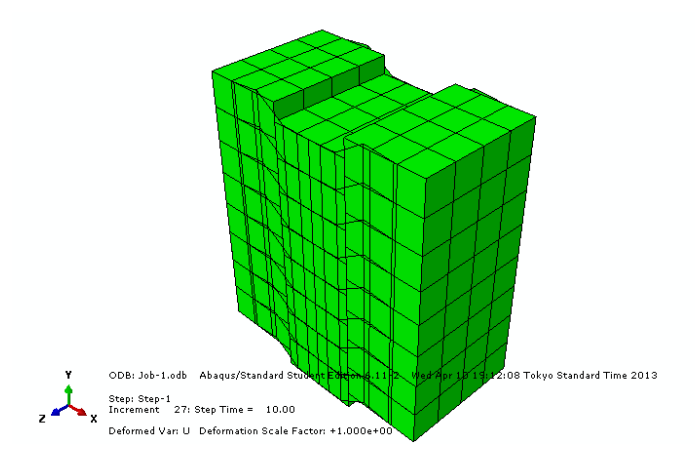


Figure 6.5 Model of retrofitted triplet specimens

6.3.3.1 Tangential Behavior

Shear stress in contact is transmitted between the attached surfaces by tangential behavior. The relationship between the stresses can be described by a friction model based on the Coulomb theory. The contact can resist shear stresses up to a certain magnitude before its

surfaces start sliding relatively. The relation between this critical shear stress and the contact pressure is defined as,

$$\tau_{crit} = \mu.N \tag{6.11}$$

 μ is the coefficient of friction, and N is the applied force normal to interface plane or slip plane. In a three dimensional model, there are two orthogonal components of shear stress (τ_1 and τ_2), which act in two perpendicular slip directions of the contact plane. These two shear stress components are combined into an equivalent shear stress for the slip calculations,

$$\bar{\tau} = \sqrt{(\tau_1^2 + \tau_2^2)} \tag{6.12}$$

Here, taking an isotropic behavior assumption, these two shear stress components were taken as equal.

Due to lack of the force normal to interface plane in case of triplet models, there is no need to define the tangential behavior.

6.3.3.2 Normal Behavior

In order to consider the over closure or interpenetration of the attached surfaces of the contact, normal stiffness of interface should be defined.

In case of triplet specimens, similar to tangential behavior, the definition of normal behavior was neglected.

6.3.3.3 Cohesive Behavior

Cohesive behavior is described by a traction-separation law between surfaces. To simulate the behavior of mortar, cohesion is restricted in the model to the surface regions that are initially in contact. In the other words, unlike usual cohesive materials, in case of masonry mortar, new contacts that occur during the analysis do not contribute to the cohesive forces.

The model assumes a linear elastic traction-separation law prior to damage. Failure of the cohesive behavior occurred by a degradation of cohesive stiffness, derived from damage process.

Once the cohesive behavior is damaged, the friction model becomes active and contributes to the shear strength. When the cohesive behavior is completely damaged, the shear strength is just provided by friction model.

> Linear elastic traction separation model

The model assumes an initial linear elastic behavior followed by the initiation and evolution of damage. The elastic constitutive matrix that relates the normal and shear stresses to the normal and shear separations across the interface is defined as,

$$t = \begin{cases} t_n \\ t_s \\ t_t \end{cases} = \begin{bmatrix} K_{nn} & K_{ns} & K_{nt} \\ K_{ns} & K_{ss} & K_{st} \\ K_{nt} & K_{st} & K_{tt} \end{bmatrix} \begin{bmatrix} \delta_n \\ \delta_s \\ \delta_t \end{bmatrix} = K\delta$$

$$(6.13)$$

where t is the nominal traction stress vector and δ , the corresponding separations. n stands for the normal direction and s and t for the in-plane principal directions ^[3]. Typical linear traction-separation model is shown in Figure 6.6.

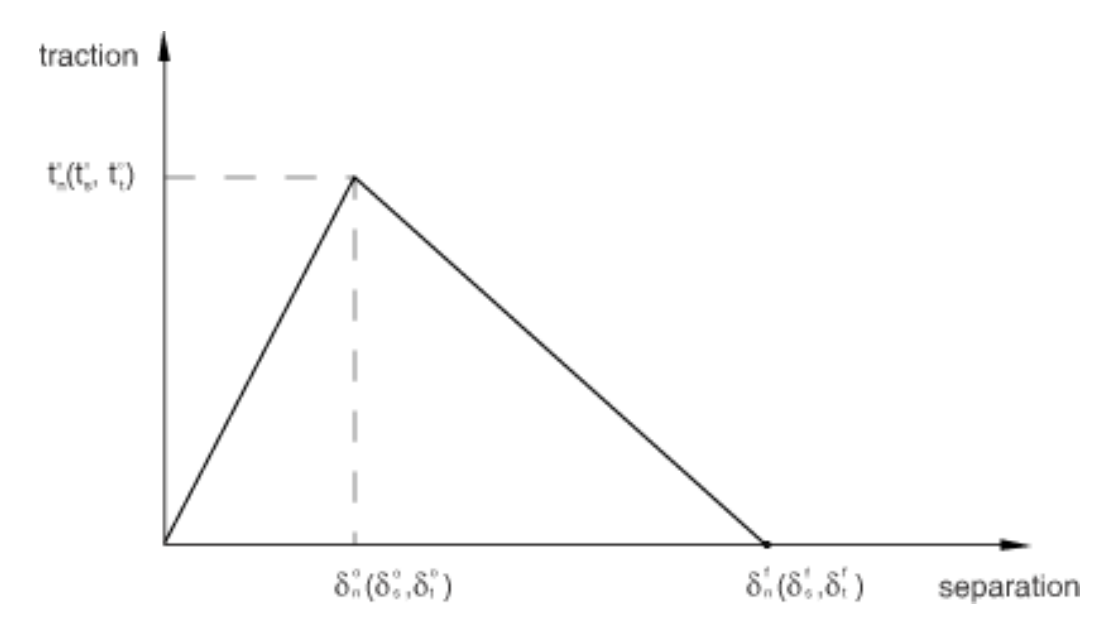


Figure 6.6 Typical linear traction-separation model

Uncoupled traction-separation behavior and the stiffness coefficients of each direction were defined using the data of Table 6.3.

Table 6.3 Stiffness coefficients of traction-separation for ECC retrofitted model

K _{nn} (MPa/mm)	K_{ss} (MPa/mm)	K_{tt} (MPa/mm)
3	30	30

The values of K_{ss} and K_{tt} were obtained from the calibration of bare triplet specimen model to the experimental data. The value of K_{nn} was defined just for preventing any possible interpenetration of interface. The displacement at failure (δ^0) for contact was found as 1.67 mm from calibration. The bond shear stress between brick and mortar versus vertical displacement of the middle brick for specimen UT2 is shown in Figure 6.7 for both cases of the experimental data and calibrated numerical model.

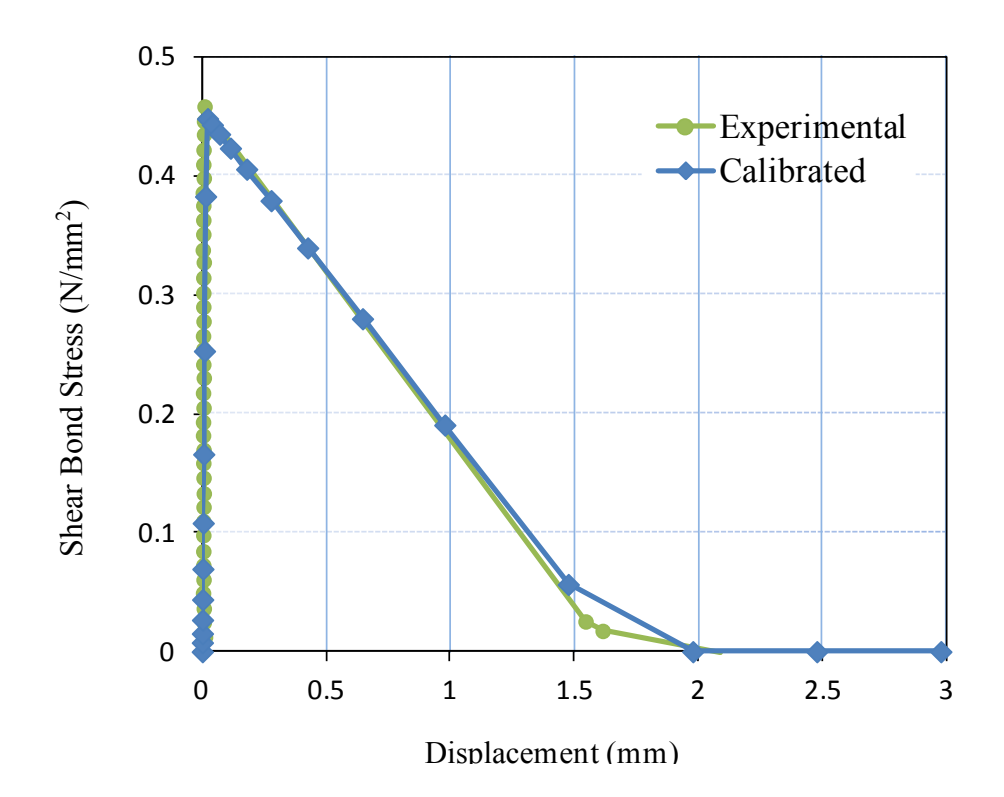


Figure 6.7 Shear bond stress vs displacement for calibrated unreinforced model and experimental data

6.3.3.4 Damage Criterion

The beginning of the degradation of the cohesive response is assumed to happen when the maximum stress criterion is accomplished,

$$\max \left\{ \frac{t_n}{t_n^0}, \frac{t_s}{t_s^0}, \frac{t_t}{t_t^0} \right\} = 1 \tag{6.14}$$

where, the peak values of the contact stress are the normal tensile strength of mortar (t_n^0) and shear bond strength between brick and mortar in two directions ($t_s^0 - t_t^0$).

Tensile strength of mortar was taken as 0.1 MPa and shear bond strength is 0.47 N/mm², obtained from the experiment results (for specimen UT2).

6.3.4 Shear Load Resistance-Displacement Behavior

The shear load resistance versus deflection of the retrofitted specimens with two different thickness of ECC overlay as 10 (specimens 10RT2 and 10RT3) and 20 mm (specimens 20RT1 and 20RT2) for both cases of analytical model and experimental data are shown in Figures 6.8 and 6.9, respectively.

These graphs are shown after the failure deflection which is around 0.2 mm in case of experimental results.

6.3.5 Results and Discussion

As it can be seen from graphs, there is a good agreement between experimental and FEM model results up to the experimental failure point. However, failure deflection of the specimens is overstimated by FEM model. Also, the shear load resistance of specimens with 10 mm thick ECC layer is slightly understimated by the model while the corresponding value for specimens with 20 mm thick layer, is overpredicted.

The maximum load carrying capacity and corresponding failure displacement of specimens 10RT3 and 20RT1 and the predicted values by the model are shown in Table 6.4. Difference between experimental and analytical shear capacity for specimen 10RT3 and 20RT1 is about 15.8% and 9.4%, respectively. As deflection, FEM model could predict the

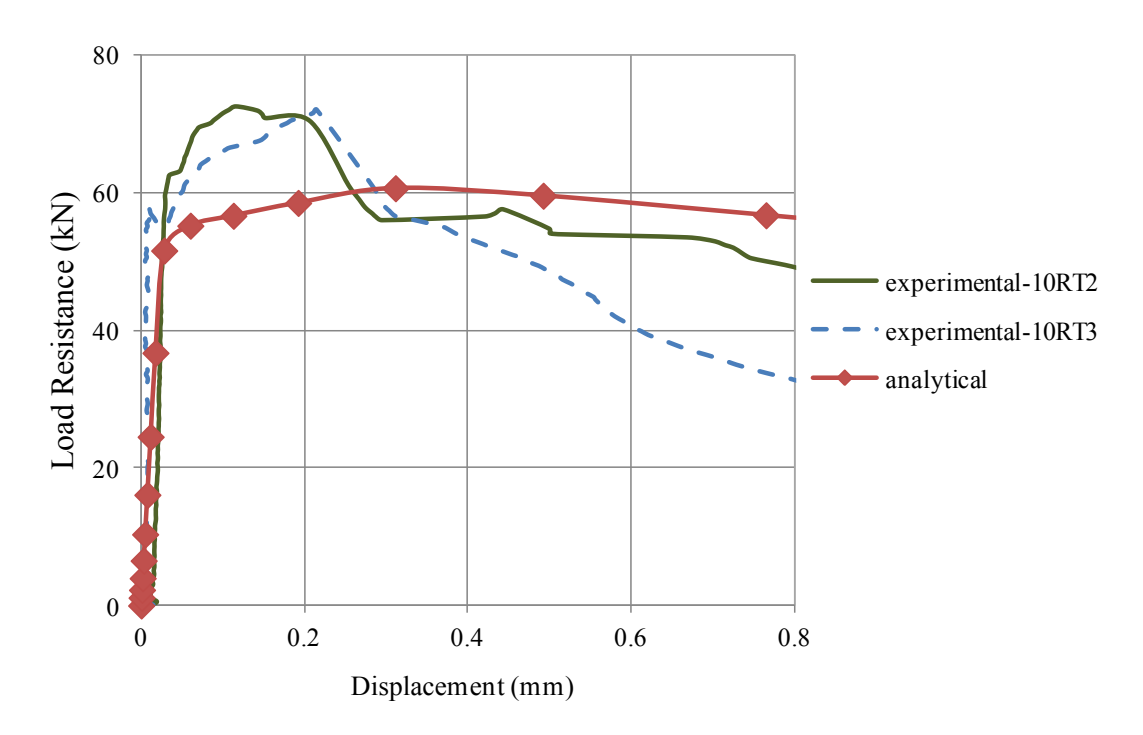


Figure 6.8 Shear load resistance vs deflection for specimens 10RT2 and 10RT3

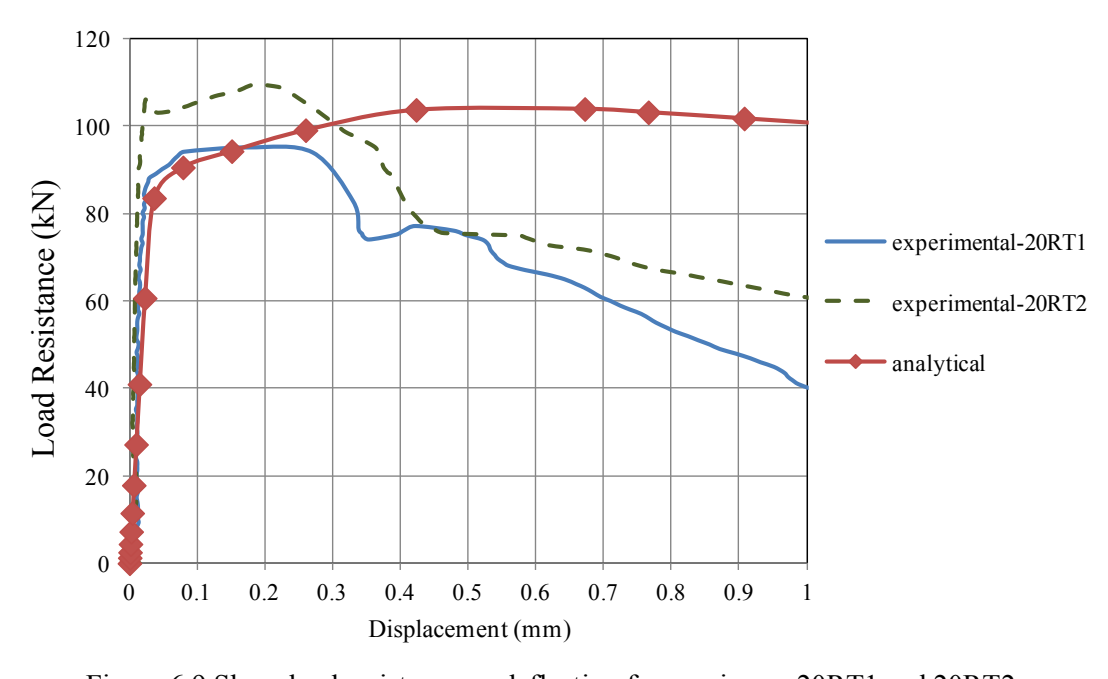


Figure 6.9 Shear load resistance vs deflection for specimens 20RT1 and 20RT2

the deflection of 10RT model more accurately than 20RT model which is related to the perfect bond assumption between brick and ECC. Based on the experimental observation, this assumption is valid for ECC retrofit thickness of 10 mm while it is not an accurate assumption in case of specimens retrofitted with ECC layer of 20 mm (debonding of ECC) and lead to an overestimation of load resistance. This issue can be solved by taking the ECC-URM bond characteristics into account which requires further experimental study in this regard.

Table 6.4 Experimental and analytical shear load capacity and failure displacement of specimens 10RT3 and 20RT1

Doromatar	Experimental		Analytical	
Parameter	10RT3	20RT1	10RT3	20RT1
Peak shear load resistance (kN)	72.02	95.00	60.64	103.95
Deflection at peak stress (mm)	0.22	0.18	0.31	0.67

6.4 Shear Strength Evaluation of AFRP Retrofitted Diagonal Specimens

For in-plane shear behavior of the URM walls retrofitted with externally bonded FRP, few design models have been developed which are mainly based on the masonry-concrete analogy.

Total shear capacity of FRP retrofitted masonry (or reinforced concrete), V, can be assumed as the sum of two terms. The first term, V_m , is the contribution of uncracked masonry and the second term, V_{FRP} , deals with the effect of shear retrofitting of FRP,

$$V = V_m + V_{FRP} \tag{6.15}$$

Among these two contributing terms, V_m may be obtained from experimental data or calculated based on the masonry design codes whereas, determination of V_{FRP} because of the numerous involving parameters is a challenging matter. These parameters such as the FRP tensile strength, modulus of elasticity, the fiber orientation, the bond characteristics between

FRP and substrate and effective strain of FRP, affect the provided shear strength. Also the strain distribution assumption and the formulation of V_{FRP} are determinative.

Because of pre-mature debonding of FRP from retrofit surface, tensile strain in FRP is much lower than its ultimate failure strain. In the other words, the high tensile strength of FRP does not fully contribute to its retrofit functionality.

There are some design models regarding the shear capacity of FRP retrofit. They can be classified into two categories based on the model formulation as: effective strain-based and truss analogy-based models ^[4]. Most of the models consider the FRP strips as the retrofit scheme but since in current study full wrapping of AFRP sheet was performed, the ones deal with this condition were studied. The confining bands utilized in this study directly contribute to the expected effective strain of FRP sheet and in this sense, the effective strain-based model category was considered in particular.

In effective strain-based approach, V_{FRP} is determined by the effective strain of FRP (ε_{fipe}). In literature, ε_{frpe} has been found through a regression of experimental data for concrete members (Triantafillou model ^[5,6]) or a fixed value of it ranging from 0.001 to 0.002 was adopted.

> Triantafillou Model

Triantafillou model is based on the analogy to the action of stirrups in reinforced concrete beams. In this model, the shear resistance mechanism is associated with the action of horizontal laminates. V_{FRP} in this model is calculated as,

$$V_{frp} = 0.9d\rho_{frp} E_{frp} r \varepsilon_{frp,u} t \tag{6.16}$$

where,

d=0.8L effective depth

 $\rho_{frp} = A_{frp} / Lt$ FRP area fraction

E_{frp} elastic modulus of FRP

 $\epsilon_{frp,u}$ ultimate failure tensile strain of FRP

r FRP efficiency factor

t,L thickness and length of retrofitted member

The effective FRP strain, $r\epsilon_{frp,u}$ or $\epsilon_{frp,e}$ can be calculated by relation (6.17) which was developed by Triantafillou through regression of experimental data for concrete members strengthened with FRP under in-plane shear,

$$r\varepsilon_{frp,u} = \varepsilon_{frp,e} = 0.0119 - 0.0205(\rho_{frp}E_{frp}) + 0.0104(\rho_{frp}E_{frp})^2$$
 (6.17)

This model is based on the testing results for concrete. Therefore, for masonry retrofit purpose; it should be validated by experimental data.

In this research work, as it explained in detail at Chapter 5, two-directional (warp and weft) aramid fiber reinforced polymer (AFRP) sheet with two different mesh density and thickness have been utilized for retrofitting of URM and diagonal compression tests were conducted on them. Moreover, in order to eliminate the pre-mature debonding of AFRP sheet, two confining bands were applied for specimen series A3, B2 and B3. Shear resistance of masonry (V_m) is calculated based on the shear strength experimentally obtained from diagonal tests on bare specimens series A1 and B1 using the relation (6.18).

$$V_m = f_{vk}td ag{6.18}$$

where, f_{vk} is the characteristic shear strength of URM specimen - which is shown for A and B specimen series as Figures 5.33 and 5.34 in Chapter 5-, t and d as defined before, are the thickness and effective depth of specimen.

Here, Triantafillou model was adopted for determining the shear contribution of AFRP sheet with confining bands with sheet properties shown in Tables 5.11 and 5.12 of Chapter 5. The experimental shear load resistance of the retrofitted specimens (V_{exp}) and the predicted results by the model (V_{ana}) are shown in Table 6.5.

Table 6.5 Experimental and analytical shear resistance of AFRP retrofitted specimens

Specimen	$V_{exp}(kN)$	V _{ana} (kN)
A21	103.1	107.1
A22	101.4	107.4
A31	145.6	107.9
A32	129.4	108.4
B21	94.5	55.6
B22	85.2	55.3
B31	89.6	72.2
B32	94.9	72.3

As it can be seen from Table data, the analytical results of specimens A21 and A22 show a good agreement with experimental data with 3.9% and 5.9% differences. These two specimens were retrofitted without any confining bands. In case of specimen series A3, B2 and B3, the shear resistance is underestimated with a factor ranging 1.3-1.6. This fact was expected since the effect of confining bands is not included in the analytical model.

Among parameters contributing in the model, confining bands highly influence the effective tensile strain of AFRP sheet. In the other words, due to debonding prevention effect of the bands, effective strain of the retrofit sheet would be higher than the one calculated with relation (6.17).

Through a reverse analysis using the model formula, the effective strain for experimental data ($\epsilon_{frp,ec}$) was obtained for each confined specimen and compared to the one predicted by

Table 6.6 Effective tensile strain of AFRP and efficiency ratio with and without confining bands

Specimen	$\epsilon_{ m frp,ew}$	$\epsilon_{ m frp,ec}$	$r_{\rm w}$	r _c
A31	0.009763	0.031820	0.28	0.91
A32	0.009762	0.021997	0.28	0.63
B21	0.009777	0.024343	0.28	0.70
B22	0.00975	0.020889	0.28	0.60
B31	0.007924	0.011159	0.23	0.32
B32	0.007944	0.012185	0.23	0.35

model ($\varepsilon_{frp,ew}$). Also, taking $\varepsilon_{frp,u}$ of AFRP equal to 0.035 [5], the efficiency factor for both cases of confined (r_c) and without confining bands (r_w) was calculated using relations (6.16) and (6.17), respectively as shown in Table 6.6. As it can be seen from Table 6.6, in case of specimen series A3 and B2 which were retrofitted with sheet material type AK-10/10 (thickness=0.048 mm), application of confining bands increased the efficiency factor from 0.28 to an average value of 0.71. In B3 specimen series, with sheet material type AK-20/20 (thickness=0.096 mm), this factor was increased from 0.23 to an average value of 0.33. In the other words, application of confining bands increased the efficiency factor about 2.5 and 1.4 times for AFRP sheet types AK-10/10 and AK-20/20, respectively. It means that the confining bands exhibit more efficiency (roughly about two times in case of this experimental study) in the specimens retrofitted with thinner sheet (lower axial rigidity) compare to thicker one (higher axial rigidity). In order to obtain a rational relation between sheet axial rigidity and confining effect, higher number of tests with different material thickness and confining patterns is needed. Also, since the relation (6.17) for effective tensile strain of FRP has originally been developed for concrete, modification for masonry application should be considered via further experimental data.

6.5 Numerical Micro-Model for AFRP Retrofitted Diagonal Specimens

Employing simple micro-model approach, FEM numerical analysis was conducted on the URM diagonal specimens retrofitted with AFRP. In a similar process as the analytical model for ECC retrofitted triplet specimens, in order to catch the brick-mortar interface parameters, calibration of unreinforced model was carried out. Then, these parameters were applied to the retrofitted model. However, because of the usual high deviation in the test results of the URM specimens, failure pattern of unreinforced diagonal specimen and consequently the deformational data cannot be accurately calibrated by numerical method. So, in the calibration of diagonal URM specimen, it was intended to adjust the ultimate failure load. Specimen series B of diagonal tests was selected as a representative for URM wall under biaxial loading condition. The experimental result of the specimen type B22 was used for the validation of AFRP-URM numerical model. Also, bare specimen type B12 was taken as the

reference for above mentioned calibration. Geometrical features and loading configuration of these specimens are explained in part 5.3.2 of Chapter 5.

The vertical load-deflection relation obtained from the numerical model was validated by the corresponding experimental data. The model structure is explained as follows.

6.5.1 Material Properties

The mechanical behavior of brick was considered as linear elastic with Young's modulus and Poisson's ratio as 17.7 kN/mm² and 0.2, respectively. The elastic properties of AFRP sheet are shown in Table 6.7. The Poisson's ratio of the sheet material was taken as 0.2. In order to take the debonding behavior of the AFRP sheet into account, the bond characteristics between the sheet and substrate should be determined which has previously been studied in several research works.

Here, a new approach for evaluation of the post-debond behavior of AFRP retrofit sheet is proposed. In this method, the overall behavior of the AFRP sheet and cohesive resin is regarded as a perfect elasto-plastic material. A bilinear tensile constitute law is assumed for this material as shown in Figure 6.10.

The yield strain in this model (ϵ_y) is assumed as the effective strain of the unconfined AFRP sheet (r_w) which is explained in part 6.4 of this chapter. The ultimate strain (ϵ_u) is regarded as the ultimate tensile strain of AFRP sheet.

Based on Table 6.6, the value of r_w for AFRP sheet type AK-10/10 (which was applied to specimen B22) is 0.28. The ultimate tensile strain of AFRP is taken as 0.035 ^[5].

In the bilinear model, the behavior of AFRP-resin assemblage is linear elastic up to the effective strain of the unconfined sheet. After this yield point, the increase in load does not affect the tensile stress and instead, leads to a plastic deformation which is represented by the debonding phenomenon.

The plastic elongation of the material is limited by the ultimate tensile strain of the material. Due to the presence of the confining bands, the value of this strain is limited to the ultimate tensile strain resisted by the AFRP sheet ($\epsilon_{tu,frp}$). So, the values of ϵ_y and ϵ_u were applied to the numerical model as 0.0098 and 0.035, respectively.

Table 6.7 Aramid sheet material specifications

Matarial	Weight	Tensile capacity	Thickness	Tensile Strength	Young's Modulus
Material	(g/m^2)	(KN/m)	(mm)	(N/mm^2)	(KN/mm^2)
AK- 10/10	180	98/98	0.048		
AK- 20/20	325	196/196	0.096	2060	118
AK-90	623	882	0.430		

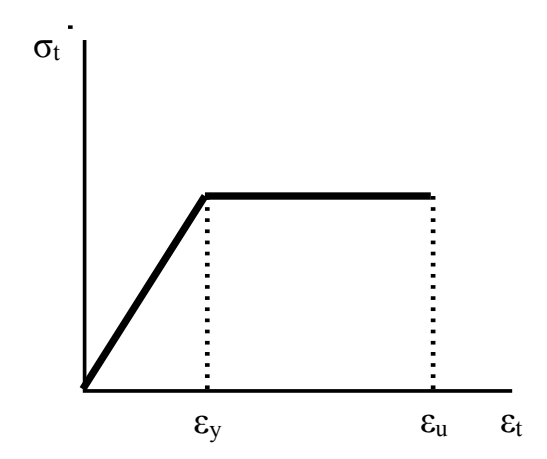


Figure 6.10 Elasto-plastic tensile stress-strain diagram for AFRP-resin

6.5.2 Discretization of Model

The brick units were modeled as eight node 3D continuum solid elements with three translation degrees of freedom at each node (C3D8R). The AFRP sheet and cohesive resin assemblage was modeled as four node quadrilateral membrane element (M3D4R) with elastoplastic behavior. The membrane element is a good choice to catch the in-plane stress and strains where the compressive stress cannot be resisted. Mesh size in the order of 30 mm was used in model. A perfect bond between AFRP-resin and masonry was defined. Similar to ECC retrofitted model, the interface between brick and mortar was modeled using contact procedure. The bottom loading shoe was assumed to be fixed in the all degrees of freedom. The incremental vertical compressive load was applied in terms of displacement on the upper

side of the top loading shoe. The model of URM and retrofitted diagonal specimen are shown in Figures 6.11 and 6.12, respectively.

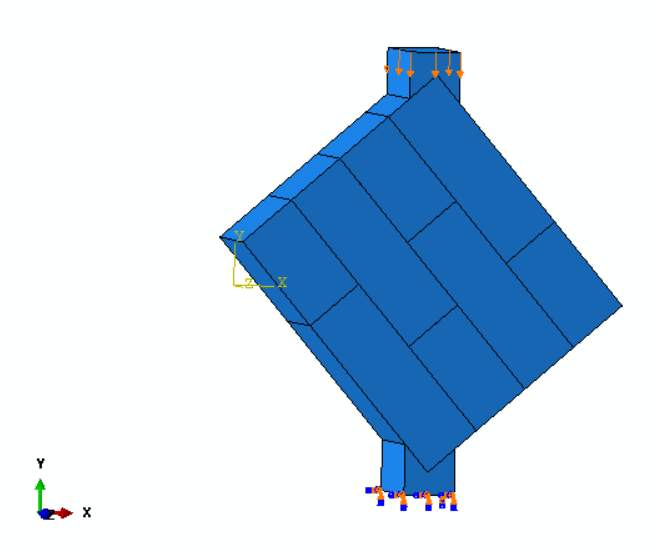


Figure 6.11 Model of unreinforced diagonal specimen

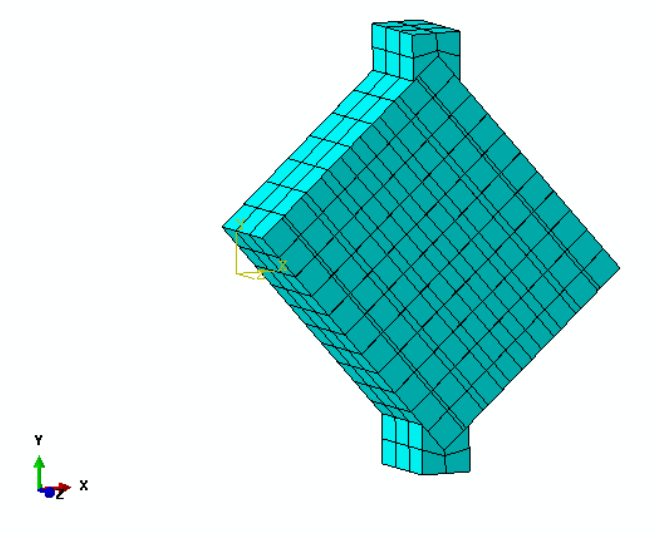


Figure 6.12 Model of AFRP retrofitted diagonal specimen

6.5.3 Characteristics of Interface

In a similar way as the ECC retrofitted model, brick-mortar contact characteristics such as the tangential behavior, normal behavior, cohesive behavior and the damage criterion were defined.

6.5.3.1 Tangential Behavior

As a result of calibration and adjustment to the experimental results of the reference bare specimen (B12), the friction coefficient, μ , was obtained as about 0.8. This value was applied to the model using isotropic penalty friction formulation in which the tangential friction is removed after the shear stress in contact reaches the critical stress determined by the friction coefficient. After removal of the friction behavior, cohesive behavior governs the contact characteristics.

6.5.3.2 Normal Behavior

Normal stiffness of contact is originated from the uniaxial compressive/tensile behavior of bed joint mortar which is a small amount in case of tensile strength for masonry mortar. However, in order to avoid the contact interpenetration and numerical convergence issues, linear model with a high value of normal stiffness as 1000 N/mm was defined.

6.5.3.3 Cohesive Behavior

Employing the linear traction-separation law, the cohesive stiffness coefficients for each planar direction of the contact were defined.

The normal and tangential stiffness of brick-masonry contact is proportional to the elastic and shear modulus of mortar, respectively. Also, similar to concrete, the elastic modulus and consequently the shear modulus of mortar can be considered proportional to $\sqrt{f_c'}$ (second root of the mortar compressive strength).

The mortar used for the construction of diagonal B specimens has a compressive strength about 1.7 times of the one used in the triplet specimens (see part 5.3.2 of Chapter 5).

Therefore, as explained above, the values of normal and tangential stiffness for diagonal specimens obtained as about 1.3 times of the corresponding values for triplet specimens. These values are shown in Table 6.8. Damage criterion and the bond strength of the contact were taken as the same values of the triplet model.

Table 6.8 Stiffness coefficients of traction-separation for AFRP retrofitted model

K _{nn} (MPa/mm)	K _{ss} (MPa/mm)	K _{tt} (MPa/mm)
3.9	39	39

6.5.4 Load-Displacement Behavior

Distribution of in-plane strain across the specimen surface is shown in Figure 6.13 in which a concentration of shear strain in AFRP sheet along the bed joint directions can be seen.

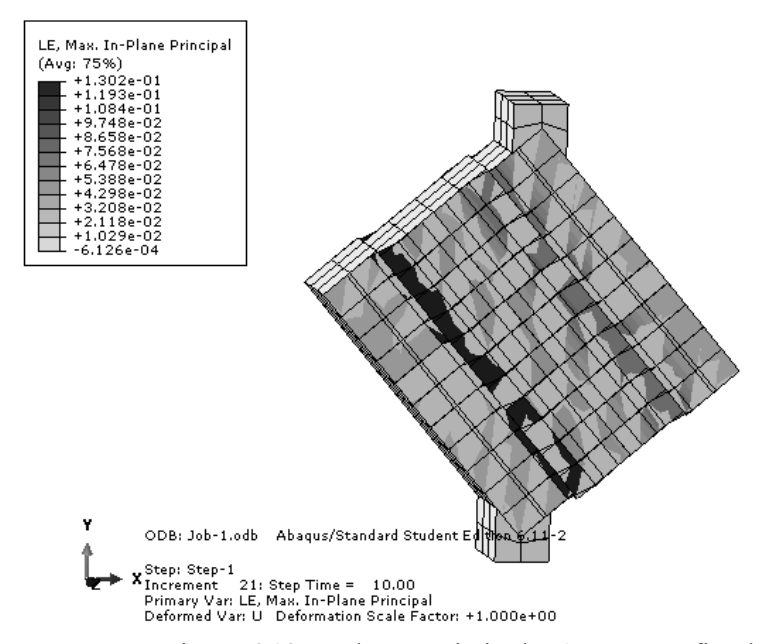


Figure 6.13 In-plane strain in the AFRP retrofitted specimen

The vertical compressive load versus deflection diagram of the retrofitted specimens with AFRP sheet type AK-10/10 (specimen type B21 and B22) for both cases of analytical model and experimental data are shown in Figure 6.14.

6.5.5 Results and Discussion

The behavior of the FEM model was in a relatively close agreement with the experimental data up to the failure point of the specimen (deformation about 4.70 mm). As observed during the experiments, post-yield behavior of the specimens started with a gradual

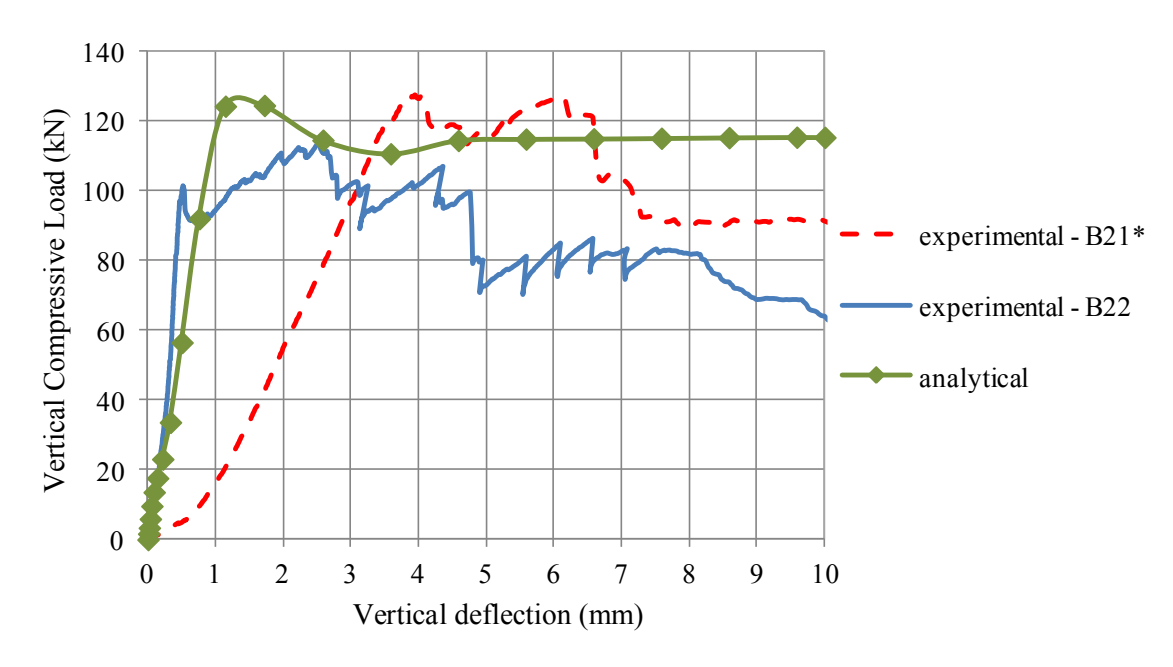


Figure 6.14 Vertical compressive load vs deflection for specimen type B21 and B22

* Including the deformation of bands at the contact point with loading shoes

debonding of the retrofit sheet in a area bordered by the confifng bands. This developing debond behavior provides the ductility of the retrofitted masonry and governs the masonry inplane behavior from the yield point up to the rupture of sheet and failure of the specimen. A similar behavioral pattern can be seen in the numerical model.

A slight post-yield hardening in the experimental diagram was observed. This hardening behavior is attributed to the truss strut mechanism in the debonded AFRP sheet.

The peak compressive load resistance in the experimental and analytical results are shown in Table 6.9. The experimental peak load in the table is the average of the results of B21 and B22 specimens. The peak load was predicted by the analytical model with a difference about 2.6% to the experimental result which shows a good agreement.

Table 6.9 Experimental and analytical results for peak compressive load of specimens B21 and B22

Parameter	Experimental	Analytical
Peak compressive load (kN)	121.20 (Average of B21 and B22)	124.40

As a result of validation, the proposed bilinear model for AFRP-resin can be considered as an appropriate method for modeling of AFRP-URM retrofit and the prediction of in-plane behavior of the AFRP retrofitted masonry wall. In the other words, instead of determination of the AFRP-URM bond characteristics which requires relatively difficult experiments, the proposed model can be used as an alternative technique for AFRP retrofit modeling.

The peak compressive load in this model is highly dependent on the definition of the yield strain of the proposed bilinear constitute law or on the effective strain of unconfined AFRP sheet. As mentioned in part 6.4 of this chapter, the effective strain for FRP in Triantafillou model, has been obtained from a regression on the concrete members retrofitted with FRP sheet. Although this effective strain lead to a good agreement in current numerical model, modification for masonry application will result in better accuracy. Also, the plastic deformation of the bilinear model (or debonding of AFRP) is dependent on the the ultimate tensile strain of AFRP sheet. This ultimate strain may not be achieved in general and so there is a need for further experiments to determine the ϵ_u for different band confinement patterns of AFRP.

References

- [1] Li, V. C., Mishra, D. K., Naaman, A. E., Wight, J. K., LaFave, J. M., Wu, H. C., Inada, Y. (1994). On the Shear Behavior of Engineered Cementitious Composites. Journal of Advanced Cement Based Materials, Vol.1, No.3, pp. 142-149.
- [2] Kanakubo, T., Shimizu, K., Kanda, T., Nagai, S. (2007). EVALUATION OF BENDING AND SHEAR CAPACITIES OF HPFRCC MEMBERS TOWARD THE STRUCTURAL APPLICATION. Proceedings of the Hokkaido University COE Workshop on High Performance Fiber Reinforced Composites for Sustainable Infrastructure System material modeling, structural design and application, Sapporo, Japan.
- [3] Hibbit, D., Karlson, B., Sorensen, P. (2002). ABAQUS/Standard theory manual. HKS.
- [4] Zhuge, Y. (2010). FRP-Retrofitted URM Walls under In-Plane Shear: Review and Assessment of Available Models. Journal of Composites for Construction, Vol. 14, No. 6, pp.743–753.
- [5] Triantafillou, T. C., Antonopoulos, C. (2000). Design of concrete flexural members strengthened in shear with FRP. Journal of Composites for Construction, Vol.4, pp.198– 205.
- [6] Triantafillou T. (1998). Strengthening of masonry structures using epoxy bonded FRP laminates. J Comp Const, ASCE; 2(2), pp. 96-104.

Chapter 7

SUMMARY AND CONCLUSION

7.1 Summary

Many of the existing buildings including historical and cultural monuments around world are constructed with unreinforced masonry (URM). A big part of these structures are located in the earthquake-prone regions of the world. In general, these buildings were built with little or no consideration for seismic design requirements. In recent earthquakes, it has been proved that many of these buildings are highly vulnerable and as a result there is a serious need for proposing appropriate retrofitting techniques for existing URM structures.

Unreinforced masonry walls are one of the most vulnerable parts of the URM structures. Their inadequate in-plane and out-of-plane seismic response are known as the most important reason for the URM partial damages and even total collapse.

In order to have a clear idea about the seismic incapability of URM walls, the principal behavioral characteristics of them considering the interaction of different loading conditions were reviewed and discussed.

This thesis focuses on the in-plane behavior of the unreinforced masonry walls. Improvement in this behavioral characteristic by suitable retrofitting methods was the main objective of this research work.

An extensive investigation has been conducted on the existing URM retrofit strategies. Their advantages and disadvantages were compared based on the experiences available in literature. As a result, it was revealed that the surface treatment is the most suitable method from both applicability and cost-performance viewpoints in the case that the covering of the wall surface is acceptable due to architectural reasons. It must be mentioned that some reliability issues for this approach have not been completely solved and need more investigation. Among the materials has been examined in the surface treatment category, ones with high deformation and tensile capacity exhibited more desirable in-plane performance in terms of the shear strength and ductility. Such kind of materials has been made available by

the composite industry in recent years. High performance composites offer a promising rehabilitation future for URM structures.

Retrofitting of URM wall with engineered cementitious composite (ECC) as a new composite material was investigated in this research work. This material has shown a high performance in the behavioral enhancing of reinforced concrete structures. ECC – also refers to as High Performance Fiber Reinforced Cement Composite (HPFRCC) in Japan, Strain-Hardening Cement-based Composite (SHCC) and bendable concrete – with multiple fine cracks is a cement-based composite material with a strain-hardening tensile behavior with an excellent capability to control the width of crack. This composite material exhibits a high deformation capacity and can absorb and dissipate high amounts of energy. Improving the low tensile strength, strain-softening and brittle behavior of URM walls with such a ductile strain-hardening material was the main motivation of this research work. Improvement in the in-plane characteristics of the ECC retrofitted masonry was evaluated through a series of tests on small-size masonry wall specimens. Monotonic shear and compression tests have been conducted on the unreinforced and ECC retrofitted specimens. Retrofitting was performed through surface treatment with different overlay thicknesses and the retrofit efficiency was evaluated for each case.

Fiber reinforced polymer (FRP) products are well-known for their retrofit capability in the variety of structure types. In case of URM structures, research works have shown a considerable improvement in the seismic behavior of FRP-URM as well. However, as it has been reported in several research works, pre-mature debonding of FRP limits its efficiency. In present study, in order to eliminate this undesirable behavior, confining bands were utilized. FRP products are available in various forms such as rods and sheets and different material bases such as carbon fiber reinforced (CFRP) and glass fiber reinforced (GFRP). Here, aramid fiber reinforced polymer (AFRP) sheet with light weight and good workability has been utilized as a retrofit solution for URM walls. Two types of masonry specimens with different size and shape were constructed and retrofitted with AFRP sheet and the confining bands were applied to some of them. Diagonal compression test was conducted on the

unreinforced and retrofitted specimens and the performance of this retrofit method and confining bands in particular was evaluated.

In order to predict the in-plane behavior of the retrofitted URM with both of the above mentioned methods (ECC and AFRP), analytical study was performed which is an important step toward the proposing a rational retrofit design model. A simple shear model introduced for ECC retrofitted masonry and the results obtained from it were validated by experimental data.

Efficient strain approach -which is originally developed for design of the FRP retrofitted concrete elements-, is adopted for URM. The effect of confining bands and their contribution to the efficient design strain of AFRP sheet was evaluated and discussed.

In order to predict the in-plane behavior of the retrofitted URM in both of ECC and AFRP techniques, numerical analysis was conducted. Available numerical modeling strategies for unreinforced masonry were introduced and discussed. Here, simple micromodel strategy was adopted in the analysis employing finite element method. In order to have reliable results, models of the unreinforced masonry specimens were calibrated using corresponding test data.

An elasto-plastic tensile model was adopted for ECC. Also, a new bilinear tensile model for AFRP-resin was proposed and applied to the numerical modeling. Analytical results of the retrofitted models were compared to the experimental ones and validated in terms of the load-deformation relation.

7.2 Findings and Conclusion

Experiments conducted on ECC retrofitted masonry showed that the shear resistance of URM was improved by an average factor of 3 per 10 mm retrofit overlay. However, due to the debonding behavior of ECC layer, this factor is not proportional to the overlay thickness. In order to have a better performance, a shear transfer mechanism should be implemented in the masonry-ECC interface. Also, a significant enhancement in the deformation capacity of URM by an average factor of 30 was observed in this retrofit method. Considering the above mentioned improvements induced by ECC retrofitting, it can be considered a reliable method.

In case of AFRP retrofitting, the shear capacity of URM was increased by an average factor of about 1.5. Also, the deformability of AFRP retrofitted masonry was obtained as about 5 times of the unreinforced one. The debonding behavior of AFRP sheet was successfully controlled by the confining bands. This effect was proved by the rupture of the sheet which means that the efficient tensile strain in AFRP reaches its ultimate value. As a result, it was concluded that the AFRP retrofitting with confining band system can be considered as an appropriate alternative technique.

As analytical study, the simple shear model for ECC retrofit showed a good agreement with experimental results in case of thin (10 mm) layer while it overestimates the shear strength of thick ECC (20 mm) overlay by a factor of 1.5. This fact is attributed to the debonding behavior of ECC which eliminates its full contribution to the shear strength of the retrofitted assemblage.

The efficiency evaluation of the confining bands in the AFRP retrofitted masonry by means of the Triantafillou model showed that the efficiency factor is inversely proportional to the thickness (axial rigidity) of the AFRP sheet. In the other words, application of these bands to thinner layers of AFRP sheet will result in higher efficiency.

Through the numerical analysis of ECC-URM model, in case of 10 mm thick ECC overlay, good agreement in terms of the shear capacity (difference about 16% to experimental data) and deformation between analytical and experimental results was obtained. In case of the 20 mm thick ECC layer, this model overestimates the shear (difference about 9% to experimental data) and deformation capacity of ECC-URM which can be attributed to the debonding effect of ECC overlay. It was found out that the adopted elasto-plastic tensile model can be used for shear design of ECC retrofit with a fine accuracy.

In the case of AFRP-URM numerical model, it was revealed that the proposed bilinear AFRP-resin model is able to predict the peak load with a good agreement (difference about 3% to experimental data). As a result, it was found out that instead of determination of the AFRP-URM bond characteristics which requires relatively difficult experiments, the proposed model can be used as an alternative technique for AFRP retrofit modeling design with a fine accuracy.

As the result of this research work, it was concluded that both ECC and AFRP (with confining band system) retrofitting can be considered as suitable methods for in-plane enhancement of URM walls. Moreover, the adopted and proposed analytical models can simulate the elastic and post-cracking behavior of retrofitted masonry with a fine accuracy and consequently can be useful for retrofit design.

7.3 Future Work

There are some issues in this research work which needs more investigation. They are recommended as the extension of this study:

- An appropriate shear transfer mechanism should be implemented in ECC-URM interface. Also, application of the ECC-URM bond characteristics to the numerical model can improve the accuracy of the results.
- 2) The effect of different confining band patterns in AFRP retrofitting could be experimentally examined. Through this process, the optimal form can be determined. However, applicability of the pattern to actual URM wall should be considered.
- 3) An empirical relation regarding the effective strain provided by the confining bands in AFRP retrofit method could be developed via further experiments.
- 4) Although the performance of retrofitting in two sides of the URM wall is higher, the effect of one side retrofitting should be investigated as well. Due to the applicability issues in some actual construction cases, two side retrofitting might not be viable.
- 5) Experimental and analytical study on the cyclic behavior of the ECC and AFRP retrofitted masonry wall is suggested as the extension of the monotonic tests conducted in this research work.